Boron isotope variations in Tonga-Kermadec-New Zealand arc lavas: Implications for origin of subduction components and mantle influences

Article *in* Geochemistry Geophysics Geosystems · February 2017

DOI: 10.1002/2016GC006523

3 authors, including:

William P Leeman
Rice University
272 PUBLICATIONS **11,173** CITATIONS

SEE PROFILE

AGU PUBLICATIONS

Geochemistry, Geophysics, Geosystems

RESEARCH ARTICLE
10.1002/2016GC006523

Key Points:
- The first comprehensive B isotope data set for the Tonga-Kermadec-New Zealand arc and associated subducting sediments
- Tonga-Kermadec lavas have higher B/Nb and δ^{11}B than the sediments, and seem to reflect dominantly fluid-related contributions from the subducting slab
- Estimates of magma source compositions and extent of melting constrain the nature of subduction contributions along the arc

Supporting Information:
- Supporting Information S1
- Figure S1
- Figure S2
- Figure S3
- Table S1

Correspondence to:
W. Leeman,
leeman@rice.edu

Citation:
Leeman, W. P., S. Tonarini, and S. Turner (2017), Boron isotope variations in Tonga-Kermadec-New Zealand arc lavas: Implications for the origin of subduction components and mantle influences, *Geochem. Geophys. Geosyst.*, *18*, doi:10.1002/2016GC006523.

Received 7 JUL 2016
Accepted 8 FEB 2017
Accepted article online 11 FEB 2017

Boron isotope variations in Tonga-Kermadec-New Zealand arc lavas: Implications for the origin of subduction components and mantle influences

William P. Leeman[1,2], Sonia Tonarini[3], and Simon Turner[4]

[1]Department of Earth Science, Rice University, Houston, Texas, USA, [2]Now at: 642 Cumbre Vista, Santa Fe, New Mexico, USA, [3]Instituto di Geoscienze e Georisorse, Consiglio Nazionale delle Ricerche, Pisa, Italy, [4]Department of Earth and Planetary Sciences, Macquarie University, Sydney New South Wales, Australia

Abstract The Tonga-Kermadec-New Zealand volcanic arc is an end-member of arc systems with fast subduction suggesting that the Tonga sector should have the coolest modern slab thermal structure on Earth. New data for boron concentration and isotopic composition are used to evaluate the contrasting roles of postulated subduction components (sediments and oceanic slab lithologies) in magma genesis. Major observations include: (a) Tonga-Kermadec volcanic front lavas are enriched in B (as recorded by B/Nb and similar ratios) and most have relatively high δ^{11}B ($>+4‰$), whereas basaltic lavas from New Zealand have relatively low B/Nb and δ^{11}B ($<-3.5‰$); (b) both δ^{11}B and B/Nb generally increase northward from New Zealand along with convergence rate and overall slab flux; (c) δ^{11}B and B/Nb decrease toward the back-arc, as observed elsewhere; and (d) low δ^{11}B is observed in volcanic front samples from Ata, an anomalous sector where the back-arc Valu Fa Spreading Center impinges on the arc and the Louisville Seamount Chain is presently subducting. Otherwise, volcanic front lavas exhibit positive correlations for both B/Nb and δ^{11}B with other plausible indicators of slab-derived fluid contributions (e.g., Ba/Nb, U/Th, (^{230}Th/^{232}Th) and ^{10}Be/^{9}Be), and with estimated degree of melting to produce the mafic lavas. Inferred B-enrichments in the arc magma sources are likely dominated by serpentinite domains deeper within the subducting slab ($\pm$altered oceanic crust), and B systematics are consistent with dominant transport by slab-derived aqueous fluids. Effects of this process are amplified by mantle wedge source depletion due to prior melt extraction.

Plain Language Summary Boron isotope and other geochemical data are used to evaluate contributions from subducted materials to magma sources for volcanoes of the Tonga-Kermadec-New Zealand volcanic arc. The data are used to estimate the composition of modified mantle sources for the arc magmas as well as the extent of melting to produce them. It is shown that the mantle was previously depleted in melt components, and then overprinted by B and other components from the subducting slab, predominantly by aqueous fluids produced by dehydration of the slab. Some elements (e.g., Th, Be, La) considered to be relatively immobile in aqueous fluids, show strong correlation with B-enrichment, suggesting that they too can be mobilized in this manner. This result is important for understanding the origin of arc magmas from other localities. In addition our data imply that slab inputs to arc magma sources are cumulative over time.

1. Introduction

Arc lavas differ from those produced in other tectonic settings in that their compositions commonly reflect contributions from subducted sediments and/or altered oceanic crust. However, there remains considerable debate concerning the nature of the "subduction component(s)," the relative roles of slab-derived fluids versus partial melts as transport media for these additions, and where and when such additions to the mantle wedge are likely to occur. Unravelling the details of melt generation may be complicated for many reasons: (a) transport processes may selectively decouple the behavior of elements having different geochemical properties [*Bebout et al.*, 1999; *Straub and Layne*, 2003], (b) processes attending ascent and storage may modify magma compositional signatures inherited from the magma source(s), and (c) the sources themselves may differ in composition over various spatial and time scales [*Leeman et al.*, 2005a]. Regarding

sediment-derived components, it is unclear whether recycling involves bulk mixing of subducted material into arc magma sources (e.g., in a subduction mélange), or selective transfer via devolatilization fluids, partial melts, or both [e.g., *Class et al*., 2000; *Elliott et al*., 1997; *Klimm et al*., 2008; *Plank*, 2005]. The apparent effects are likely to vary depending on the specific elements being considered. Because subduction zones are sites of major material recycling back into the upper mantle, resolution of such questions is essential to better understand the physical processes and loci of melt generation as well as the effects of subduction recycling on mantle and crustal evolution.

Here we focus on the utility of boron as a petrogenetic tracer because this element is known to be efficiently mobilized in aqueous fluids [*You et al*., 1993, 1995; *Brenan et al*., 1998a, 1998b], to have low affinity for all major mantle minerals [e.g., *Chaussidon and Libourel*, 1993; *Ottolini et al*., 2004], and to have low concentrations in typical mantle and lower crustal rocks [cf. *Leeman and Sisson*, 1996]. Thus, it is expected that B systematics of ascending magmas are relatively insensitive to modification by wall rock interactions. On the other hand, because B is enriched in altered oceanic crust [*Thompson and Melson*, 1970; *Seyfried et al*., 1983; *Spivack and Edmond*, 1987; *Leeman*, 1996; *Staudigel et al*., 1996], most marine sediments [*Ishikawa and Nakamura*, 1992; *Leeman and Sisson*, 1996], and serpentinized upper oceanic mantle [*Bonatti et al*., 1984; *Benton et al*., 2001; *Hattori and Guillot*, 2003; *Tenthorey and Hermann*, 2004; *Scambelluri et al*., 2004; *Savov et al*., 2005; *Vils et al*., 2008, 2009; *Tonarini et al*., 2011; *Pabst et al*., 2012; *Scambelluri and Tonarini*, 2012; *Deschamps et al*., 2013; *Harvey et al*., 2014; *Ryan and Chauvel*, 2014; *Martin et al*., 2016], subduction of such materials can lead to anomalous enrichment of B in subarc mantle domains [*Ryan and Langmuir*, 1993; *Leeman*, 1996; *Savov et al*., 2005]. Relative to other incompatible elements, B tends to be selectively enriched in most arc lavas—with maximum enrichments (at any given subduction zone) observed in frontal rather than back-arc regions [*Leeman et al*., 1994, 2004; *Ishikawa and Nakamura*, 1994; *Ryan et al*., 1995; *Tonarini et al*., 2001]. Also, anomalous enrichment of B is commonly associated with unusual tectonic settings, such as areas where fracture zones are subducted [*Singer et al*., 2007; *Manea et al*., 2014]. Moreover, positive correlations between B enrichment (e.g., B/Be) and $^{10}Be/^{9}Be$ in arc lavas provide "smoking gun" evidence that the B signal is in some manner slab-derived [*Morris et al*., 1990; *Ryan et al*., 1995; *Ishikawa et al*., 2001]. Similar correlations with other elemental and isotopic tracers of slab contributions support this inference [*Leeman*, 1996; *Noll et al*., 1996; *Chan et al*., 1999, 2002; *Straub et al*., 2004]. Enrichment of B with respect to relatively fluid-immobile incompatible elements (e.g., Zr, Hf, Nb, Ta) effectively requires an aqueous fluid phase as opposed to either slab-derived silicate melt or supercritical fluid as the primary transport medium for B enrichment in arc magma sources [cf. *Brenan et al*., 1998a; *Kessel et al*., 2005]. This distinction is of particular import when considering thermal conditions in subduction zones, as such decoupling of B should preferentially occur in cold subduction zones (i.e., at temperatures below material solidi or supercritical conditions). It is important to note that temperature conditions (here, referred to as "thermal structure") in subduction zones can vary significantly depending on such tectonic factors as age of the subducting slab and rate of convergence [cf. *Wiens and Gilbert*, 1996; *Van Keken*, 2003; *England and Wilkins*, 2004; *England and Katz*, 2010]. Thus, as discussed below, metamorphism, devolatilization, and, ultimately, melting of slab components may follow diverse pathways depending upon subduction zone thermal structure. Mobility of specific elements will also be influenced by their affinity to minerals in equilibrium with the transfer medium (solid/melt and solid/fluid distribution coefficients; cf. *Marschall et al*. [2006], *Spandler and Pirard* [2013]), and that can vary with P-T conditions.

Several studies have exploited B isotopic variations between seawater, sediments, and altered oceanic crust to investigate origins of the so-called "fluid component" in arc lavas [e.g., *Ishikawa and Nakamura*, 1994; *Ishikawa and Tera*, 1997, 1999; *Ishikawa et al*., 2001; *Tonarini et al*., 2001, 2011; *Straub and Layne*, 2002; *Rosner et al*., 2003; *Leeman et al*., 2004; *Ryan and Chauvel*, 2014]. These studies describe systematic variations in B isotopic composition that are attributed to additions of ^{11}B-rich (or isotopically heavy) slab-derived fluids to the arc magma sources. However, estimated compositions and amounts of the subduction component vary significantly from arc to arc, and are difficult to reconcile in terms of a simple universal mixing model. Differences in thermal conditions within subduction zones, hence in the dehydration and metamorphic processes operating therein, may strongly influence the compositions and amounts of fluids released as well as the probability that slab melting may occur beneath specific volcanic arcs or segments thereof [cf. *Moran et al*., 1992; *Konrad-Schmolke and Halama*, 2014]. Such factors certainly influence the spatial distribution and nature of slab contributions to arc magmatism. For example, *Tonarini et al*. [2011] stress that thermal

conditions in subducting slabs result in a strong dehydration gradient along the upper boundary of the slab compared to its interior. Thus, it is likely that slab-derived fluid contributions are initially dominated by the uppermost parts of the slab (sediments, variably altered oceanic crust, subduction mélange, etc.). But, with increasing depth of subduction, interior parts of the slab (serpentinized oceanic mantle) become warmer and may contribute an increasing proportion of the overall fluid flux [*Straub and Layne*, 2002; *Tonarini et al*., 2011; *Walowski et al*., 2015].

Understanding the linkages between tectonic and physical controls on B systematics in arc lavas may provide useful insights into subduction processes in general. Thus, we undertook a B isotope investigation of volcanic rocks from the well-characterized Tonga-Kermadec-New Zealand (TKNZ) arc. These arc lavas encompass a transition from the highly incompatible element-depleted, fluid-rich Tonga sector to the progressively more sediment-dominated Kermadec and New Zealand sectors. Moreover, dramatic along-strike variation in subduction rate corresponds to significant differences in subduction zone (SZ) thermal structure [cf. *Syracuse et al*., 2010]. This, in turn, may lead to spatially distinct histories of (a) slab metamorphism and dehydration, (b) metasomatism of arc magma sources, and (c) magma generation. Our focus on B geochemistry provides unique perspectives on these processes.

2. Background and Previous Work

The Tonga-Kermadec-New Zealand (TKNZ) arc formed in response to subduction of the Pacific plate beneath the Australian plate, and extends ~2500 km northward from New Zealand (Figure 1). Convergence rates reach a global maximum (~24 cm/yr) in the north of Tonga and decrease southward by roughly fourfold approaching New Zealand [*Bevis et al*., 1995; *Zellmer and Taylor*, 2001]. Because slab thermal structure is proportional to convergence rates, it is predicted that slab temperatures decrease northward from New Zealand, and may presently be the coolest beneath northern Tonga [*Wiens and Gilbert*, 1996; *Wiens*, 2001]. We also call attention to the fact that the Valu Fa Spreading Center (VFSC) impinges the back-arc side of the Tonga arc near the island of Ata, and incipient back-arc spreading is also recognized near Fonualei [*Zellmer and Taylor*, 2001; *Keller et al*., 2008; *Escrig et al*., 2012; see these references for details]. Such areas are of particular note because they correspond to regions of anomalously warm upwelling mantle proximal to the subducting plate. In these regions, the mantle wedge and possibly portions of the downgoing slab could be warmer and more strongly dehydrated compared to adjacent "normal" arc sectors [*Harmon and Blackman*, 2010; *Dunn and Martinez*, 2011; *Wei et al*., 2015]. It is also apparent that mantle sources for back-arc lavas in these regions and in the eastern Lau Basin have been variably modified by inputs of fluids or melts from the TKNZ subduction zone [e.g., *Escrig et al*., 2009, 2012; *Wei et al*., 2015]. Chemical and thermal exchange beneath the TKNZ arc and back-arc regions may be further complicated by arc-parallel convection [e.g., *Turner and Hawkesworth*, 1998; *Smith et al*., 2001; *Conder and Wiens*, 2007; *Menke et al*., 2015].

As one relatively direct means of unravelling such complexities, the lavas erupted along the arc have been studied in detail. These rocks largely comprise basalt to basaltic andesite, but include compositions as evolved as dacite and rhyolite. It is inferred that the mafic primitive melts are derived from a mantle wedge that becomes increasingly depleted in conservative incompatible elements (those not replenished by slab contributions; cf. *Pearce and Peate* [1995] and *Pearce et al*. [2005]) toward the north as a consequence of extensive back-arc melt extraction associated with formation of the Lau Basin and its counterparts to the south [*Ewart and Hawkesworth*, 1987; *Gamble et al*., 1993a, 1993b; *Ewart et al*., 1998; *Smith and Price*, 2006; *Caulfield et al*., 2008]. In this region, the melt-depleted nature of the wedge renders it to be highly sensitive to fluid or melt contributions from the subducting plate. Crustal structure also varies from essentially oceanic beneath Tonga-Kermadec to continental beneath New Zealand, and this difference (as well as the nature of underlying lithospheric mantle) also may influence magmatic compositions.

The incoming sediment sequence on the Pacific plate is relatively thin (ca. 70 m) near the Tongan sector, but thickens southwards along the Kermadec arc due to increased deposition of terrigenous turbidites approaching New Zealand [*Burns et al*., 1973; *Gamble et al*., 1996; *Macpherson et al*., 1998; *Timm et al*., 2014]. Sediment sequences outboard the Tongan trench (Figure 1) at DSDP/ODP Sites 596 (pelagic sediments) and 204 (pelagic and volcaniclastic sediments proximal to the Louisville Seamount Chain; "LSC") have been discussed by *Turner et al*. [1997] and *Ewart et al*. [1998]. Based on U-Th isotope constraints, *Turner et al*. [1997] suggest that the minimum transfer time for any Louisville-derived sediment component beneath the

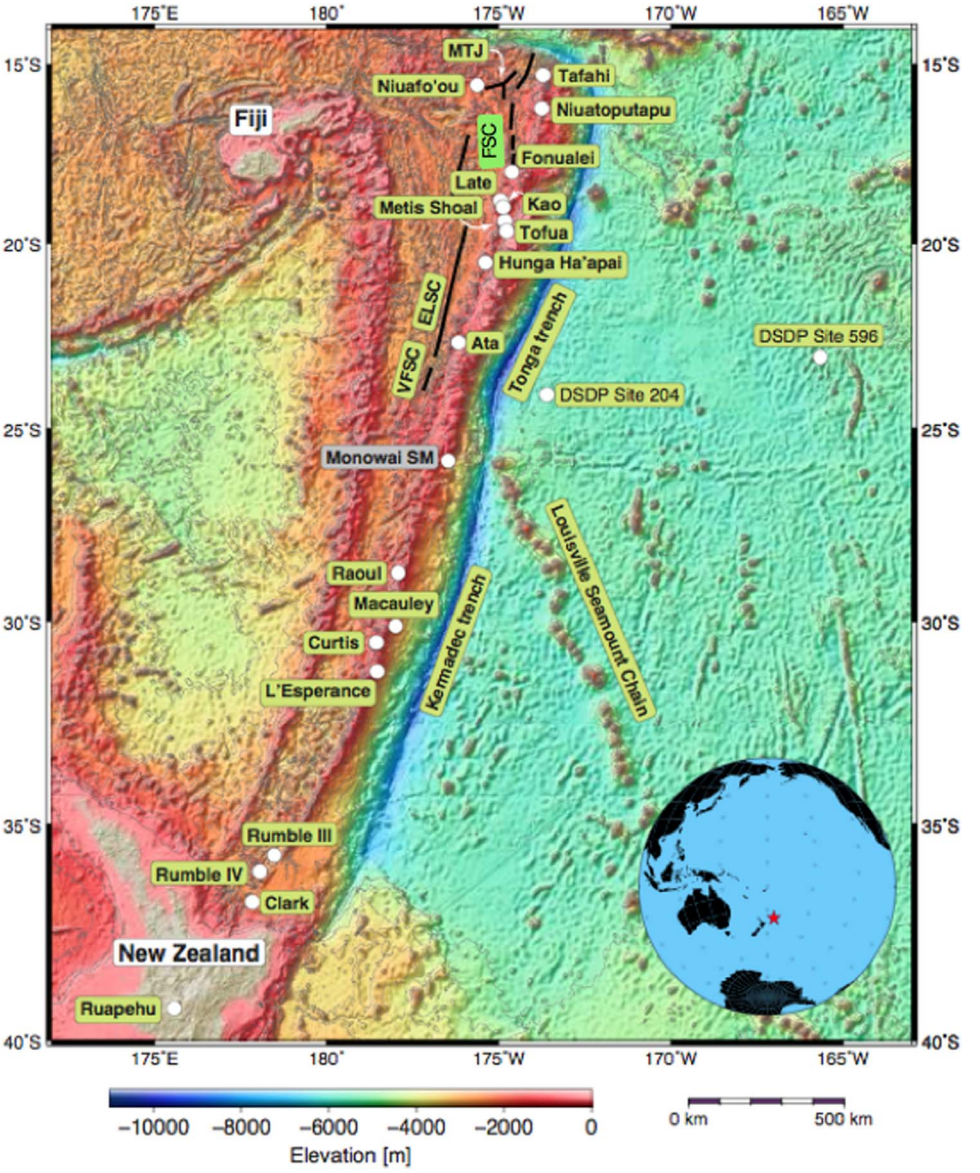

Figure 1. Regional setting for the Tonga-Kermadec-New Zealand arc, showing key geographic and tectonic features. VFSC = Valu Fa Spreading Centre, ELSC = Eastern Lau Spreading Centre, FSC = Fonualei Spreading Centre, MTJ = Mangatolo Triple Junction. White circles indicate localities from which samples are analyzed in this study, excepting Monowai (highlighted in gray box) for which literature data are utilized. Map was produced using GMT software [*Ryan et al*., 2009].

arc is ~350 ka [cf. *Regelous et al*., 1997, 2010]. Though poorly constrained, the maximum sediment transfer time may be on the order of a few Ma based on geometric observations in Tonga, wherein the Louisville volcaniclastic signature can be recognised in lavas erupted 2–4 Ma after the locus of subduction of the LSC had swept further southward along the arc [*Turner and Hawkesworth*, 1997]. *George et al*. [2005] used ^{10}Be isotopic data to further evaluate this scenario, and suggested from Be-Li-Th relationships that an inferred sediment component in TKNZ lavas could have been added as a partial melt formed at ~2 GPa and ≥800°C. However, this result is puzzling in light of the predicted cool slab conditions as modeled by *Syracuse et al*. [2010], and corroborated by estimates based on H_2O/Ce ratios [cf. *Caulfield et al*., 2012a; *Cooper et al*., 2012]. The thermal models of *Syracuse et al*. [2010] suggest that beneath Tonga, slab surface temperatures are likely below experimentally determined water-saturated sediment solidi (Figure 2a). Moreover, a steep thermal gradient is predicted within the uppermost slab such that Moho and subjacent mantle temperatures are less than 200°C at subarc depths. Under such conditions melting is precluded within the slab and hydrous phases (many B-bearing) remain stable throughout broad portions of the slab. In contrast, slab

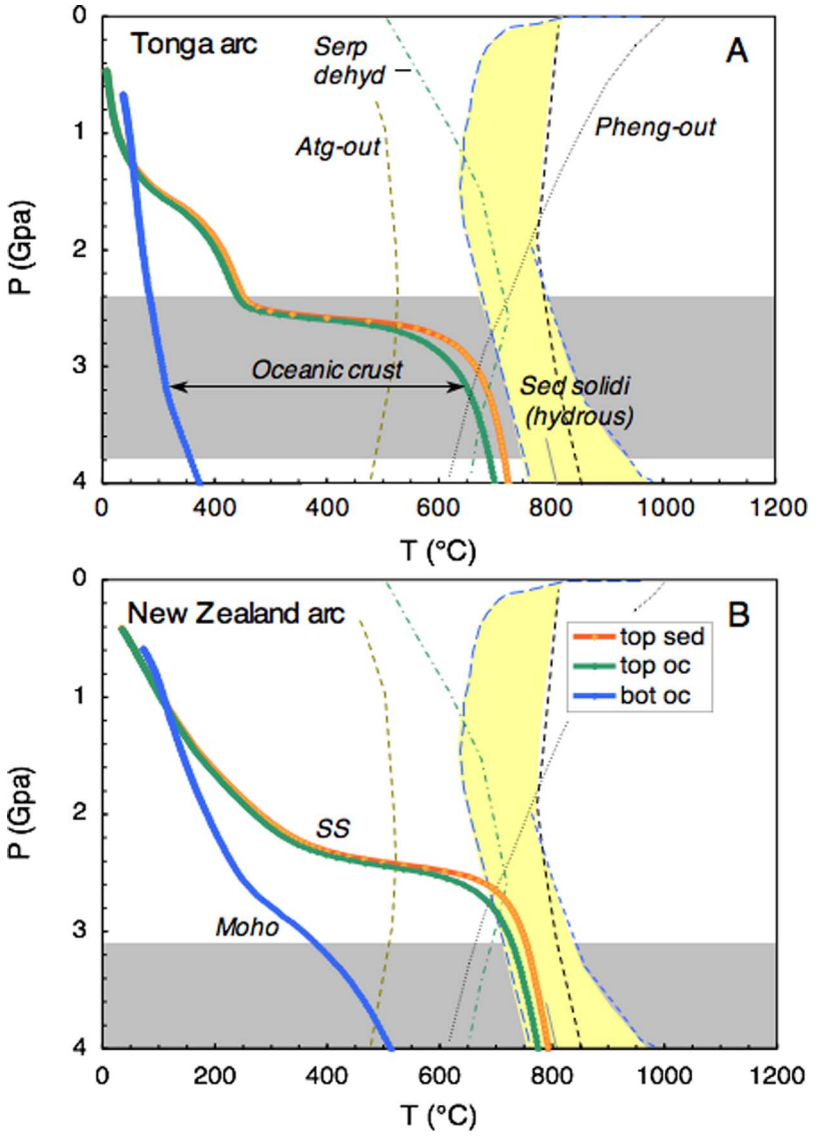

Figure 2. Pressure-Temperature sections for (a) Tonga and (b) New Zealand arc segments. P-T profiles are shown for the slab surface (red), base of the sedimentary column (black), and oceanic Moho (blue) as predicted by "D80" models of *Syracuse et al*. [2010]. Gray-shaded bands correspond to pressure ranges beneath the volcanic arc based on depths to the subducting slab from *Hayes et al*. [2014]. Yellow shaded band outlines loci of water-saturated solidi for representative sediments as compiled by *Hermann and Spandler* [2008]. Curves are also plotted for key reactions that control water release and/or destabilization of important B-host minerals: (1) "phengite-out" in metasediments, (2) "antigorite-out" in serpentinites, and (3) serpentine dehydration [cf. *Hermann and Spandler*, 2008]. The breakdown of phengite in sedimentary compositions and of antigorite in serpentinites dramatically lowers solid/fluid partition coefficients for B in these materials and facilitates its removal from the subducting slab in dehydration fluids [*Marschall et al*., 2006; *Padrón-Navarta et al*., 2013].

surface temperatures are predicted to increase southward and for Kermadec and New Zealand (Figure 2b) overlap some sediment solidi estimates. Although the slab is predicted to be warmer beneath these sectors of the arc, expected Moho temperatures of 400–500°C still favor preservation of hydrous phases throughout the mantle and much of the oceanic crust sections of the slab. Because B is likely to be depleted from subducted materials due to progressive metamorphism [*Moran et al*., 1992; *Marschall et al*., 2009], complicated scenarios are required to account for the observed B-enrichments in TKNZ lavas (and their sources) if melting conditions are approached in the subducting slab.

Sr and Pb isotopic compositions are consistent with significant fluid-borne inputs of these elements from subducted, altered oceanic crust [e.g., *Turner et al*., 1997; *Ewart et al*., 1998; *Regelous et al*., 2010]. The latter authors estimate that as much as 40–90% of Pb in northern Tonga lavas could be derived from basaltic

crust of the subducting LSC, and exceeds that likely derived from the mantle wedge. Several groups also have assessed the magnitude of relative elemental contributions from subducted pelagic sediments to Tonga-Kermadec lavas using the more refractory Nd, Hf, and Be isotopes. Although estimates vary from study to study, there is consensus that slab contributions for these elements are very small and typically less than 1% in all but the southernmost sector of the arc [*Ewart and Hawkesworth*, 1987; *Turner et al*., 1997, 2009; *Ewart et al*., 1998; *George et al*., 2005; *Gamble et al*., 1996, 1997; *Regelous et al*., 2010; *Todd et al*., 2010, 2011; *Rooney and Deering*, 2014]. Together, these studies suggest that Tonga is a relatively cool end-member subduction zone wherein slab-derived fluids strongly leverage the composition of a mantle wedge that was previously depleted in incompatible elements (e.g., $B \ll 0.1$ ppm; cf. *Ryan et al*. [1996]) owing to presubduction melt extraction history. The nature and importance of sediment contributions remain matters of debate.

A notable feature of the Tonga arc is the observation of highly radiogenic $^{206}Pb/^{204}Pb$ in volcanics from the northernmost two islands (Tafahi and Niuatoputapu) that originally was inferred to be derived from the LSC [*Regelous et al*., 1997; *Turner et al*., 1997]. More recently, this feature has been ascribed to proximity to the Samoan (and perhaps other) plume(s) [*Wendt et al*., 1997; *Ewart et al*., 1998; *Falloon et al*., 2007; *Lytle et al*., 2012]. Still elevated but more muted $^{206}Pb/^{204}Pb$ signals have now been observed in arc lavas (e.g., Monowai) above the current site of intersection of the seamount chain with the arc just to the south of the island of Ata [*Timm et al*., 2011] as well as in lavas from the northern parts of the remnant Lau arc [*Hergt and Woodhead*, 2007]. Perhaps more importantly, *Regelous et al*. [2010] suggested that the Louisville seamount Pb must have been added after addition of pelagic sediment to the mantle wedge beneath Tafahi and Niuatoputapu. This development has reinvigorated discussions of the mechanism and timing of addition of the Louisville-like component—that is, it may have been stored for several Ma in the lithosphere that now lies beneath the northern arc, and is currently being added to the wedge beneath Monowai [*Timm et al*., 2013].

In general, fluid and sediment signatures tend to be inversely correlated in arc lavas and the TKNZ arc has been considered to have among the strongest "fluid signatures" known (e.g., with Ba/Th ratios ranging from 200 up to at least 1000; *Turner et al*. [1997]). U-series isotope data have been used to suggest that the fluid addition responsible for these signatures commenced about 50 ka ago [*Regelous et al*., 1997; *Turner et al*., 1997] and continued essentially to the present. In contrast, observed ^{226}Ra-disequilibrium in the youngest lavas implies very rapid melt formation and ascent rates (on the order of millennia; *Turner et al*. [2000]). The incompatible element inventory of the fluid component relative to total concentrations in the erupted products was estimated by mass balance by *Turner et al*. [1997].

In the only previous study of boron isotopes in the TKNZ arc, *Clift et al*. [2001] reported SIMS (ion probe) data for arc lavas from eight volcanoes and for glass shards from fore-arc sediments from ODP Hole 840. These authors suggested that high $\delta^{11}B$ values in Tongan lavas reflect a strong seawater fluid signature; in contrast, lower $\delta^{11}B$ values in Kermadec lavas were attributed to a greater influence of terrigenous sediment from New Zealand. However, it should be noted that these data are extremely varied and unsystematic ($\delta^{11}B = -11.6$ to $+37.5‰$, with differences of up to $18‰$ for replicates of single samples!), and therefore must be considered highly suspect. The present investigation was undertaken to clarify the B systematics in this arc.

3. Analytical Techniques

The samples analyzed include representative lavas from the studies of *Ewart and Hawkesworth* [1987], *Graham and Hackett* [1987], *Gamble et al*. [1993a], and *Turner et al*. [1997], and sediments previously described by *Turner et al*. [1997] and *Plank and Langmuir* [1998]. Data are presented for standards in Table 1 and for all analyzed samples in Table 2. B concentrations initially were determined by prompt-gamma neutron activation (PGNA) with precision and accuracy typically better than 10–15% at the levels in most samples [*Leeman*, 1988]. Because some B concentrations reported by *George et al*. [2005] differ considerably from our PGNA data, most samples used for B isotopic work were reanalyzed for B content at Rice University by inductively coupled plasma-atomic emission spectroscopy (ICP-AES) using a Varian Vista spectrometer; repeat analysis was not possible in a few cases owing to insufficient sample powder. Samples were subjected to HF-HCl digestion in the presence of mannitol and with closed Teflon vials to avoid B volatilization.

AGU Geochemistry, Geophysics, Geosystems
10.1002/2016GC006523

Table 1. Reference Samples Analyzed

Analyses at:	Rice University (Analyst = Leeman)								C.N.R. (Tonarini)	
Standard:	JA-2	JB-2	JA-3	JB-3	JR-1	B-5	MAG-1	BHVO-1	RGM-1	JB-2
Element:	B	B	B	B	B	B	B	B	B	B
RV	21.1 ± 1.9	29.98 ± 0.74	26.5 ± 0.6	20.7 ± 0.3	132 ± 1	10.1 ± 1.2	136 ± 5	3.0 ± 0.3	27.4 ± 2.8	29.98 ± 0.74
This Study (B by AES):									*(ID)*	*(ID)*
Avg.	**20.9**	**29.6**	**24.3**	**18.6**	**124.1**	**10.0**	**142**		**27.2**	**28.5**
SD	2.1	1.7	1.1	1.8	3.6	1.5	4.1		0.4	0.5
%CV	10.0	5.7	4.5	9.7	2.9	15.0	2.9		1.5	1.6
n	17	29	14	22	15	22	3		1	4
This Study (B by PGNA; McMaster Univ.):										
Avg.	**19.9**	**28.5**	**22.9**	**18.0**	**132**		**134**	**2.5**	**27.8**	
s.d.	0.6	1.8	0.9	0.8	2.8		8.3	0.6	2.1	
%CV	3.0	6.3	3.9	4.4	2.1		6.2	24.0	7.6	
n	3	3	5	3	2		31	39	34	
Analyses at:	Boston University [*Davidson et al.*, 2013] (T. Plank, personal communication, 2017)									
Standard:					JA-2					
Element:	Zr	Nb	Y	La	Yb	Th	Ba	Be	Hf	U
RV	108.5 ± 2.6	9.3 ± 0.24	15.6 ± 0.17	15.46 ± 0.4	1.65 ± 0.04	4.8 ± 0.11	308.4 ± 5.1	2.26 ± 0.19	2.84 ± 0.06	2.18 ± 0.06
Analyzed With Samples From This Study:										
	109.9	**9.54**	**16.7**	**14.46**	**1.53**	**4.68**	**313.3**	**2.50**	**2.69**	**2.13**
SD	0.7	0.25	0.3	0.47	0.04	0.01	5.7	0.06	0.07	0.001
%CV	0.64	2.6	1.8	3.2	2.6	0.17	1.8	2.5	2.8	0.03
n	2	2	2	2	2	2	2	2	2	2
Standard:					*BIR-1*					
Element:	Zr	Nb	Y	La	Yb	Th	Ba	Be	Hf	U
RV	14.8 ± 0.22	0.553 ± 0.014	15.6 ± 0.17	0.627 ± 0.012	1.631 ± 0.015	0.0328 ± 0.0015	6.75 ± 0.13	0.102 ± 0.011	0.582 ± 0.009	0.0105 ± 0.0004
Analyzed With Samples From This Study:										
	15.6	**0.575**	**15.9**	**0.651**	**1.63**	**0.032**	**6.71**	**0.116**	**0.624**	**0.0105**
SD	0.6	0.006	0.3	0.027	0.07	0.002	0.17	0.046	0.009	0.0004
%CV	3.7	1.1	2.2	4.2	4.0	6.9	2.6	39.7[a]	1.4	4.1
n	3	3	3	3	3	3	3	3	3	3

Recommended values (RV) for BIR-1, JA-2, JB-2, BHVO-1, and RGM-1 are from GEOREM website *Jochum et al.* [2005].
RVs for B in JA-3, JB-3, and JR-1 are from *Nagaishi and Nakamura* [2009].
RV for B in B-5 is from *Gonfiantini et al.* [2003].
RV for B in MAG-1 is from *Govindaraju* [1994].
Note: "*n*" = number of independent replicate analyses by each method for each standard.
[a]Replicate reproducibility for Be is considerably better at the higher concentrations observed in TKNZ samples (ca. ±20% above 0.2 ppm and better than ±10% above 0.4 ppm (Plank, personal communication, 2017).

Table 2. Boron Isotopic and Selected Trace Element Data for TKNZ Lavas and Local Sediments

Locality	Sample	S Lat. (°)	E Long. (°)	SiO_2 (%)	TiO_2 (%)	B ppm[a]	Zr ppm	Nb ppm	Yb ppm	Be ppm	Th ppm	U ppm	$^{11}B/^{10}B \pm 2s$	$\delta^{11}B \pm 2s$
Back-Arc Region (W of Tonga)														
Niuafo'ou (back-arc, BA)	31461	15.60	175.65	50.0	1.345	4.6	92.6	3.251	3.06	0.525	**0.256**	**0.080**	4.0408 ± 18	−0.7 ± 0.4
Replicate $\delta^{11}B$													4.0420 ± 18	−0.4 ± 0.4
Average $\delta^{11}B$														*−0.6 ± 0.3*
Niuafo'ou (back-arc, BA)	N110	15.60	175.65	50.7	1.704	***2.7***	102	3.96	3.46	0.505	0.363	0.127	nd	nd
Tonga Islands														
Tafahi (Taf)	TAF45/7	15.87	173.92	53.1	0.470	12.2	16.3	0.530	1.160	0.229	**0.107**	**0.072**	4.0825 ± 19	9.6 ± 0.5
Niuatoputapu (NTT)	NTT29/3	15.95	173.97	60.5	0.533	12.4	36.5	1.625	2.148	0.512	**0.390**	**0.168**	4.0676 ± 12	5.9 ± 0.3
Fonualei (Fon)	Fon-31	17.70	174.33	60.8	0.665	22.6	52.1	0.898	2.649	0.729	**0.321**	**0.307**	4.0668 ± 23	5.7 ± 0.6
						26								
Fonualei (Fon)	Fon-39	17.70	174.33	65.5	0.601	27.7	46.7	0.934	2.407	0.707	**0.487**	**0.472**	4.0715 ± 4	6.9 ± 0.1
						25								
Late	Late-7	18.82	174.67	53.4	0.502	10.7	21.2	0.217	1.373	0.222	**0.136**	**0.111**	4.0791 ± 15	8.8 ± 0.4
						14								
Kao	T103c	19.05	175.02	54.1	0.792	20.0	38.9	0.38	1.89	0.300	**0.188**	**0.140**	4.0719 ± 15	7.0 ± 0.4
Metis Shoal (MS)	11108	19.18	174.86	64.5	0.392	48.4	43.3	1.082	1.890	0.270	**0.308**	**0.230**	4.0763 ± 24	8.1 ± 0.6
Tofua (Tof)	26835	19.75	175.08	54.1	0.494	13.6	21.4	0.191	1.420	0.202	**0.128**	**0.109**	4.0732 ± 14	7.3 ± 0.3
Tofua (Tof)	26907	19.75	175.08	54.4	0.544	13.3	25.2	0.223	1.648	0.251	**0.130**	**0.118**	4.0725 ± 18	7.1 ± 0.4
Hunga Ha'apai (HH)	HH BTM	20.55	175.42	54.6	0.491	17.6	23.0	0.220	1.416	0.208	**0.121**	**0.116**	4.0882 ± 19	11.0 ± 0.5*[b]
Leach residue	HH BTM												4.0826 ± 17	9.6 ± 0.4
Hunga Ha'apai (HH)	HH TOP	20.55	175.42	56.0	0.607	23.9	25.8	0.363	1.724	0.232	**0.164**	**0.133**	4.1059 ± 15	15.4 ± 0.4*
Replicate $\delta^{11}B$						*25*							4.1043 ± 22	15.0 ± 0.5*
Average $\delta^{11}B$														*15.2 ± 0.4**
Valu Fa sector														
Valu Fa Spreading Center (VF)	D2-05	22.33	176.66	55.8	1.773	9.8	71.4	2.217	3.4	0.576	**0.352**	**0.159**	4.0639 ± 19	5.0 ± 0.5
Ata	482-8-1	22.33	176.20	52.0	0.631	21.1	31.1	0.451	1.480	0.322	**0.365**	**0.171**	4.0281 ± 14	−3.8 ± 0.3
Ata	482-8-3	22.33	176.20	52.8	0.804	29.0	39.9	0.48[c]	1.894	0.352	**0.417**	**0.189**	4.0225 ± 7	−5.2 ± 0.2
								[1.427]						
Kermadec Islands and seamounts														
Raoul (R)	T5	29.25	177.87	56.9	0.977	16.7	53.4	0.553	2.809	0.431	**0.439**	**0.175**	4.0680 ± 28	6.0 ± 0.7
Raoul (R)	7125	29.25	177.87	50.3	0.730	*10*	26.3	0.303	1.438	0.207	**0.197**	**0.075**	4.0636 ± 20	4.9 ± 0.5
Replicate $\delta^{11}B$													4.0626 ± 61	4.7 ± 1.5
Average $\delta^{11}B$														*4.8 ± 0.2*
Raoul (R)	23386	29.25	177.87	56.5	0.714	10.5	29.2	0.30	2.59	0.220	0.191	0.076	4.0631 ± 4	4.8 ± 0.1
Macauley (Mac)	45658	30.22	178.55	48.9	0.658	8.2	30.0	0.440	1.241	0.344	**0.467**	**0.169**	4.0509 ± 16	1.8 ± 0.4
Replicate $\delta^{11}B$													4.0487 ± 18	1.3 ± 0.4
Average $\delta^{11}B$														*1.5 ± 0.5*
Macauley (Mac)	10380	30.22	178.55	49.3	0.901	*14*	38.4	0.57	1.62	0.360	0.581	0.180	4.0632 ± 17	4.8 ± 0.4
Curtis SM (C)	14849	30.58	178.60	66.3	0.761	20.1	68.6	0.66	2.78	0.450	**0.855**	**0.652**	4.0662 ± 17	5.6 ± 0.4
Replicate $\delta^{11}B$													4.0684 ± 10	6.1 ± 0.2
Average $\delta^{11}B$														*5.9 ± 0.4*
L'Esperance (Esp)	14831	31.43	178.90	53.3	1.064	19.8	44.7	0.489	2.353	0.417	**0.577**	**0.165**	4.0720 ± 21	7.0 ± 0.5
						24								
Southern Seamounts														
Rumble III SM (RS3)	AU36986	35.75	−178.48	52.6	0.722	10.4	*48*	*0.5*	2.67		**0.416**	**0.176**	4.0891 ± 36	11.2 ± 0.9*
Replicate $\delta^{11}B$						*10*							4.0909 ± 20	11.7 ± 0.5*
Average $\delta^{11}B$														*11.5 ± 0.4**
Leach residue	AU36986												4.0670 ± 19	5.8 ± 0.5
Rumble IV SM (RS4)	X168/1A	36.26	−178.00	52.8	0.833	15.7	59.6	1.562	2.057	0.436	**0.669**	**0.223**	4.0598 ± 13	4.0 ± 0.3
Replicate $\delta^{11}B$													4.0581 ± 14	3.6 ± 0.3
Average $\delta^{11}B$														*3.8 ± 0.4*
Clark submarine volcano	X451a	36.45	−177.84	50.5	0.622	4.7	91.1	2.136	1.537	1.234	**1.391**	**0.555**	nd	nd
New Zealand														
Atiamuri (NZ)	PK-1	38.38	−176.00	51.2	1.292	*5.7*	*103*	*3.5*	2.32		1.54	0.28	4.0207 ± 17	−5.7 ± 0.4

AGU Geochemistry, Geophysics, Geosystems

10.1002/2016GC006523

Table 2. (continued)

Locality	Sample	S Lat. (°)	E Long. (°)	SiO_2 (%)	TiO_2 (%)	B ppm[a]	Zr ppm	Nb ppm	Yb ppm	Be ppm	Th ppm	U ppm	$^{11}B/^{10}B \pm 2s$	$\delta^{11}B \pm 2s$
Replicate $\delta^{11}B$													4.0177 ± 19	−6.4 ± 0.5
Average $\delta^{11}B$														*−6.0 ± 0.7*
Ongaroto (NZ)	BH-3	38.39	−175.94	51.3	1.090	*3.2*	*108*	*4.2*	2.18		1.01	0.08	4.0296 ± 18	−3.5 ± 0.4
Replicate $\delta^{11}B$													4.0299 ± 20	−3.4 ± 0.5
Replicate $\delta^{11}B$													4.0291 ± 16	−3.6 ± 0.4
Average $\delta^{11}B$														*−3.5 ± 0.2*
Additional Samples Analyzed for B Content Only														
Havre Trough	PPTUW/5	33.54	−178.75	51.2	1.523	*8.7*	126	1.71	2.9		0.167	0.062	nd	nd
Kakuki, NZ	BH-4	38.48	−176.17	49.1	0.907	*1.9*	*79*	*3*	1.60		0.51	0.10	nd	nd
Tarawara, NZ	C-675	38.27	−176.52	51.4	0.848	*4.0*	*82*	*2*	1.87		1.64		nd	nd
Waimerino, NZ	WB	39.10	−175.00	52.9	0.484	*6.5*	*47*	*1.5*	1.44		1.93		nd	nd
Mangawhero, NZ	L1015A	39.25	−175.57	52.8	0.662	*6.1*	57	1.77	1.55		1.18	0.33	nd	nd
Ruapehu, NZ	E7	39.28	−175.57	54.2	0.706	*8.0*	*68*	*3*					nd	nd
Ruapehu, NZ	A8	39.28	−175.57	56.6	0.665	*9.2*	*61*						nd	nd
Ruapehu, NZ	H7A	39.28	−175.57	56.8	0.725	*26*	*114*	*3*					nd	nd
Whakapapa, NZ	D2	39.28	−175.57	57.2	0.715	*19*	*94*						nd	nd
Ruapehu, NZ	M11	39.28	−175.57	57.5	0.675	*21*	*102*	*4*					nd	nd
Ruapehu, NZ	M9	39.28	−175.57	59.1	0.644	*24*	*124*	*4*					nd	nd
Ruapehu, NZ	B2	39.28	−175.57	59.2	0.674	*19*	*130*						nd	nd
Ruapehu, NZ	N7	39.28	−175.57	64.3	0.794	*44*	*209*	*8*					nd	nd
Ruapehu, NZ	N112A	39.28	−175.57	66.9	0.633	*48*	*180*	*5*					nd	nd
Sediments From DSDP Hole 596														
Yellow brown clay (1.1 mbsf)	T1/596-1,1	23.85	165.65	56.8	0.904	**107.1**	93.7	10.68	3.27	2.373	9.00	1.78	4.0540 ± 18	2.6 ± 0.4
Replicate $\delta^{11}B$						105.5							4.0543 ± 18	2.6 ± 0.4
Average $\delta^{11}B$														*2.6 ± 0.1*
Medium brown clay (5.5)	T2/596-1,cc	23.85	165.65	53.9	1.015	**95.4**	136.2	8.34	7.81	1.755	6.35	1.83	4.0517 ± 15	2.0 ± 0.4
Dark brown clay (13.7)	T3/596-2,6	23.85	165.65	48.9	0.773	118.5	201.2	16.10	38.99	2.164	24.48	4.07	4.0568 ± 18	3.3 ± 0.4
						119.8								
Dark brown clay (22.1)	T4/596-3,5	23.85	165.65	56.6	0.677	150.6	177.9	16.11	15.37	2.295	10.63	1.48	4.0503 ± 12	1.7 ± 0.3
Dark brown clay/chert 36.9)	T5/596-5,2	23.85	165.65	56.9	0.479	138.3	204.6	7.97	17.03	2.083	4.01	1.66	4.0383 ± 13	−1.3 ± 0.3
Yellow brown porcellanite (38.0)	T6/596-5,cc	23.85	165.65	91.8	0.111	**46.0**	43.8	1.71	2.64	0.598	0.71	1.14	4.0424 ± 12	−0.3 ± 0.3
						44.4								
Dark yellow clay (46.8)	T7/596-6,5	23.85	165.65	66.4	0.337	122.4	133.0	6.63	12.13	1.543	3.03	1.40	4.0360 ± 14	−1.9 ± 0.3
Yellow brown chert (50.6)	T8/596-7,cc	23.85	165.65	92.4	0.105	**49.1**	43.0	1.76	2.86	0.510	0.80	1.27	4.0340 ± 12	−2.4 ± 0.3
						47.9								
Dark brown clay (66.7)	T9/596A-1,1	23.85	165.65	43.0	0.224	**91.0**	150.7	5.32	16.25	4.084	2.21	2.87	4.0404 ± 18	−0.8 ± 0.4
						87.6								
Black clay (73.0)	T10/596-1,5	23.85	165.65	12.4	0.256	282.4	146.6	3.06	17.14	2.192	0.83	4.76	4.0513 ± 12	1.9 ± 0.3
Replicate $\delta^{11}B$													4.0523 ± 12	2.1 ± 0.3
Average $\delta^{11}B$														*2.0 ± 0.2*
Sediments From DSDP Hole 204														
Volcaniclastite (92-93)	204-7-1	24.95	174.11	44.7	2.263	50.8	278	37.1	1.65		1.37	0.58	4.0713 ± 11	6.8 ± 0.3
Pelagic clay (140-141)	204-4-4	24.95	174.11	47.5	4.242	145.1	137	16.1	1.98		2.95	1.40	4.0663 ± 13	5.6 ± 0.3
Metasedimentary Basement, North Island, NZ														
Torlesse graywacke	MY					*57*							nd	nd
Torlesse graywacke	N112E					*46*							nd	nd
Torlesse [*Price et al.*, 2015]; B = average of samples above	Avg. of 9			69.3	0.59	*51.5*	199	11.9	2.7		14.2	3.1	nd	nd

[a]Boron contents reported are via ICP-AES (Rice Univ.), ID (bold values) or *PGNA* (*italicized values*) on different aliquots; analyses by multiple methods are listed where available.

[b]B isotopic data for unleached samples denoted by "*" are likely affected by seawater contamination, and ignored in the data analysis.

[c]Nb for Ata sample 482-8-3 is reported as average of five other Ata samples (SD = 0.06 ppm) reported by *Davidson et al.* [2013]; the actual analysis is an outlier (reported below).

Nb, Zr, Yb, and Be data are from sources as indicated below:

XRF: *Italic* font [*Graham and Hackett*, 1987; *Ewart and Hawkesworth*, 1987; *Gamble et al.*, 1993].

ICPMS: black font [*Plank and Langmuir*, 1998; *George et al.*, 2005; *Davidson et al.*, 2013].

ICPMS: bold blue font [*Gamble et al.*, 1996; *Ewart et al.*, 1998; *Regelous et al.*, 2008; *Price et al.*, 2012].

ID: U and Th data, bold black font [*Turner et al.*, 1997, 2000].

INAA: bold green font [*Gamble et al.*, 1993].

Geochemistry, Geophysics, Geosystems

10.1002/2016GC006523

Isothermal evaporations were carried out using aluminum heating blocks maintained at $T < 70°C$. The method of standard additions was applied to minimize solution matrix effects. Sample replicates and standard rock analyses indicate that long-term accuracy and precision are within about 10% relative at the B concentration levels encountered. Where PGNA data are available, agreement is typically within the precision of the respective methods. In addition, ICP-AES data agree well (within 4%) with isotope dilution determinations (see below) for Tonga sediments. The new B concentrations are considered to supersede all previously reported data for these samples. Methods of analysis are distinguished in Table 2.

Major element data used in this paper are from the references cited above; analyses are recalculated to total 100% with all iron as FeO*. Major element data and Sr-Nd-Pb and U-series isotopic data for the arc lavas are from *Ewart and Hawkesworth* [1987], *Gamble et al*. [1993a], and *Turner et al*. [1997, 2000] with suggested updates from *Hergt and Woodhead* [2007] where appropriate. Trace element data for most samples in this study are taken from *Davidson et al*. [2013], who report reproducibilities of better than 3% for Zr and Nb (and other elements; cf. Table 1) for the JA-2 reference standard; the latter data are internally consistent and supersede original analyses in *Turner et al*. [1997] that were compiled from several sources. It should be noted that unpublished data for the BIR-1 standard (cf. Table 1) confirm that roughly comparable accuracy and precision persist to concentration levels similar to those in the TKNZ samples. Trace element and radiogenic isotope analyses from other sources [*Gamble et al*., 1993; *Ewart et al*., 1998; *Regelous et al*., 2008; *Price et al*., 2012] are used for some of the samples studied. Data sources for each sample are indicated in Table 2. Major and trace element data for the analyzed sediments are from *Turner et al*., [1997], *Ewart et al*. [1998], and *George et al*. [2005] for DSDP Hole 204, and from *Plank and Langmuir* [1998] for ODP Hole 596. Concentration data reported in Table 2 are used in the figures presented in this paper.

Boron isotopic composition was determined by the dicesium borate method using a VG Isomass 54E positive thermal ionization mass spectrometer, following separation of boron by ion-exchange procedures as described by *Tonarini et al*. [1997]. Total procedural blanks (8–12 ng) are negligible relative to the amount of sample processed. Correction for isotopic fractionation associated with mass spectrometric analysis was made using a fractionation factor (including correction for ^{17}O contribution; cf. *Tonarini et al*. [1997]), calculated as $\{(R_{cert} + 0.00079)/R_{meas}\}$, relative to NIST SRM 951 ($R_{meas} = {}^{11}B/{}^{10}B_{meas} = 4.0498 \pm 0.0010$). An aliquot of this standard was processed identically with each batch of samples. Boron isotopic composition is reported in conventional delta notation ($\delta^{11}B$) as per mil (‰) deviation from the accepted composition of NIST SRM-951 ($R_{cert} = 4.04362$; *Catanzaro et al*. [1970]). Long-term reproducibility of isotopically homogeneous samples treated with alkaline fusion chemistry is approximately $\pm 0.5‰$ [*Tonarini et al*., 2003] and replicate analyses of all samples agree within this limit. Accuracy was evaluated independently via multiple analyses of GSJ-JB2 basalt reference standard, for which we obtained an average $\delta^{11}B$ of $7.13 \pm 0.19‰$ ($2\sigma_{mean}$; $n = 17$) during the course of this study. B contents in several sediment samples were determined via isotope dilution following separate fusions with K_2CO_3 and ion exchange purification; the spike solution was prepared from the NIST SRM-952 standard. Although repeat analyses of a given solution agree within 0.2%, replicate analyses of rock standards (JB2 and RGM1) indicate slightly worse reproducibility (within a few percent) attributed largely to addition of the spike solution to samples following the alkaline fusion step [*Tonarini et al*., 1997, 2003].

Also, because many samples were collected from sea cliffs or dredged, there was concern about contamination from seawater (4.6 ppm B, $\delta^{11}B = 40‰$). For example, a small degree of seawater interaction (water:rock < 5) with the Valu Fa dredged sample could produce its observed $\delta^{11}B$ ($+5.0‰$) from a rock having a composition in the range of MORB (ca. $\delta^{11}B = -5‰$ and B/Nb < 1). Thus, for a few samples showing conspicuously high $\delta^{11}B$, isotopic composition was remeasured following 30 min leaching in warm B-free water (this procedure was found to produce no significant isotopic fractionation; cf. *Tanaka and Nakamura* [2005]). In all cases, leach residues have somewhat lower $\delta^{11}B$ than the equivalent unleached powder. These data are considered to be more representative of the actual compositions, and are used in lieu of the unleached analyses (for the same samples) for all discussion in this paper; however, these data could represent *upper limit* values for $\delta^{11}B$. Unfortunately, there was insufficient sample to carry out more detailed leaching studies. Although anomalously high $\delta^{11}B$ in some cases possibly could reflect "seawater contamination", simple mixing calculations indicate that improbable amounts of contaminant are needed to account for observed discrepancies (e.g., >25% to raise $\delta^{11}B$ from $+10‰$

to +15‰ in sample HH TOP), and B content would be lowered instead of raised by this process. All isotopic data are reported in Table 2.

Before describing our results, we address and discard the data of *Clift et al*. [2001]. First, their replicate measurements for each of nine lavas exhibit large ranges in δ^{11}B (the ranges averaging almost 11‰!); such variability renders these data virtually uninterpretable. In two cases, direct comparison can be made with our data. For Fon-31, we measure 5.7‰ (they report a range of 11–18‰); our analysis of Fon-31 is supported by a measurement of 6.9‰ for sample Fon-39. For sample HH-Top we report replicate analyses of 15.0‰ and 15.4‰ (*Clift et al*. report a range of 11–28‰). As seen in Table 1, our replicates for all samples agree within the expected analytical precision. Regarding B contents, we also note large discrepancies in the SIMS data reported by *Clift et al*. [2001]. For a given sample, repeat measurements by ion probe typically range by a factor of two, and in some cases by more than an order of magnitude. For Fon-31, we measure 22.6 ppm (their range is 4.1–6.8 ppm) and for HH-Top we measure 23.9 ppm (their range is 2.0–4.3 ppm); independent PGNA data for different aliquots of these two samples (26 and 25 ppm, respectively) are similar to our ICP-AES data. Given the poor accuracy and precision of the *Clift et al*. data, they are given no further consideration in this paper.

Regarding B concentrations reported previously for Tonga-Kermadec samples by *George et al*. [2005], a few of these same samples were reanalyzed in our investigation. Where direct comparison can be made, the following is observed—Metis Shoal (11108): 53 versus our 48.4 ppm; Valu Fa (L2-5A = D2-05): 9.4 versus our 9.8 ppm; Ata (482-8-3): 12.1 versus our 29.0 ppm; Clark (X451a) 4.7 versus our 4.7 ppm. Different samples were analyzed for other locations, but in many cases the data of *George et al*. [2005] appear to be considerably higher than our results for comparable samples. *Keller et al*. [2008] also report B data for one Tofua sample (T02.4, 26.1 ppm B at 58% SiO_2) that is higher than values we have measured (13.3 and 13.6 ppm at ~54% SiO_2); in this case, the difference in B content may be related to differing degrees of magma evolution. For the sake of internal consistency, discussion of TKNZ samples is based primarily on our B data set. However, our results can be compared with B data for back-arc samples from the Fonualei Spreading Center (FSC) [*Keller et al*., 2008].

4. Results

For convenience of discussion, our data for the arc lavas are presented in the following sample groupings: (1) Tonga (or Tofua) arc (from north to south: Tafahi, Niuatoputapu, Fonualei, Late, Kao, Metis Shoal, Tofua, and Hunga Ha'apai); data for Ata, are distinguished for special consideration; (2) Kermadec islands and seamounts (Raoul, Macauley, Curtis, and L'Esperance); (3) Southern seamounts (Rumble III and IV, Clark); (4) New Zealand (Taupo Volcanic Zone, N. Island); (5) the back-arc (BA), as represented by the northernmost island, Niuafo'ou, and (6) the VFSC, represented by a single dredged sample. Previous studies have documented the existence of significant geochemical differences between these geographic areas, which is not surprising given their wide spatial distribution (Figure 1). Although our study clearly is of a reconnaissance nature, we attempt to relate the B geochemistry of these arc lavas to both tectonic and petrogenetic processes.

Finally, data for DSDP/ODP core samples outboard of the Tongan subduction zone provide some constraints on the nature of subducted sediments in this arc. The 70 m sedimentary section at site 596 east of the Tonga Trench is highly condensed representing deposition since Miocene time. Lithological units comprise (1) pelagic clay with zeolite (ash), (2) brown-black clay rich in Fe and Mn hydroxyoxides, (3) chert and porcellanite layers, and (4) hydrothermal sediments (containing up to 51.3% FeO). Pelagic clays are dominant and contain ca. 90–150 ppm B. The one Fe-rich hydrothermal sediment analyzed contained 282 ppm B, but such material is a minor component (lower 2 m of section). Two samples from the DSDP Hole 204 core were analyzed as a preliminary assessment of sediments proximal to the LSC. A pelagic clay contained 145 ppm B, and a volcaniclastic sand contained 51 ppm B. Boron isotopic compositions of the ODP Hole 596 sediments ranged narrowly (δ^{11}B: +3.3 to −2.4‰) and are slightly lower than for the DSDP Hole 204 samples (5.6–6.8‰). B contents were also determined for two metagraywackes of the Torlesse Fm., North Island, NZ; these contain an average of 51.5 ppm B (i.e., similar to observations of *Ellis and Sewell* [1963]). Together with ICPMS data for average Torlesse greywacke [*Price et al*., 2015], these results allow provisional estimates of B/Zr and B/Nb in the crustal basement proximal to the Taupo Volcanic Zone (TVZ). Because

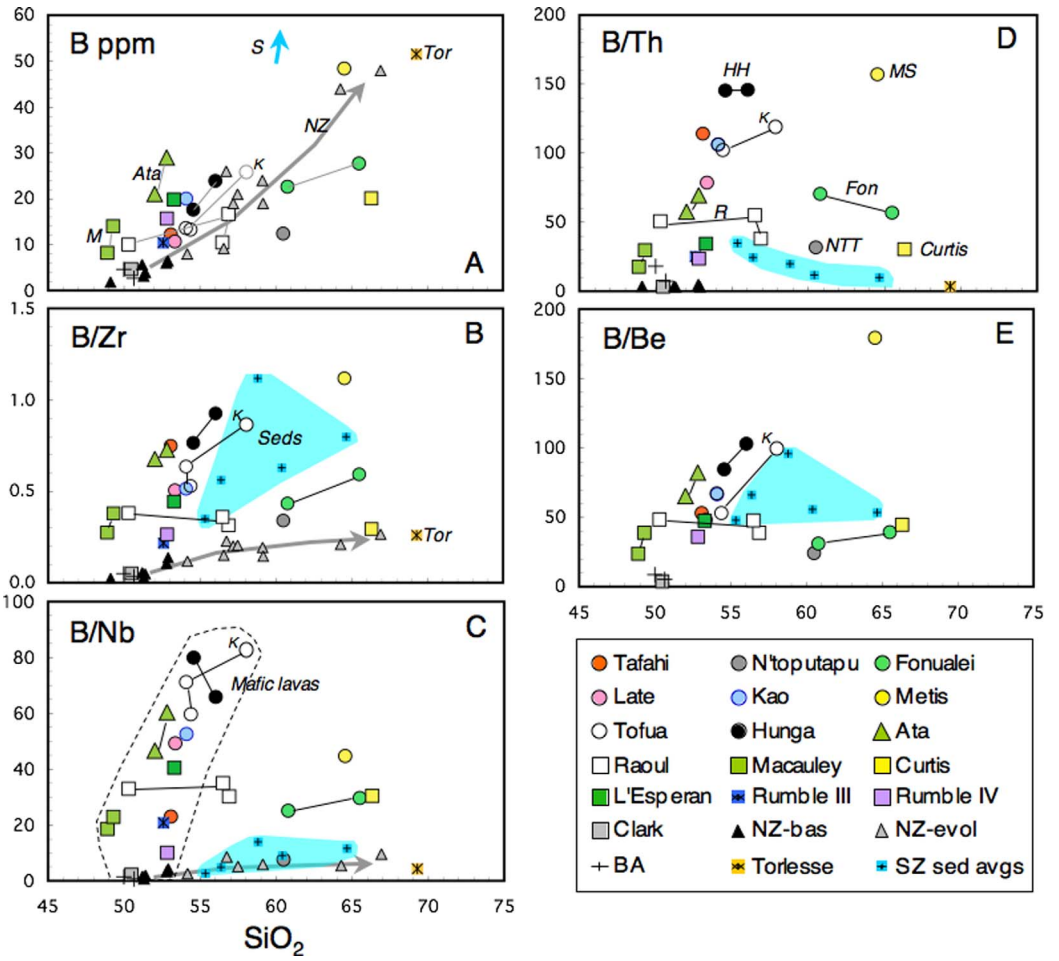

Figure 3. Plots showing the variation in B systematics with SiO_2. (a) B contents increase with differentiation in related lava suites but also show a large regional variation at similar SiO_2. (b) B enrichment (B/Zr) generally increases northwards along the arc but also within specific Tongan lava suites. In contrast, B/Zr varies modestly within some suites (e.g., Raoul Island and Ruapehu) as expected for closed system differentiation. (c) Similar variations for B/Nb ratios display clearer distinction between mafic lavas and more evolved ones. Ditto for B/Th (d) and B/Be (D). These diagrams show that overall B-enrichment can be reliably quantified using any of the ratios shown. Note: tie lines connect samples from the same geographic location. Different symbols for each locality are used throughout the paper where individual samples are plotted. Letters by sample points indicate location (see Table 2, first column); e.g., R = Raoul, M = Macauley. New Zealand data, mostly from Ruapehu and environs, are distinguished as basaltic (black triangles) versus evolved (gray triangles) compositions; gray arrows highlight evolution of these lavas. Small "K" denotes Tofua sample from *Keller et al.* [2008]. Note that all Tonga samples except Ata are shown as circles, whereas Kermadec samples are shown as squares. Fields ("Seds") indicate ranges for average compositions of local sediments (cf. supporting information Table S1); blue arrow ("S") points to "Sed" field that plots off-scale at higher B contents.

weighted average compositions of these sediments [cf. *Plank*, 2014; *Turner et al.*, 1997; *Price et al.*, 2015] are likely to be more representative of bulk subducted sediment packages, such estimates are reported in supporting information Table S1 and used in most diagrams in this paper.

4.1. Boron Variation With Magma Type and Other Factors

We first examine B systematics as a function of rock composition. B contents range from about 2 to 50 ppm, generally increasing with SiO_2 content (Figure 3), albeit with notable scatter. The wide range (2–30 ppm B) observed in basaltic ($\leq$53% SiO_2) lavas suggests that source composition exerts a dominant control. Ratios of B to nominally fluid-immobile elements (e.g., Zr, Nb, Th, Be) provide consistent measures of the relative B enrichment in the respective source domains. Here we base regional comparisons on B/Nb ratios even though, for most New Zealand samples studied, only less precise XRF Nb data are available. Considering the low and similar values of experimentally determined mineral-melt partition coefficients for B and Nb [*Brenan et al.*, 1995], B/Nb ratios are expected to change little during fractional crystallization ("FC") and to closely mimic source compositions during partial melting. Overall, these ratios exhibit wide variability (B/Nb ranges from ca. 1 to 80) and define systematic geographic patterns as discussed below.

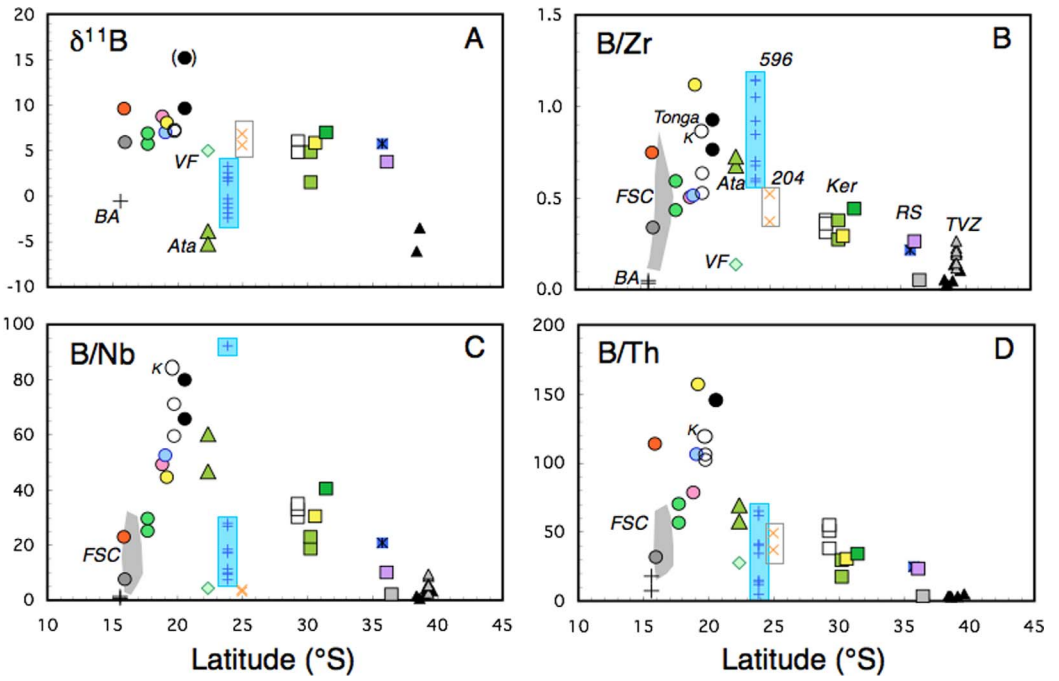

Figure 4. Variation in B systematics with latitude along the TKNZ arc. (a) δ^{11}B generally increases northward from New Zealand, with notable exceptions. Extremely high values (e.g., HH TOP, in parentheses) may reflect SW contamination. In contrast, δ^{11}B is conspicuously low in the far back-arc (Niuafo'ou), in New Zealand, and at Ata (proximal to the VFSC). (b) B/Zr, (c) B/Nb, and (d) B/Th elemental ratios generally increase northward from New Zealand as far as Ata, spike noticeably at Hunga Ha'apai, then decrease sharply toward the northernmost islands. The latter segment trends (esp. for B/Nb) are nearly linear, merge with the fields for lavas from the FSC (located in the proximal back-arc region) and terminate with the far back-arc lavas of Niuafo'ou. All arc samples are enriched in B relative to intraplate basalts (e.g., B/Nb = ~0.06); New Zealand and back-arc samples have ratios similar to intraplate basalts, and ratios for the one Valu Fa sample are slightly higher. Data for analyzed DSDP/ODP sediments are overlaid for comparison at appropriate latitudes. Symbols for arc lavas as in Figure 3.

It is difficult to assess fully the influence of local processes without detailed work at each volcano. However, our data for TVZ lavas (mostly Ruapehu basalt to dacite) define systematic trends that seem consistent with expected incompatible element behavior during FC and/or magma mixing (Figure 3). For example, the small increase in B/Nb (also B/Zr) with increasing SiO_2 in Ruapehu lavas is consistent with admixture of average Torlesse basement rocks to differentiates of local basaltic magmas [cf. *Graham and Hackett*, 1987; *Gamble et al*., 1999; *Price et al*., 2005, 2007, 2012]. This appears to be the case for other volcanic centers along the arc [e.g., Raoul: *Smith et al*., 2010; Fonualei: *Turner et al*., 2012; Tofua: *Caulfield et al*., 2012b; *Barker et al*., 2013]. However, increases in B/Nb (e.g., in samples from Fonualei, Ata, or Hunga Ha'apai) cannot generally be attributed to basement assimilation as B/Nb ratios for average local sediments (<15) and altered oceanic crust (ca. 20) are well below those of the arc lavas, and thus cannot explain the observed increases. Alternatively, variations in the arc lavas could reflect source heterogeneities established as a consequence of variable subduction inputs.

As noted earlier, B contamination from seawater is a distinct possibility, particularly for submarine samples. Although published isotopic and trace element data on the same powders provide little indication that this is a significant problem for other elements, several dredged samples do contain a leachable ^{10}Be component that is attributed to seawater contamination [*George et al*., 2005]. As discussed earlier, for some samples we find that mild leaching also removes a heavy B (i.e., high δ^{11}B) component that is likely to be seawater-derived. Nevertheless, most of the data define coherent variations that seem to reflect primary petrogenetic processes. For example, systematic variations in the slab-derived flux (i.e., net B inputs) versus the degree of prior incompatible element depletion in the mantle wedge could impart regional variation in apparent B-enrichment (see section 5).

A first-order observation is that B/Nb tends to increase northward from New Zealand (cf. Figure 4c). This trend is clearest among the basaltic rocks, whereas relatively evolved lavas from northerly Tonga islands (especially, Fonualei and Niuatoputapu) have lower ratios that presumably reflect the source compositions

for these magmas or their precursors. On the other hand, lavas from the Kermadec sector and the Rumble seamounts display little variation with SiO_2 and their B/Nb ratios are intermediate between most samples from Tonga and New Zealand. Finally, in the context of a possible Samoan plume influence in the northern part of the arc, we note that Samoan basalts have low B (4.2 ± 1.2 ppm) and B/Nb (0.067 ± 0.012) relative to Tonga-Kermadec lavas [*Workman et al*., 2006].

4.2. Geographic Variations in Boron Enrichment

Regional variations in B systematics are shown as a function of latitude (Figure 4). Again, a general northward increase in relative B-enrichment is evident as defined by B/Zr, B/Nb, and B/Th ratios, all of which define similar spatial variations. Taking B/Nb as an example, the volcanic front lavas define two conspicuous trends with peaks near Hunga Ha'apai ("HH" in plots). To the south, these ratios decrease in near-linear fashion to lows at New Zealand and the southernmost seamounts. To the north from Hunga Ha'apai, B/Nb ratios decrease systematically to the northernmost islands (Niuatoputapu and Tafahi; with no discernable break; this array merges with the trend for FSC lavas in the near back-arc region, and ends with the far back-arc lavas of Niuafo'ou. These remarkable patterns imply the existence of a discontinuity in the arc with distinct B systematics north and south of the area between Ata and Hunga Ha'apai (ca. latitude 21°S). The one sample from the VFSC is not strictly part of the arc, but its B/Nb, B/Th, and B/Zr ratios are intermediate between those of NMORB and the arc lavas, consistent with some subduction influence on its back-arc source [cf. *Kamenetsky et al*., 1997].

Regarding B isotopic composition, there is a general northward increase from New Zealand (δ^{11}B values from −6‰ to −3.5‰) to the Rumble seamounts (3.8–5.8‰), the Kermadec sector (4.8–7.0‰, with one low value of 1.5‰ at Macauley), and Tonga sector (5.7–9.6%, excluding the HH TOP outlier). Two samples from Ata have δ^{11}B values (−5.2‰ to −3.8‰) significantly below the general arc trend. Together with samples from New Zealand and the back-arc, these samples fall in the range reported for many oceanic island and mid-ocean ridge basalts [cf. *LeRoux et al*. 2004; *Tanaka and Nakamura*, 2005; *Brounce et al*., 2012; *Genske et al*., 2014], whereas data from Tonga are among the highest δ^{11}B values known from Pacific volcanic arc lavas. We consider it unlikely that the TKNZ values reflect contamination of ascending magmas by altered oceanic crust (i.e., in shallow magma chambers) upon which the volcanoes rest. Simple mixing calculations using average altered oceanic crust ("AOC"; 26 ppm B and $\delta^{11}B = 0.8$ ‰; *Staudigel et al*. [1996]) cannot significantly elevate δ^{11}B; and even considering maximal δ^{11}B (+24‰) measured in oceanic crustal rocks [e.g., *Ishikawa and Nakamura*, 1992; *Smith et al*., 1995; *Yamaoka et al*., 2012], assimilation of >25% of such material is required to raise magmatic δ^{11}B as much as 5‰ (using Hunga Ha'apai as an example).

Low δ^{11}B values for NZ basaltic lavas could reflect interactions with low-δ^{11}B crustal rocks (or sediments), or could be inherited from a little modified intraplate type of mantle source. At this time, the only comparative data for New Zealand are from geothermal fluids from the Taupo Volcanic Zone (TVZ) that also have low δ^{11}B values (−6‰ to −2‰; *Millot et al*. [2012]), as well as radiogenic $^{87}Sr/^{86}Sr$ (0.7055–0.7096). Because B and Sr compositions of such fluids largely are inherited via interaction with local reservoir rocks [cf. *Pennisi et al*., 2000; *Leeman et al*., 2005b], the observed δ^{11}B values reasonably represent either TVZ silicic volcanic rocks, the underlying Torlesse-type basement rocks, or both since the TVZ rhyolites likely incorporate significant melt components from the basement [cf. *Deering et al*., 2011]. However, because the analyzed basalts are relatively primitive, with up to 9% MgO, we tentatively favor the view that their δ^{11}B values are representative of the underlying mantle in this region. The one back-arc lava analyzed (−0.7‰) is in the upper range for intraoceanic basalts, but suggests a significant decrease in δ^{11}B behind the volcanic front—as is typically observed for other cross-arc transects [*Ishikawa and Nakamura*, 1994; *Ishikawa et al*., 2001; *Tonarini et al*., 2001; *Leeman et al*., 2004].

Our data for local sediments are compared with the lavas in Figure 4. Ten samples (mostly pelagic clays) from the ODP Hole 596 core have δ^{11}B (−2.4 to +3.3‰) significantly lower than most Tongan lavas, whereas two samples (pelagic clay and volcaniclastite) from the DSDP Hole 204 core have δ^{11}B values (5.6‰ and 6.8‰) within the range for the arc lavas. B/Nb ratios for most of the sediments (range = 7–28, excluding black clay) overlap the lower end of the range for the arc lavas,

In summary, our major observations are as follows: (1) There is a general regional increase in δ^{11}B, B/Nb, and similar ratios toward the north from New Zealand; this correlates with a significant northward increase in plate convergence rate for the arc, hence cooler temperatures at a common reference depth on the top

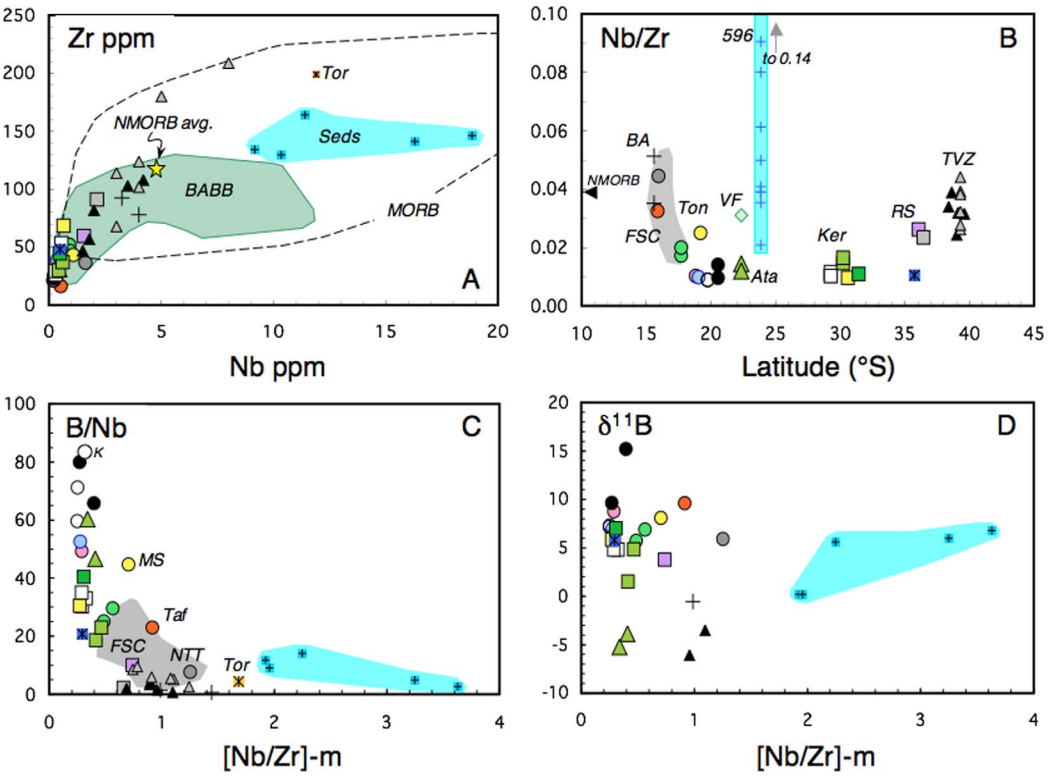

Figure 5. (a) Zr versus Nb content of TKNZ lavas. Fields are shown for MORB and BABB segment averages from *Gale et al.* [2013], along with their average NMORB composition (star). Also shown are estimated average compositions of subducting sediments (blue field) and Torlesse basement from New Zealand. (b) Latitudinal variation in Nb/Zr ratios for TKNZ lavas. Data ranges are shown for DSDP 596 sediments and for FSC lavas. Nb/Zr values for central arc lavas are strongly depleted with respect to NMORB average (tick on left side). Acronyms (Ton, Ker, RS, TVZ) indicate arc sectors. (c and d) B/Nb ratios and δ^{11}B values for TKNZ lavas versus NMORB-normalized Nb/Zr values; also shown are fields for sediment averages (blue) and FSC lavas (gray). Symbols for arc lavas as in Figure 3.

of the subducting plate; (2) In detail, B/Nb and similar ratios define a conspicuous "spike" near latitude 21°S (southern Tonga), with distinct patterns of B-enrichment north and south of that latitude that likely reflect compositional gradients in arc magma sources; (3) There is a hint of a cross-arc decrease in δ^{11}B and B/Nb toward the back-arc, as observed elsewhere; and (4) Anomalously low δ^{11}B is observed in samples from Ata, where the back-arc VFSC impinges on the arc system and the LSC is being subducted. In subsequent sections of this paper, we also incorporate published data for the submarine Monowai volcano [*Timm et al.*, 2011] to partially fill the gap in our coverage between Ata and the northern Kermadec islands.

5. Discussion

To better understand the nature of along-strike variability in the composition of TKNZ arc magmas, we consider Zr-Nb systematics (Figure 5). These elements are highly incompatible (Nb more so than Zr; *Brenan et al.* [1995] and *Pfänder et al.* [2007]) in major mantle minerals and nominally immobile in slab-derived fluids. Thus, Nb/Zr ratios in the mantle can be significantly reduced in response to melt extraction. Additionally, Nb and Zr abundances in the arc magmas are strongly influenced by prior melting history of their mantle source. Overall, TKNZ lavas are among the most Nb- and Zr-depleted lavas known—more so than most mid-ocean ridge (NMORB) or back-arc basin (BABB) basalts (Figure 5a). Nb/Zr values in all TKNZ samples are low ($<$0.04) relative to primitive mantle ("PM"; $\sim$0.06) [*McDonough and Sun*, 1995], and are consistent with selective depletion of the more incompatible Nb due to prior extraction of melts from their source regions (also borne out by data for other incompatible elements; *Ewart and Hawkesworth* [1987], *McCulloch and Gamble* [1991], *Woodhead et al.* [1993], *Turner et al.* [1997], *Haase et al.* [2002], *Smith and Price* [2006], and *Wysoczanski et al.* [2006]).

In particular, lavas from the central part of the arc (latitudes from 18°S to 33°S) have extremely low Nb/Zr ratios (ca. 0.01)—about 4 times lower than average NMORB (or its Depleted MORB Mantle source, "DMM"; cf. Figure 5b, *Salters and Stracke* [2004]). Only lavas from the northernmost islands (Tafahi, Niuatoputapu), the back-arc, and New Zealand have Nb/Zr as high as or greater than the NMORB average. It is significant that TKNZ lavas with the lowest Nb/Zr ratios (here normalized to the NMORB average; "[Nb/Zr]-m") exhibit systematically higher B-enrichment as evidenced by B/Nb ratios (Figure 5c). Overall the data define a continuous array that merges with data from the FSC, and potentially extends to compositions of New Zealand basement and local subducting sediment averages. We note that the distinct gradients in B/Nb, etc. along the arc (Figure 4) span the region of near constant and low Nb/Zr. This implies that, at least in the central part of the arc, the gradients are likely controlled by variations in the magnitude and/or composition of subduction components added to the mantle wedge; source influence (increasing Nb/Zr) may be significant at the extreme ends of the arc. Boron isotopic compositions are not obviously correlated with [Nb/Zr]-m (Figure 5d), which suggests that boron added to the arc magma sources has diverse origins or has experienced different isotopic fractionation paths.

As a corollary, the near-constant source Nb/Zr values along much of the arc indicate that presubduction melt depletion of the mantle wedge was fairly uniform in degree. Refertilization of upper mantle domains beneath northernmost Tonga and the proximal back-arc region [cf. *Ewart et al*., 1998; *Falloon et al*., 2007; *Regelous et al*., 2008; *Keller et al*., 2008; *Tian et al*., 2011; *Lytle et al*., 2012] by in-flow of relatively enriched mantle could account for increased Nb/Zr in this region. At the southern end of the arc, increasing Nb/Zr toward New Zealand implies a gradient in mantle depletion there as well—that is, decreasing southward. These observations raise questions regarding the extent to which arc magma chemistry may reflect (1) along-strike differences in degree of melt-depletion of arc magma sources vis à vis (2) variations in magnitude and nature of subduction contributions.

5.1. Nature of Arc Magma Sources

To address these issues, it is useful to know the compositions of magma sources along the arc. These are best estimated by considering elements whose abundances in the magma source are least likely to have been augmented by subduction contributions; primary candidates are TiO_2, Y, and Yb [*Pearce and Peate*, 1995; *Pearce et al*., 2005, and references therein]. Abundances of TiO_2 and Yb (also Y, not shown) in TKNZ lavas define a coherent array (Figure 6a) that closely follows the predicted melting path for a spinel lherzolite source with DMM composition (cf. supporting information Table S1 for model parameters). Comparison with predicted batch melt fractions indicates that TKNZ arc and back-arc magmas could form by roughly 35 to 5% melting of such a source. But because source depletion appears to vary from DMM and differ in detail along the arc, we need to quantify the degree of melt depletion relative to DMM to refine estimates of melt fraction (F).

This is done for source TiO_2 content using ratios of TiO_2/Y and TiO_2/Yb as normalized to the same ratios in NMORB [*Gale et al*., 2013] and following the approach of *Gribble et al*. [1998] and *Kelley et al*. [2006]. Using both ratios, source TiO_2 contents were calculated for selected primitive basaltic magmas from each location investigated. Additionally, data from Monowai Seamount [*Timm et al*., 2011] and submarine Volcano A [*Cooper et al*., 2010] can be compared with our results. Monowai is of particular interest because of its proximity to the subducting Louisville Seamount Chain, south of Ata Island (Figure 1). Published data for Volcano A are limited to boninitic lavas and can be compared to nearby Hunga Ha'apai. No B data are available for either of these localities. Average TiO_2 values ($\pm$SD) are given in supporting information Table S1, and details of the calculations are summarized in the supporting information. Because we restricted calculations to samples with $SiO_2 <$ ca. 55%, MgO $>$ 5%, and calculated equilibrium olivine composition of at least Fo_{83}, reliable estimates are not available for localities in this study (Niuatoputapu, Fonualei, Metis Shoal, Curtis) where only more evolved lavas have been analyzed.

The same sample analyses were corrected individually by incremental addition of equilibrium olivine to equivalent melts in equilibrium with a Fo_{90} source so as to estimate "TiO_2-90" values for each locality (cf. supporting information; *Lee et al*. [2009]). These values and source TiO_2 estimates allow computation of *F* values for each location following the approach of *Kelley et al*. [2006]. Results are given in supporting informationTable S1. As seen in Figure 6b, melt fraction increases with latitude from about 10% to 15% in New Zealand to 20–25% in Tonga, with exceptions at Monowai (28%), Tafahi (35%), and back-arc Niuafo'ou (7%).

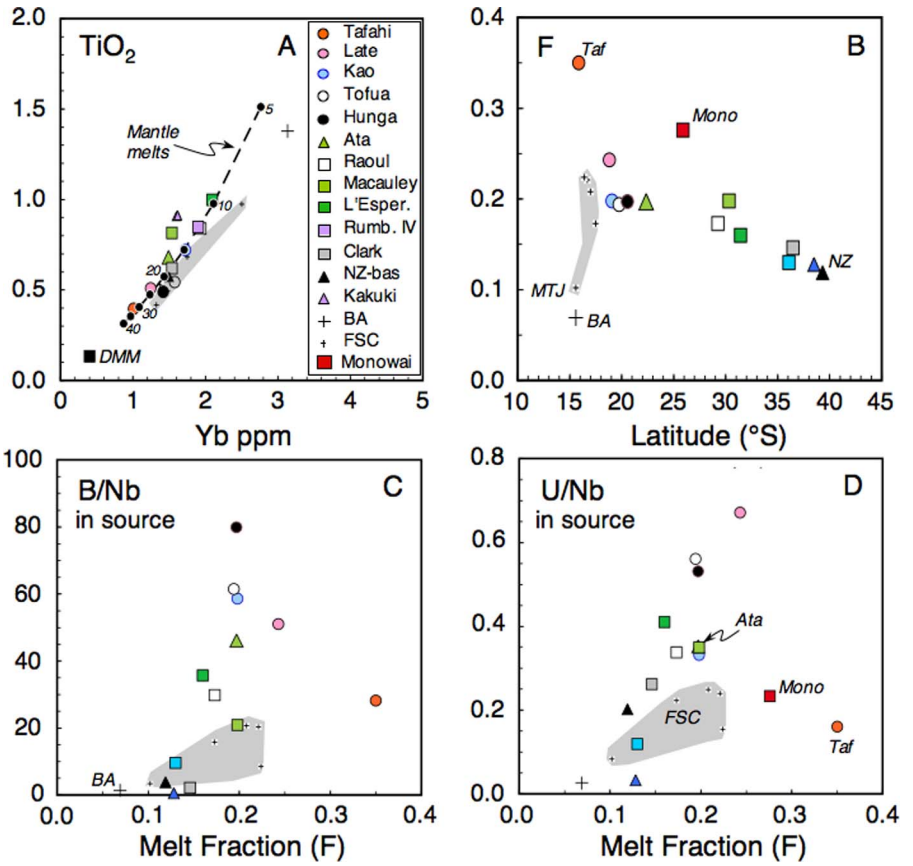

Figure 6. (a) TiO_2-Yb array for TKNZ lavas, with superposed data array for FSC. Dashed curve shows locus for batch melts of a spinel lherzolite source (ol:opx:cpx = 0.6:0.3:0.1) with initial composition of DMM (0.133% TiO_2, 0.4 ppm Yb). Percent melt is indicated by numbers along the curve. (b) Spatial variation in estimates of melt fraction. (c and d) Plots of source B/Nb and U/Nb ratios versus calculated melt fractions. See text and supporting information for details of calculations. Symbols as in Figure 3, but excluding locations without primitive lavas. Kakuki is a primitive basalt from the TVZ [*Price et al*., 2012]. Monowai data are from *Timm et al*. [2011].

We note that estimated *F* value for Volcano A is consistent with the main trend for the arc (not shown, cf. supporting information Table S1). *F* values were also estimated for FSC (Figure 6b) using the data of *Keller et al*. [2008]; our results (10–22%) are virtually identical to estimates by *Escrig et al*. [2012] using their own data set for the same areas. These data indicate that degree of melting decreases with distance behind the volcanic arc.

With the exception of Tafahi, average B/Nb ratios for each locality are positively correlated with estimated melt fraction (Figure 6c). U/Nb ratios also correlate well with melt fraction, with exception of Tafahi and Monowai (Figure 6d). Considering that both B and U are expected to be readily mobilized in aqueous fluids, these correlations support the notions that melt fraction is proportional to the amount of slab-derived fluid that was added to the respective magma sources, and that subduction contributions appear to vary in a systematic manner along the arc. The FSC data appear to define distinctly lower slopes (Figures 6c and 6d); given the back-arc setting, this may be attributed to smaller inputs of slab-derived B and U (i.e., fluid) to the mantle in this region. The observed correlations also could reflect systematic changes in the composition of the added subduction component. It is unclear why Monowai and Tafahi do not follow the main arc trend, Tafahi is the northernmost Tongan island, and prior works demonstrate that it is exceptional in many ways (alluded to in our earlier remarks). Monowai, straddles the sector where the LSC is being subducted, and could well have complications arising therefrom.

Finally, using average compositions of the most primitive basaltic lavas from each locality and the corresponding *F* values, we estimated concentrations of B, Ba, U, Th, La, Yb, Be, Nb, Zr, in the respective magma sources for a spinel lherzolite melting model (supporting information Table S1 and Figure S2). These results are discussed in more detail in the supporting information. Principal outcomes for the TKNZ arc lavas

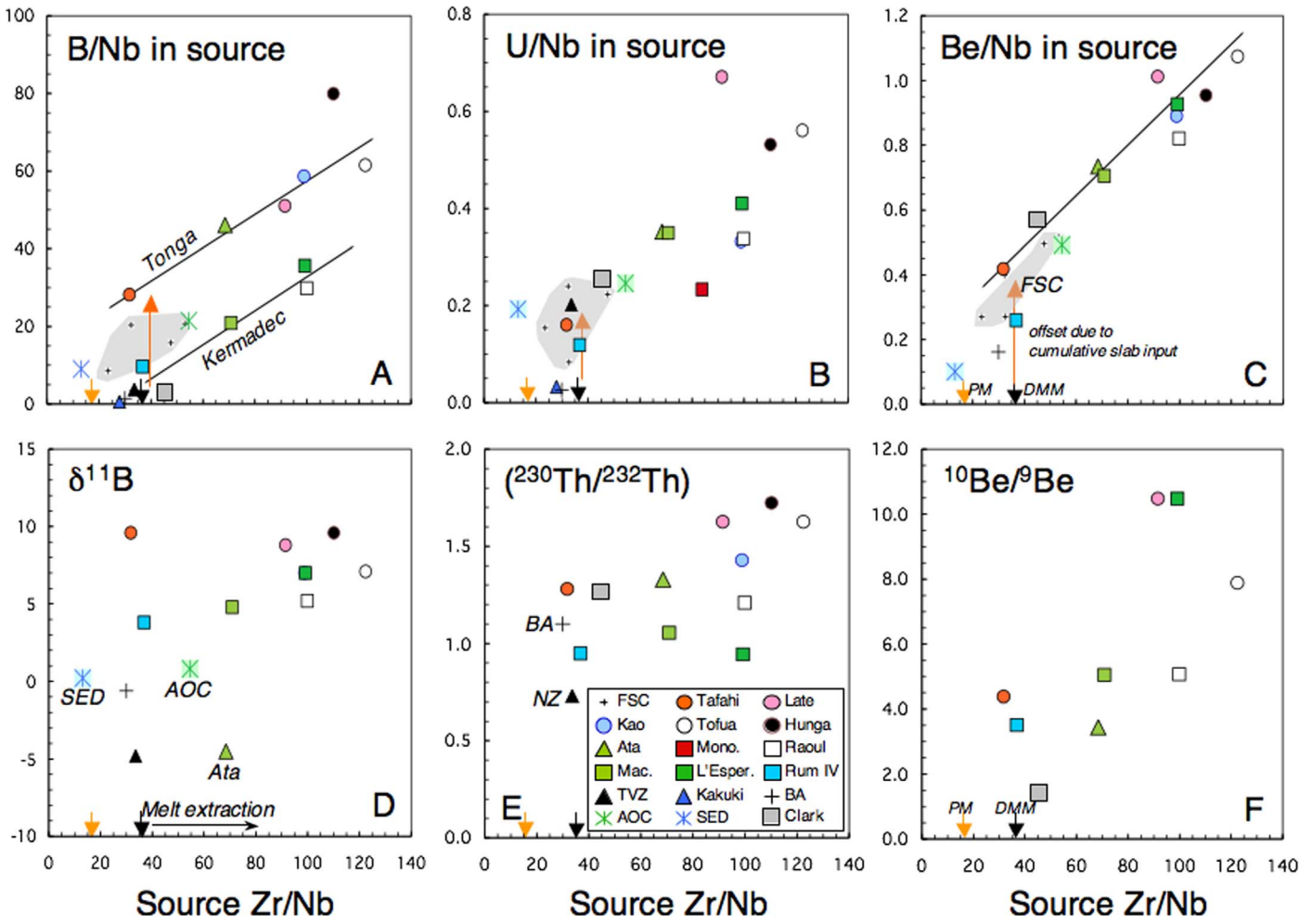

Figure 7. (a) B/Nb, (b) U/Nb, and (c) Be/Nb ratios calculated for sources of TKNZ magmas versus source Zr/Nb. Source depletion increases with Zr/Nb. PM and DMM mantle compositions, average sediment (SED), altered oceanic crust (AOC), and fields for FSC sources are shown for comparison. Vertical orange arrows indicate magnitude of offset from DMM to array for Tonga sources. (d) δ^{11}B, (e) (^{230}Th/^{232}Th) activity ratios, and (f) ^{10}Be/^{9}Be ratios for TKNZ lavas versus source Zr/Nb. Positive correlations with Zr/Nb are consistent with increasing leverage of subduction contributions over more depleted sources. Symbols and data as in Figure 6.

include the following: (1) B and, to lesser extent, Ba are extremely enriched in the arc magma sources relative to estimated DMM values, such that nearly all B and most Ba must be slab-derived; (2) Th, U, La, and Be are also enriched relative to DMM, consistent with significant slab inputs for these elements; (3) Yb is similar to DMM/PM values, and generally consistent along the arc; (4) Zr is also relatively consistent along the arc, but slightly lower than DMM values except in southern locales where Zr appears to be locally enriched; (5) Nb is ultradepleted along most of the arc, but increases to DMM levels or higher in the southern and northern sectors (Figure 5b).

These estimates are used to examine source abundances of B, U, and Be relative to Nb, and corresponding isotopic compositions as a function of source depletion as inferred from Zr/Nb ratios (Figure 7). Note that binary mixing relations in these element ratio plots should be linear. B and Th isotopic ratios were measured on the samples used to estimate source elemental compositions; ^{10}Be/^{9}Be ratios from *George et al*. [2005], often on different samples, are taken as representative of the inferred sources. The element ratios are positively correlated and consistent with stronger enrichments of B, U, and Be as sources become more refractory (increasing Zr/Nb). The near-linear array for Be/Nb (Figure 7c) for TKNZ (and FSC) is consistent with addition of an essentially uniform Be-rich component to sources along the arc that also are similar (or collinear) in composition (excepting Rumble IV and back-arc Niuafo'ou, for which source estimates lie off the delineated array). Arrays for U/Nb (Figure 7b) and particularly B/Nb (Figure 7a) are more scattered and, for the latter, essentially distinct for the Tonga and Kermadec sectors. Average subducting sediment and

altered oceanic crust estimates lie near the arc arrays, but closer to the origin than most of the inferred source compositions. Bulk addition of these materials to the arc magma sources cannot produce the observed arrays, although they could contribute to solute loads in slab-derived fluids. Additives are needed that are enriched in B, U, and Be, that are somewhat heterogeneous for U and, for B, distinctive for the two arc sectors. Moreover, the arrays are offset to higher B/Nb, U/Nb, and Be/Nb ratios than estimated for PM and DMM compositions. Assuming the actual source end member(s) lie along the inferred source arrays, they must have accumulated some B. U, and Be prior to establishment of those arrays. This could have occurred over protracted duration of subduction. It appears that such accumulation for B was more pronounced for Tonga than for Kermadec mantle domains. Smaller offsets for the FSC source compared to the adjacent Tonga volcanic front are consistent with decreasing slab inputs toward the rear of the arc system.

Isotopic compositions of B, Th, and Be are also positively correlated with apparent source depletion (Figures 7d–7f), albeit less so than the elemental ratios. Excluding Ata, the back-arc and New Zealand, δ^{11}B values are slightly offset for different arc segments, being slightly lower for Kermadec lavas. The same can be said for (^{230}Th/^{232}Th) activity ratios and for ^{10}Be/^{9}Be ratios (excepting a high value for L'Esperance). Because the latter two ratios decay with time (to equivalence with respect to (^{238}U/^{232}Th) ratio, and zero, respectively), they require that the mixing process(es) responsible for the observed arrays are relatively recent (see later discussion). Of course, some of the scatter in those arrays could result from differences in times of mixing (and/or duration of storage) to produce the sampled mantle domains. In essence, the data are consistent with addition of one or more B-U-Be-rich components (presumably slab-derived fluids) to regionally variable mantle domains that were previously melt-depleted but subsequently replenished to differing degree with respect to the fluid-mobile trace elements.

Compositions of radiogenic Sr-Nd-Pb isotopes (averaged for each locality) are also compared with estimated source depletion (Figure 8 and supporting information Table S1). These data are subdivided into two distinct groups. The first includes source domains beneath New Zealand and southern seamounts, back-arc, and Tafahi from the northernmost end of the arc. This array is viewed as potentially representative of the least melt-depleted (i.e., lowest source Zr/Nb) mantle preserved in proximity to the TKNZ arc; the NMORB average of *Gale et al*. [2013] has comparable Zr/Nb. Note that distal lavas of the FSC originate in this array and become more "arc-like" with proximity to the volcanic front [*Escrig et al*., 2012]. A second grouping comprises all other lavas from the TKNZ volcanic front. Sr isotopic ratios vary little with increasing source depletion (Zr/Nb), but are slightly more radiogenic than NMORB (Figure 8a). Nd isotopic ratios are MORB-like (Figure 8b) and generally decrease with source depletion. Pb isotopic ratios are slightly more radiogenic than the NMORB average and also decrease with source depletion (Figures 8c and 8d), and in a general sense from south to north along the arc. We note that the trends in Pb isotopic values verge away from estimated sediment composition (^{206}Pb/^{204}Pb = 18.8, ^{208}Pb/^{204}Pb = 38.8; *Regelous et al*., 2010; also cf. supporting information Table S1) in this region. This observation does not exclude some inolvement of sediment-derived Pb, but is consistent with its diminishing importance toward the north. Assuming these latter trends reflect addition of a slab-derived fluid to the arc magma sources, it is inferred to carry dominantly MORB- or AOC-like Sr-Nd-Pb, with little implication of pelagic sedimentary components (this is also seen in Supplemental Figure S3 for Sr and Nd isotope compositions versus B/Zr and δ^{11}B in individual samples). However, the nature of subducted components may also vary with position along the arc. As proposed by *Turner et al*. [1997], volcaniclastic sediments derived from the LSC could be involved in the north Tonga mantle sources. In contrast, lavas from the southern end of the arc have isotopic affinities to local sediments and could be derived from sources with such contributions. Note that the local sediments have low Zr/Nb ratios and their addition could to some degree counterbalance effects of prior melt extraction on source Zr/Nb.

In summary, addition of slab-derived fluid to the mantle wedge is commonly invoked as a trigger for forming arc magmas. This scenario predicts a correlation between the amount of fluid added and the degree of induced melting that ensues [cf. *Stolper and Newman*, 1994; *Kelley et al*., 2006]. Assuming that ratios of fluid-mobile to non-fluid-mobile elements are proportional to fluid flux, this appears to be the case for the TKNZ arc based on calculated source compositions. In addition, B/Nb and similar ratios define an inverse correlation with measures of melt-depletion of magma sources, particularly for the arc front lavas, that requires a multistage (or progressive) history for the magma sources. That is, B enrichment attending subduction is superimposed on earlier stages of melt depletion that produced low Nb/Zr (also La/Yb, not shown) as well as very low contents of B and other incompatible elements in the residual mantle; prior melting is expected

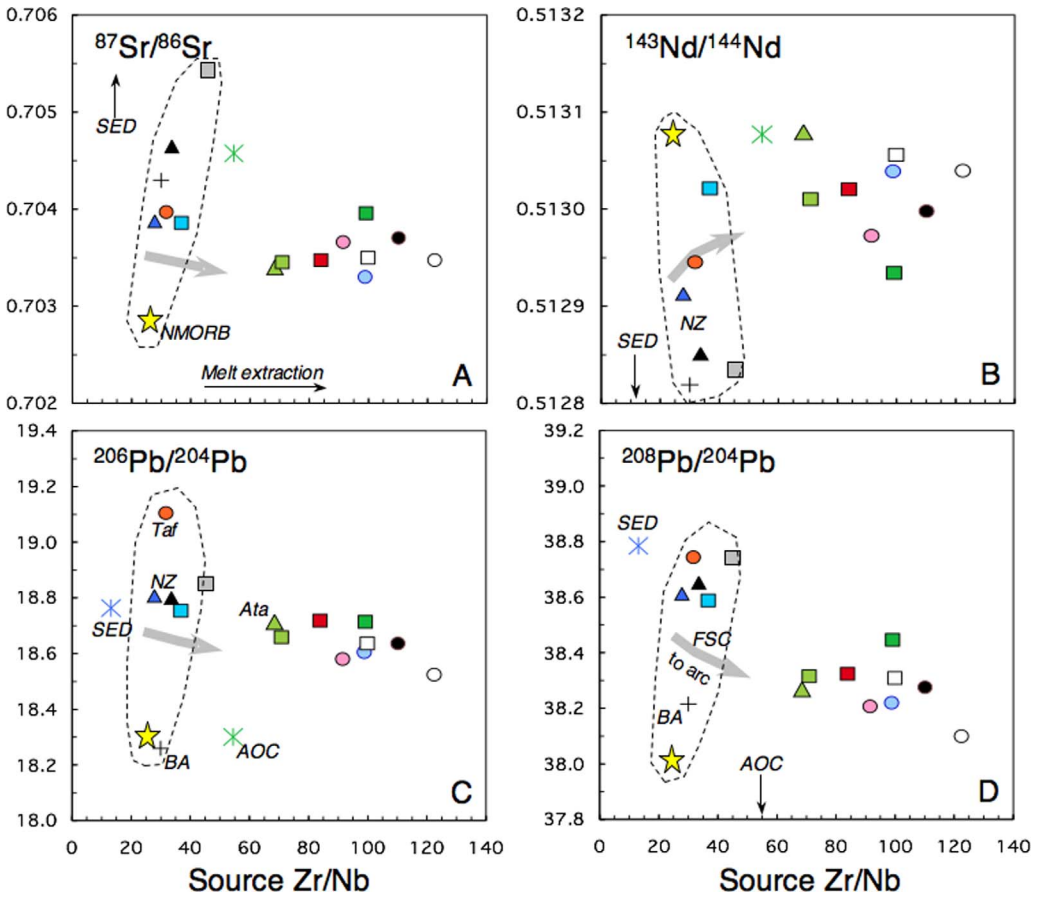

Figure 8. (a) Sr, (b) Nd, (c and d) Pb isotopic compositions of TKNZ lavas as functions of source Zr/Nb. Isotopic compositions for TKNZ lavas are from *Turner et al*. [1997] or *Ewart et al*. [1998] as amended by *Hergt and Woodhead* [2007]. These data are plotted as averages for each locality; also shown are average SED, AOC, and NMORB compositions (cf. supporting information Table S1). Pb compositions of AOC are inferred from the study of *Castillo et al*. [2009]. Average isotopic compositions of FSC segments [*Escrig et al*., 2012] are used to define the trends shown by gray arrows. Dashed field comprises samples from DMM (MORB-like) mantle sources. Symbols as in Figure 3.

to have had relatively little effect on δ^{11}B (which should remain near or below typical mantle values (ca. $-5‰$ to $-10‰$). Present-day B-enrichment (as evidenced by B/Nb ratios) and elevated δ^{11}B in the arc magmas can be explained by subsequent inputs of slab-derived fluids of slightly different composition along the arc. To further evaluate this hypothesis, we next consider B systematics in greater detail.

5.2. Constraints From Boron Elemental Systematics

The effects of adding slab-derived fluids and other subduction components to the mantle wedge are shown schematically for B-Nb elemental systematics in Figure 9. For a given source composition, contents of highly incompatible elements in a partial melt will vary inversely with melt fraction produced. Thus, ratios for similarly incompatible elements should mimic those of the source. This is the case for B and Nb as their partition coefficients between common mantle minerals and equilibrium melts are similarly low [*Brenan et al*., 1995, 1998a, 1998b]. Other beneficial consequences are that melting models for these elements are not very sensitive to source mineral modes (esp. at melt fractions greater than a few percent), or to the mode of melting (e.g., batch versus fractional melting). Considering that TKNZ arc magma sources are relatively depleted compared to "primitive mantle", low-clinopyroxene spinel lherzolite or harzburgitic lithologies are considered appropriate [*Bourdon et al*., 1999; *Wood and Turner*, 2009; cf. our Figure 6a]. Significantly, it is virtually impossible to produce a series of melts with B/Nb ratios spanning the observed TKNZ range by melting such sources unless they have been modified to have elevated B/Nb prior to melt formation.

Open system processes (i.e., variable slab inputs to the mantle wedge) are required to create a spectrum of sources with the observed nearly two orders of magnitude range in B/Nb in the TKNZ lavas. Such

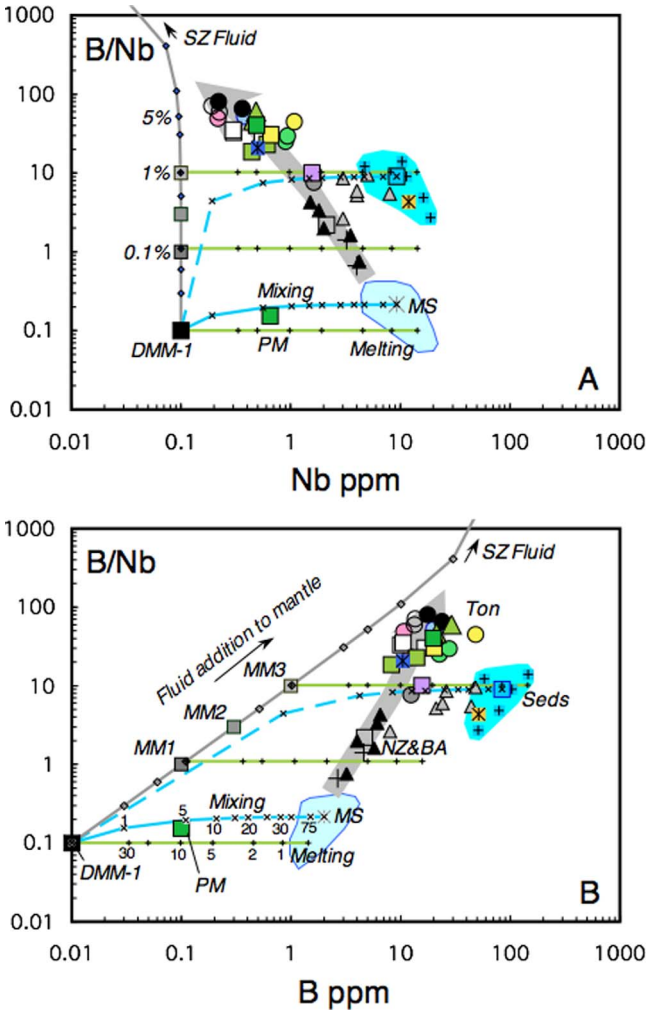

Figure 9. Models of source modification by addition of fluids or sedimentary components to hypothetical mantle end members superimposed on data for TKNZ lavas for (a) B/Nb versus Nb content, and (b) B/Nb versus B content; data symbols as in Figure 3. The principal arc trends for mafic lavas are highlighted by broad gray arrows, and more evolved lavas are generally offset to the right of these arrows. Relevant sediment averages are plotted as well. Two extreme mantle compositions are shown. The first is a MORB-source mantle that has been further depleted by removal of 1% partial melt ("DMM-1"; 0.01 ppm B, 0.1 ppm Nb; cf. Table S1 and supporting information); this composition is appropriate for the lowest Nb/Zr Tonga lavas. A more enriched composition ("PM"; 0.1 ppm B, 0.65 ppm Nb) is shown for comparison; for clarity, model curves are not shown for this end member. The effect of adding a B-rich subduction zone fluid (100 ppm B, 0.1 ppm Nb) to DMM-1 is shown by gray mixing curves (diamonds at 0.01%, 0.05%, 0.1%, 0.5%, 1%, 3%, 5%, 10%, and 20% fluid). Subsequent partial melting of such variably modified mantle compositions can best account for the range in B-enrichment observed in the TKNZ lavas. Representative melting curves are plotted for DDM-1 and two modified mantle (MM1, MM3) sources (green lines with plus signs at 0.5%, 1%, 2%, 5%, 10%, 20%, and 30% melting). Note that the degree of melting required to produce mafic TKNZ magmas appears to increase with B-enrichment of the source. The effect of adding sedimentary components is illustrated with two extreme end members: bulk sediment represented by local sediment averages (Seds field), and equivalent metasediments (MS field) that have undergone B-depletion during subduction. The latter compositions are estimated using an equation for B-depletion based on empirical data for prograde metamorphic sequences [*Moran et al*., 1992] (Leeman, unpublished data) and assuming that the sediments reach a temperature of 800°C. [Depletion factor = 1.034–0.0125*(T°C/100)2 – 0.0264*(T°C/100)]. Trajectories are shown for mixing bulk sediment with DMM-1 (blue dashed curves with *x*'s at 1, 5, 10, 15, 20, etc., up to 100% sediment end member). A similar curve (blue solid line) is shown for mixing B-depleted metasediments with DMM-1. Melts of these materials will produce similar mixing trajectories but with smaller proportions to achieve comparable shifts in source composition (not shown for clarity). Addition of these sedimentary components or melts thereof cannot produce source B/Nb ratios greater than ca. 10 (i.e., suitable only for New Zealand samples.

compositional variability in the arc magma sources may be achieved by several end-member processes, or possibly combinations thereof (Figure 9). For simplicity, we consider modification of the mantle wedge by addition of either (1) aqueous fluid, (2) bulk sediment, or (3) sediment melt. Given predicted thermal conditions in the subducting slab (cf. Figure 2), we do not consider melting of oceanic crust likely for the TKNZ arc (and particularly Tonga). In the first case, an aqueous fluid is considered in which B is highly soluble whereas Nb is not. Here, we do not specify the source of the B other than that it is likely to be the

subducting slab. The fluid composition assumed is conservative in that B content (100 ppm) is lower than some predictions [cf. *Brenan et al*., 1998b; *Marschall et al*., 2006], and B/Nb in the fluid could be much higher. Such fluids essentially act as a B-spike to the mantle, and relatively small additions would be sufficient to create the spectrum of source B/Nb needed to produce TKNZ magmas, with nearly all of the B in the modified sources being slab-derived. Subsequent partial fusion of these variably modified mantle domains (see representative horizontal melt paths) can produce melts having a range of B/Nb ratios that depend on the degree of source modification. In this scenario, along-arc fluid contributions to the magma sources must vary in proportion to observed B/Nb ratios in the arc lavas (cf. Figure 4). If the fluids are more or less uniform in composition, this would be equivalent to varying fluid volume flux in proportion to local B/Nb values. The slopes of the TKNZ main trend data (exclusive of evolved andesite-dacite compositions) in Figures 9a and 9b are consistent with greater melt productivity from the most highly modified mantle sources. That is, the lava arrays converge toward the source mixing lines with increasing B/Nb. This qualitatively matches the effect of water addition on partial melting for a given bulk composition; that is, the degree of melting increases in proportion to amount of water added to the source [cf. *Stolper and Newman*, 1994]. In detail, if magmas along the arc are derived from distinct sources of variable fertility, then (1) a family of fluid-mixing curves would be produced originating from those sources, and (2) inferred degrees of modified mantle (MM) source melting would shift accordingly. Furthermore, the amount of fluid required to attain a specific source B/Nb value would vary inversely with source fertility as the fluid will have more leverage with diminishing incompatible element content in the sources. Fluid compositions could also vary spatially or temporally within the arc system. For these reasons, the models shown in Figure 9 are considered as exemplars, and not unique.

Given that sediment involvement has been proposed for the TKNZ arc, we also consider the implications of adding subducted sediment components to mantle sources. However, because local subducting sediment averages have lower B/Nb ratios ($<$15) than observed in most Tonga-Kermadec lavas, bulk sediment incorporation can only be significant for lavas from the southern seamounts and New Zealand and cannot account for elevated B/Nb in more northerly locations. If B is quantitatively retained in the bulk sediment up to melting conditions, at least 1–5% sediment must be added to a DMM-1 type mantle to shift source B/Nb values to those (1–5) observed in New Zealand basalts (Figure 9), and this may be consistent with Sr-Nd isotopic compositions of these lavas [*Rooney and Deering*, 2014]. Partial melts of sediments would have higher incompatible element contents than the bulk sediment, thus reducing the amount of material that must be added to the mantle wedge to achieve a given range in source B/Nb, but the mixing curves would have essentially the same trajectory as for bulk sediment. However, the efficacy of this process is weakened by the probability that B and other fluid-mobile elements are selectively removed by dehydration and metamorphic processes prior to onset of melting [cf. *Moran et al*., 1992; *Marschall et al*., 2007]. The extent of this effect is modeled using the *Moran et al*. [1992] empirical observations of B-depletion as a function of metamorphic grade (or T°C), from which we estimate greater than 95% loss of B from sediments heated to $\sim$800°C (see Figure 9 caption). In this case, B/Nb ratios in sediment melts or B-depleted subducted metasediment may be too low to elevate the mantle source compositions to B/Nb values observed in the lavas.

It is worth noting that, in Figure 9, New Zealand basalts lie on trends consistent with mafic lavas from the TKNZ arc as a whole, whereas data for Ruapehu evolved lavas (gray triangles) form distinct subhorizontal trends that project toward compositions of sediments (or local Torlesse basement). The latter trends are consistent with petrologic evidence that Ruapehu andesites and dacites are produced by FC of intermediate composition (i.e., basaltic andesite) magmas and further modification by mixing of such magmas with silicic crustal melts and/or assimilated crustal material [*Graham and Hackett*, 1987; *Price et al*., 2012]. Such processes appear to be common elsewhere in the TKNZ arc [e.g., *Gamble et al*., 1993a; *Smith et al*., 2010], and can contribute to horizontal dispersion of compositional arrays like those in Figure 9. For this reason, the data for basaltic lavas provide closer constraints on mantle source processes.

5.3. Constraints From Boron Isotopic Systematics

Variation in boron isotopic and related compositional data is shown in Figure 10. Comparison of the TKNZ data with those from other arc systems provides a general context for more detailed analysis. The Tonga-Kermadec data are rather typical of other western Pacific arcs (Izu-Bonin: *Ishikawa and Nakamura* [1994], *Straub and Layne* [2002]; Kurile: *Ishikawa and Tera* [1997]; Marianas: *Ishikawa and Tera* [1999]; Kamchatka: *Ishikawa et al*. [2001]), all of which are associated with relatively cool subduction zones. Data for these arcs

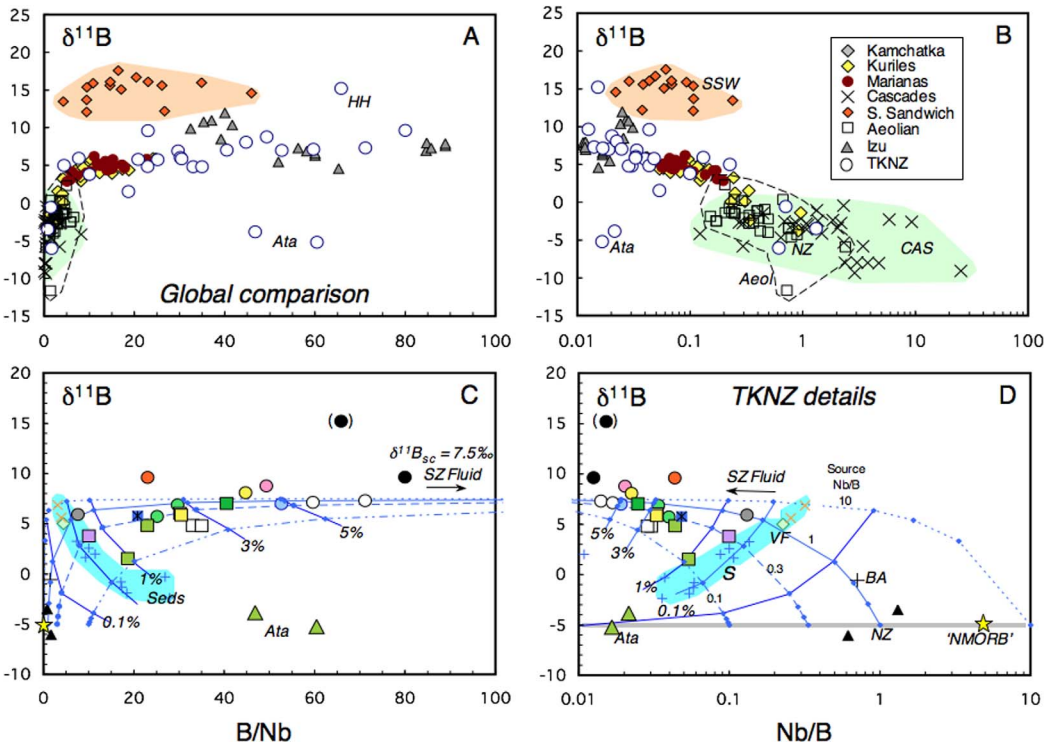

Figure 10. Boron isotopic compositions of arc lavas as a function of B/Nb or Nb/B. (a and b) Show TKNZ data in the context of other volcanic arcs. The B/Nb plot emphasizes the nature of B-rich additives (slab-derived subduction components), whereas the Nb/B plot emphasizes processes in the arc magma sources (mantle wedge effects). The Cascades and Aeolian arcs are associated with warm subduction zones, the western Pacific arcs (Mariana, Izu, Kurile, Kamchatka, Tonga-Kermadec) represent cool subduction zones, and S. Sandwich arc is associated with strong accretionary erosion of the forearc. (c and d) Show the TKNZ data in detail with representative process models. Symbols as in Figure 3. Mixing curves are shown for addition of a hypothetical slab-derived fluid (100 ppm B, 0.01 ppm Nb, $\delta^{11}B = 7.5‰$, and B/Nb = 10000) to a range of mantle sources having MORB-like $\delta^{11}B$ ($-5.0‰$), 0.1 ppm Nb, and variable B (Nb/B = 10 to 0.1). Intersecting lines link these various models at fixed proportions of fluid added (0.1–5%).

are consistent with $\delta^{11}B$ values in the subduction component ("$\delta^{11}B_{SC}$"; see below) similar to those at Tonga-Kermadec. For comparison, much lower $\delta^{11}B_{SC}$ (near $+1‰$) is consistent with low $\delta^{11}B$ values in lavas from the very warm Cascade arc. There, it is proposed that ^{11}B was selectively removed from the subducting slab during advanced dehydration beneath the fore-arc region [*Leeman et al*., 2004]. Effectively, early quantitative removal of B from the slab in hot subduction zones minimizes overprinting of the mantle wedge B systematics by infiltrating slab-derived fluids. Regarding isotopic compositions, it is widely agreed that, as subducting slabs are heated and progressively dehydrated, the released fluids will selectively remove ^{11}B, causing gradual reduction of $\delta^{11}B$ [*Peacock and Hervig*, 1999]. A similar situation may prevail in the Aeolian arc due to slow convergence [*Tonarini et al*., 2001]. In contrast, very high $\delta^{11}B_{SC}$ (near $+16‰$) for the South Sandwich arc has been attributed to subduction erosion of previously metasomatized frontal arc mantle that has been enriched in ^{11}B by shallow subduction zone fluids [*Straub and Layne*, 2002; *Savov et al*., 2005; *Tonarini et al*., 2011]. As discussed in these papers, retention of B in subducting slabs likely depends on the stability and spatial distribution of B-host minerals (dominantly serpentinite and phyllosilicate phases) under gradational thermal conditions as the slab is progressively heated.

These data are modeled in terms of additions of subduction components to arc magma sources in the mantle wedge. Again, B/Nb ratio is used as a proxy for boron enrichment in the magma sources, and should essentially depend on the magnitude of fluid additions to the respective mantle domains (assuming negligible fluid solubility of Nb). In detail, the amount of fluid required to produce a specific source B/Nb value will vary inversely with the B content of that fluid or directly with degree of source depletion. As in previous models, we used a fixed B content of 100 ppm for illustration. The entire full range of observed B/Nb values can be produced by adding up to 5% of this fluid to the model source (or $<1\%$ fluid at higher B content ca. 1000 ppm); this addition need not be instantaneous, and is likely to be cumulative over time. Although

initial δ^{11}B values in slab components (abyssal peridotites, oceanic crustal rocks, etc.) can be high in some cases (10–40‰) [*Martin et al*. [2016] due to interaction with seawater, they are typically lowered by dehydration processes, making it difficult to know a priori the isotopic composition of material being added to arc magma sources. Boron isotopic variations in arc lavas provide the most direct constraints on this question.

For example, at relatively high B/Nb, mixing curves for fluid addition define plateaus approximating the isotopic composition of this subduction component ($\delta^{11}B_{SC}$). Accordingly, data for the Tonga sector and for some Kermadec lavas indicate that the subduction component added to their sources must have a $\delta^{11}B_{SC}$ value near 7.5‰ (Figure 10c). Data for Hunga Ha'apai (leacheate residue) and Tafahi permit involvement of heavier contributions ($\delta^{11}B_{SC}$ approaching 10‰), and some Kermadec samples are consistent with $\delta^{11}B_{SC}$ as low as 5‰. Thus, a representative composition for slab-derived contributions in the main arc is taken as 7.5 ± 2.5‰. Similarly, lower δ^{11}B values in the southernmost lavas (Figure 4) can be explained by southward decrease in $\delta^{11}B_{SC}$ values. This in turn could result from enhanced isotopic fractionation (selective loss of ^{11}B) in the slab due to steeper thermal gradients and more pronounced dehydration [*Marschall et al*., 2009]. As long as fluid B/Nb values are large, and source B/Nb low, model curves in Figure 10c will converge to fluid δ^{11}B values after adding only small amounts (≪1%) of fluid, essentially forming "plateaus" approximating the fluid composition. Changing δ^{11}B values of the fluid additive would effectively shift the array of curves up or down (Figures 10c and 10d). For example, compositions of the anomalous Ata lavas could be produced if $\delta^{11}B_{SC}$ approaches MORB-like values (−5‰) in that region. We consider this scenario unlikely unless temperature conditions in the Ata source differ sufficiently from adjacent arc sectors to cause such a shift by isotopic fractionation (i.e., greater dehydration of the subducting slab in this area). Interestingly, B-enrichment in the lavas does decrease sharply south of Hunga Ha'apai (cf. Figures 4b–4d), and this is reflected in relatively low B/Nb (compared to all northern Tonga except Tafahi) estimated for the Ata source (Figure 7a). So there possibly is a thermal effect just north of Ata. On the other hand, a dehydration process that could lower δ^{11}B by ∼15‰ would also be expected to reduce B content and B/Nb to values well below those in the Ata lavas. As seen in Figure 10d, scatter in the TKNZ data is permissive of significant variation in source Nb/B ratios (from unity for New Zealand or Niuafo'ou, to 0.1 for Macauley and Raoul, and as low as 0.02 for Ata). A similar range is seen in the analyzed sediments, and presumably such variations could develop over time in the mantle wedge (equivalent to the offsets discussed in Figure 7). The simplest explanation for Ata may be that the subduction component there is completely different (with low $\delta^{11}B_{SC}$ and elevated B_{SC}).

A general explanation for source variability with regard to Nb/B is that this is controlled by regional differences in degree of presubduction mantle depletion, coupled with spatially variable later inputs of B from the subducting slab. The amount of subducted B is expected to be least near New Zealand (owing in part to a warmer slab) and in the back-arc regions (owing to progressive slab depletion). Because Nb/Zr and source Nb are evidently higher in those areas, we predict that they will be characterized by the highest Nb/B ratios (albeit significantly lower than the average NMORB source). Conversely, because most of the arc sits over mantle wedge domains that previously experienced the greatest melt extraction, arc magma sources there could have Nb contents approximately one fourth as high (ca. 0.05 ppm; supporting information Figure S2). In such mantle domains, slab-derived B enrichments will be proportionately larger. Using source Nb estimates (supporting information Table S1), and minimal Nb/B values for the Tonga and Kermadec sectors (cf. Figure 10), we estimate those local arc magma sources to have maximal B contents near 3.5 and nearly 2.0 ppm, respectively (supporting information Table S1 and Figure S2). Thus, maximal B-enrichments for the arc magma sources relative to DMM are nearly two orders of magnitude (at least ca. 80-fold).

Basalts from New Zealand and back-arc Niuafo'ou also have low δ^{11}B values (−1‰ to −6‰) overlapping those in many intraplate and mid-ocean ridge basalts. This is commonly the case for back-arc samples, where slab fluid inputs are inferred to be greatly diminished, and/or δ^{11}B values predicted to decrease with depth owing to progressive release of ^{11}B-enriched fluids from the subducting slab [*Ishihawa and Nakamura*, 1993; *Straub and Layne*, 2002; *Tonarini et al*., 2011; *Harvey et al*., 2014]. For New Zealand, where contributions of slab-derived fluids appear to be small, the mantle in this region could have a distinctive intraplate-like composition given similarity between B-Nd-Sr isotopic compositions of basalts there and at Niuafo'ou, where there is no continental or evolved oceanic crust. Still, mantle sources in both places have ca. 0.2 ppm B (supporting information Table S1 and Figure S2), and B/Nb ratios that are enriched more than 15-fold relative to typical oceanic island basalt sources (0.06 ± 0.02; *Ryan et al*. [1996]) and more than 5-fold

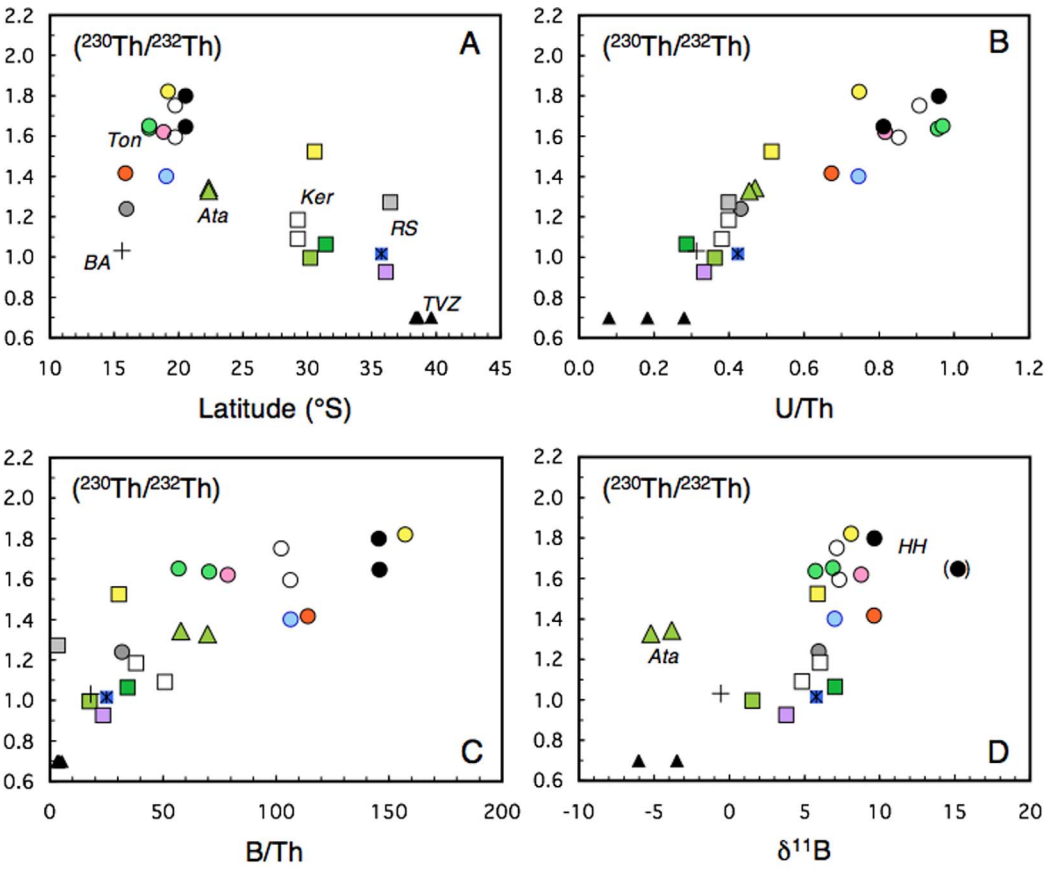

Figure 11. Diagrams showing variation in (^{230}Th/^{232}Th) activity ratio with (a) latitudinal position along the arc, and as functions of (b) U/Th, (c) B/Th, and (d) δ^{11}B. Positive correlations among all these parameters suggest that B-enrichment also is recent or "real-time." Th activity ratios are from *Turner et al.* [1997] for Tonga-Kermadec and extrapolated from *Price et al.* [2007] for New Zealand. All other data were measured on samples used in this study. Data symbols as in Figure 3.

relative to average NMORB. These enrichments are readily explained by addition of small amounts of B-rich fluids with low δ^{11}B.

5.4. Implications for U-Series Isotopes

In this section, we revisit implications of U-series isotopes in the context of the present study (Figure 11). Systematic variation in (^{230}Th/^{232}Th) activity ratios along the arc (Figure 11a) mimics spatial variations in other parameters (cf. Figure 4) that are linked to subduction contributions. The large range in (^{230}Th/^{232}Th) values in the TKNZ rocks most likely reflects a combination of prior melt depletion and any fluid addition of U to the wedge $>$ 350 ka ago [i.e., addition of U $<$ 8 ka ago will not change this ratio, but will lead to (^{238}U/^{230}Th) $>$ 1], whereas addition of U within $>$ 10 kyr and $<$ 350 ka will lead to associated increases in (^{230}Th/^{232}Th). Values of the (^{230}Th/^{232}Th) activity ratio in TKNZ lavas are strongly correlated with U/Th, B/Th, and δ^{11}B in samples analyzed for B content (Figures 11b–11d). These correlations clearly show that selective enrichment of U parallels that of B, both of which are consistent with infiltration of U-rich and B-rich fluids [cf. *Bali et al.*, 2011]. The extent of these enrichments is roughly proportional, and most extreme in the Tongan sector. It should be noted that low (^{230}Th/^{232}Th) values for New Zealand are taken from different samples [*Price et al.*, 2007], but are representative of all available data for that region. The two Ata basalts also appear to sample a source that experienced both B-enrichment and U-enrichment, again with distinctly lower δ^{11}B. Finally, differences between the back-arc sample (BA) and others from the arc front are consistent with diminished fluid input behind the arc.

We next re-examine the timing of slab contributions; that is, what is meant by "recent." On the U-Th equiline diagram (Figure 12), a notable feature of the Tonga-Kermadec rocks is their large range in both (^{230}Th/^{232}Th) versus (^{238}U/^{232}Th) activity ratios [*Regelous et al.*, 1997; *Turner et al.*, 1997]. Although the data

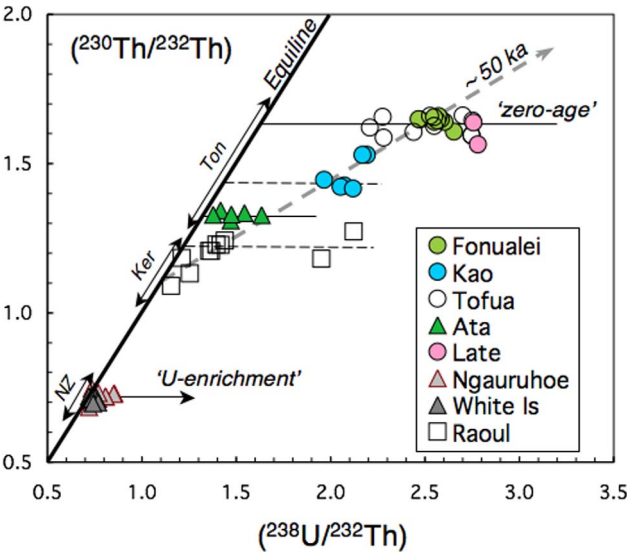

Figure 12. U-Th equiline diagram for TKNZ lavas. Data from *Turner et al.* [1997, 2012], *Heyworth et al.* [2007], *Price et al.* [2010], and *Caulfield et al.* [2012b]. All samples plotted are characterized by some degree of ^{226}Ra-disequilibrium that is taken to signify recent disturbance in the magma source. Note that magnitude of U-enrichment relative to the equiline generally increases toward the north (particularly in the Tonga sector; Figure 11a) where, owing to more rapid plate convergence, there is a proportionately larger subduction mass flux. Dashed gray line represents early interpretation that inferred an approximate "age" of 50 ka for the data array as a whole. Horizontal lines are consistent with most of the data for individual locations (with notable scatter for Kao and Raoul, that include older, less precise data); these imply near "zero-age" additions of U to local sources, with increasing magnitude toward the north as also seen in U/Nb (Figure 6d) or U/Th (Figure 11b) elemental ratios.

array was initially interpreted to reflect U addition to a uniform, sediment-modified mantle wedge composition (i.e., a single point where the sloped data array intersects the equiline) at ca. 50 ka, the B data presented here and new U-Th data obtained by *Caulfield et al.* [2012b] and *Turner et al.* [2012] suggest an alternative interpretation.

Both depletion of Th by melt extraction and episodic addition of U by fluids can lead to increases in mantle wedge U/Th ratio and, allowing for decay of ^{238}U, subsequent increases in (^{230}Th/^{232}Th). Thus, multistage scenarios in which both the extent of mantle wedge melt-depletion and relative addition of slab-derived fluids increase northwards along the arc predict that the corresponding resultant mantle wedge compositions will tend to move progressively up the equiline. As illustrated on Figure 12, data for most individual islands approximate subhorizontal arrays extending to the right of the equiline, and these generally step to higher (^{230}Th/^{232}Th) toward the north. The implication is that the U addition responsible for the observed U-Th disequilibria is relatively recent (i.e., within the last few millennia), which in turn suggests that the observed ^{226}Ra excesses [*Turner et al.*, 2000] are coupled and essentially reflect the same episodes of fluid addition. This interpretation nicely reconciles differences in the timing of fluid additions initially inferred from U-disequilibria and Ra-disequilibria data. Realistically, the fluid addition process has been ongoing since arc initiation, and element concentrations in the mantle wedge must be considered to be a time-integrated record of this process rather than a snapshot of only the most recent or "real-time" subduction effects. If presubduction depletion of Th and U in the mantle wedge is similar along central portions of the arc (i.e., as inferred for Nb), then the northward increasing magnitude of (^{238}U/^{232}Th) shifts must dominantly reflect northwardly increasing fluid flux (i.e., consistent with increasing convergence rate). This notion is supported by the correlation seen between magnitude of source U/Nb and calculated melt fractions (Figure 6d). As just discussed for B, the impact of fluid inputs on mantle composition may be amplified to the extent to which the mantle has been previously stripped of Th due to prior melt extraction.

These observations are consistent with general modification of the mantle wedge, and specifically arc magma sources, in response to infiltration of slab-derived fluids. The U-series data verify this to be a relatively recent (ongoing?) phenomenon, but the B data (especially offsets in B/Nb; Figure 7a) suggest some extended history of accumulation of the fluid mobile elements—the full extent of which may not be preserved with the short-lived radioisotopes.

5.5. Implications for Be Isotopes

Perhaps the most compelling indicator that near-surface materials in the downgoing slab are involved in subduction-related magmatism is the unique presence of cosmogenic ^{10}Be in many young arc lavas (cf. Figure 13). Relative enrichment of this tracer (measured as ^{10}Be/^{9}Be ratio) is well correlated with enrichment of B (as B/Be) in several arcs [*Morris et al.*, 1990]. *George et al.* [2005] report such data for T-K lavas (Figure 13a), that define a positive correlation between ^{10}Be/^{9}Be ratio and B/Be, but with several notable outliers (Raoul, Tofua, Metis Shoal). These authors attribute selective enrichments of ^{10}Be to involvement of a subducted

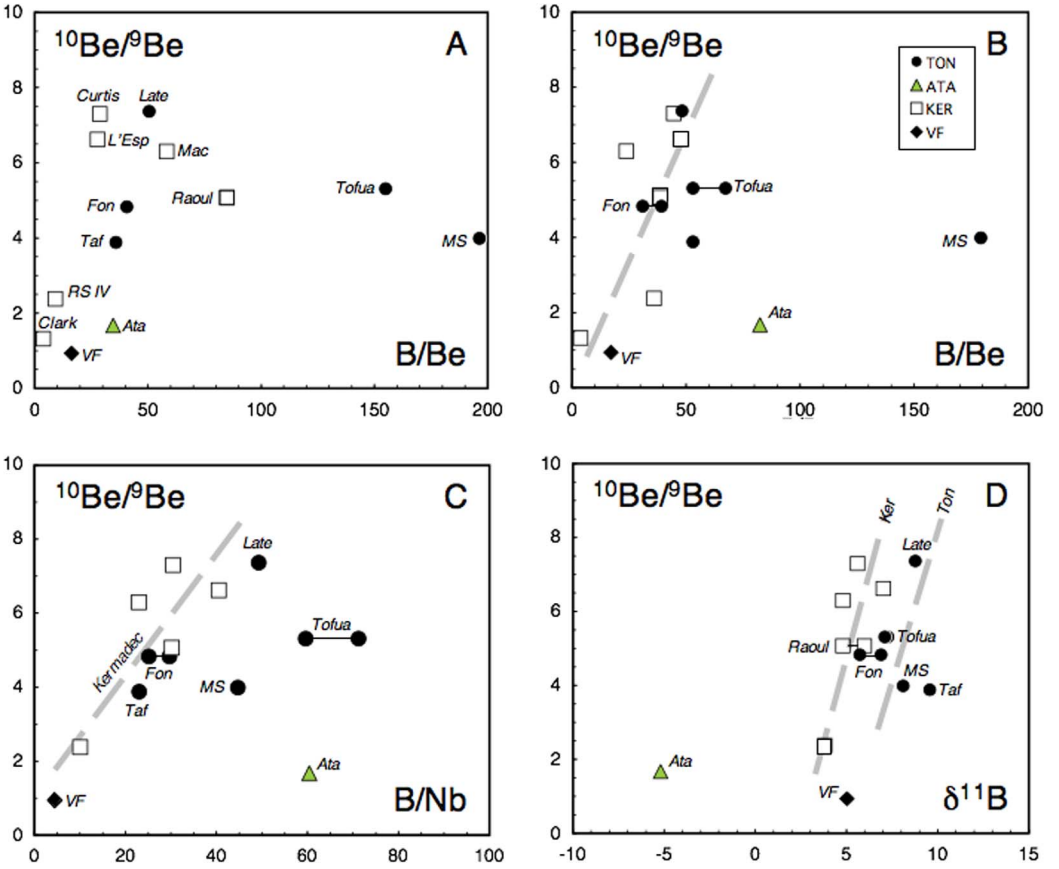

Figure 13. Plots of $^{10}Be/^{9}Be$ versus (a) B/Be, using data of *George et al*. [2005]; and (b) B/Be, (c) B/Nb, and (d) $\delta^{11}B$, using our data for the same or comparable samples. Note that in all but four cases the $^{10}Be/^{9}Be$ data are from different samples than those in our study. Horizontal bars connect samples with similar chemistry from the same island, indicating probable ranges in B/Be or B/Nb for these localities based on data from this study. Symbols are simplified to indicate affinity with Tonga (circles) or Kermadec (squares) sectors, as well as the unusual Ata and Valu Fa samples. Approximate trends in Figurex 13b and 13c for Kermadec samples (heavy dashed lines) highlight tentative correlations between B and Be systematics. In Figure 13d, two trend lines are shown, corresponding to the offset in $\delta^{11}B$ between Kermadec and Tonga lavas (cf. Figures 4a and 7a).

sedimentary component, although simple bulk addition of sediment seems precluded. We briefly review the constraints from Be isotope data, considering that positive $^{10}Be/^{9}Be$ values require enrichment of arc magma sources in slab-derived ^{10}Be, and magma generation and ascent within a time scale less than ca. 8 Ma (including subduction transport time). The latter constraint is based on the fact that the slab inventory of ^{10}Be decays with a half-life of 1.387 Ma [*Korshinek et al*., 2010]. It is commonly assumed that ^{10}Be resides largely in subducted sediments, and that its transport to the mantle wedge must be via a sediment melt component owing to the notion that Be is sparingly soluble in aqueous fluids. However, as previously noted, *You et al*. [1994] demonstrated that ^{10}Be is effectively mobilized from pelagic sediments by hydrothermal fluids at 350°C, and suggested the viability of Be transport via fluid mobilization in subduction zones. In this study, we also present evidence that Be is significantly enriched in TKNZ magma sources (Figure 7e), and that this parallels enrichments of B and U, both of which correlate with degree of melting to produce the arc lavas (Figures 6c and 6d). Thus, we consider that enrichments of both Be and B are facilitated by transport in slab-derived fluids. This does not preclude sediment melting as a contributing factor, but does raise doubt as to its necessity.

Direct comparison of our data with the Be data of *George et al*. [2005] is complicated by the fact that different samples were used in all but four cases. For the others, our results are combined with Be isotope data from *George et al*. [2005] for comparable samples to allow preliminary evaluation of the B-Be systematics. Because of discrepancies noted earlier regarding B concentration data, we compare the original B/Be data with ours (Figures 13a and 13b); for our samples we utilize Be concentrations in Table 2. Of the original

outliers, only Metis Shoal remains as a distinct outlier. Considering that this is one of the samples analyzed in common, and that the B data are in reasonable agreement, it is a confirmed anomaly. Because the Metis Shoal dacite (65% SiO_2) carries a disequilibrium assemblage of "phenocrysts" indicative of mixing between mafic and silicic magmas [*Ewart et al*., 1973], its significance is unclear. We also find that, using our B data for the Ata sample analyzed in common, it becomes an outlier in Figure 13b. In this case, our higher B content is substantiated by comparable data for a second Ata sample; thus, Ata stands out as anomalous in yet another regard. Comparing Be isotope data with B/Nb ratios, we again see a strong correlation between B and ^{10}Be enrichments (Figure 13c), but with the outliers of Ata, Metis Shoal, and now Tofua. Still, the overall correlation suggests that Be, like B, is plausibly transported by aqueous fluids.

Lastly, we compare the B and Be isotopic data for each location (Figure 13d). A reasonable correlation is evident between δ^{11}B and ^{10}Be/^{9}Be for Kermadec, whereas the Tonga data are largely clustered but offset to higher δ^{11}B reflecting the along-strike differences in δ^{11}B (cf. Figures 4 and 10). The sample from Ata stands alone and has the lowest ^{10}Be/^{9}Be and δ^{11}B values of all TKNZ samples. There is no a priori reason why these parameters need be directly linked, as ^{10}Be and B are likely hosted in different parts of the slab. That is, with B residing primarily in altered oceanic crust and/or serpentinized ultramafic lithologies [cf. *Tonarini et al*., 2011; *Ryan and Chauvel*, 2014], whereas ^{10}Be is preferentially concentrated in the uppermost sedimentary veneer (any inventory in deeper, older sediments presumably having decayed away).

However, the inferred correlation between B-enrichment and isotopic composition with ^{10}Be/^{9}Be for Kermadec samples is considered robust (evident in all panels of Figure 13) and is of particular significance. First, it is consistent with the notion that transport of B and Be into arc magma sources is linked by a common fluid infiltration process. Second, if ^{10}Be and B are derived primarily from the sediment veneer, a coupling of their enrichments would imply that temperatures near the slab surface must be cooler than the sediment solidus (otherwise B would be selectively attenuated by dehydration processes approaching such high temperatures). However, it is also possible that B-rich fluids originate from greater depths within the slab and entrain ^{10}Be from the uppermost slab sediments as they ascend—in which case, warmer slab surface temperatures could be viable. This scenario is compatible with the existence of multiple types or sources of slab components that may modify parts of the mantle wedge [cf. *Ryan and Chauvel*, 2014], albeit for TKNZ a fluid-dominated component seems adequate to explain available data for the arc lavas.

5.6. Implications for Subduction Zone Thermal Conditions and Sources of Boron

This study bolsters existing evidence that arc magmas are selectively enriched in boron, and in the TKNZ arc system such enrichments are among the highest known. The underlying cause for such enrichments has been attributed to selective transfer of boron from the subducting slab, which is considered to be a major repository for this element. The primary reservoirs for B in subduction zones are serpentinized peridotites that have reacted with seawater-related hydrothermal fluids in the shallow mantle, altered oceanic crustal rocks (gabbros and lavas) and the overlying sediments. Inventories of B in these materials, and B isotopic compositions of many, have been discussed extensively [*Leeman and Sisson*, 1996; *Bebout et al*., 1999; *Savov et al*., 2005; *Vils et al*., 2008, 2009; *Kodolányi et al*., 2012; *Deschamps et al*., 2013; *Harvey et al*., 2014; *Ryan and Chauvel*, 2014; *Martin et al*., 2016]. Boron systematics in sediments have been summarized by *Ishikawa and Nakamura* [1993]; *Leeman and Sisson* [1996] and *Romer et al*. [2014], and references therein; for our purposes the new analyses reported in this paper for DSDP/ODP cores offshore of the TKNZ arc are considered to be representative.

Extraction of boron from these sources is strongly supported by the correlated enrichments of B and ^{10}Be in modern arc lava suites [*Morris et al*., 1990], and this is the case for TKNZ [*George et al*., 2005]. On the other hand, the elevated δ^{11}B values observed in most of the volcanic front lavas are more consistent with compositions of abyssal peridotites and serpentinites (references cited above). Frontal arc erosion and subduction of such rocks is suggested by available geologic and geophysical surveys of the TKNZ arc system [e.g., *Contreras-Reyes et al*., 2011; *Timm et al*., 2014]. However, dehydration reactions during subduction (or equivalent metamorphic processing) commonly result in a progressive decrease of δ^{11}B in the residual slab materials owing to selective fractionation of heavy ^{11}B into the released fluids [*Scambelluri et al*., 2004; *Marschall et al*., 2007, 2009; *Tonarini et al*., 2007, 2011; *Martin et al*., 2016]. In some cases [*Scambelluri and Tonarini*, 2012] this may not occur, and elevated δ^{11}B values ($>20‰$) can be retained in serpentinized peridotites. In any case, the initial compositions of subducted slab materials are expected to be isotopically heavier than

fluids released from the slab directly beneath volcanic arcs [*Peacock and Hervig*, 1999]. The difference depends to some extent on the temperature gradient experienced during subduction, but could be as much as 5–10‰ based on empirical studies and models [*Marschall et al*., 2006, 2007]. With some exceptions, marine sediments and altered oceanic crust generally have δ^{11}B values [*Ishikawa and Nakamura*, 1992; *Smith et al*., 1995; *Yamaoka et al*., 2012; *Romer et al*., 2014] lower than observed in most volcanic front lavas from the Tonga and Kermadec arc sectors, and this is true for our data for sediments outboard the arc. Thus, considering the fractionation effects that accompany subduction, it seems improbable that such materials can account for the observed B compositions in the northern reaches of the arc. Previously altered and/or serpentinized ultramafic rocks similar to those sampled in the Mariana forearc [*Benton et al*., 2001; *Savov et al*., 2005] or the South Sandwich forearc [*Tonarini et al*., 2011] would be more suitable sources for B-rich fluids.

Juxtaposed against the prevalent trends for Tonga-Kermadec are the anomalous lavas from Fonualei and especially Ata that exhibit minor to large negative anomalies in δ^{11}B relative to adjacent volcanoes. Their proximity to impinging back-arc spreading centers raises the possibility that convective flow of warm back-arc mantle could accelerate dehydration of the slab (or perhaps metasomatized portions of the overlying mantle wedge), resulting in more dramatic lowering of δ^{11}B in proximal domains, hence in the fluids released therefrom. It is also possible that deeply subducted and more ^{11}B-depleted mantle upwells into the nascent spreading center [cf. *Escrig et al*., 2009, 2012], albeit such material would likely be B-depleted and thus have little leverage on B systematics in the present mantle wedge. In the case of Ata, the observation of relatively high B/Nb ratios seems antithetic to such scenarios and other alternatives should be considered. For example, *Timm et al*. [2013] have suggested that subduction of the Louisville seamounts beneath this region may have contributed radiogenic Pb to southern Tonga magma sources, including those of the Monowai seamounts and Ata. If so, it is possible that they also contributed B with OIB-like low δ^{11}B to the Ata magma source. The low ^{10}Be/^{9}Be value in one Ata sample as well as less radiogenic Sr and more radiogenic Nd in Ata lavas compared to nearby arc sectors (Figures 4 and 12) also set them apart from most other Tongan lavas, and are consistent with a distinctive (more OIB-like) source. Our analysis of one Louisville-derived volcaniclastic sediment has high δ^{11}B (+6.8‰) but, upon subduction, δ^{11}B values of such material could be lowered substantially. So, the real mystery of Ata boils down to how its source developed its high B/Nb-low δ^{11}B character. This question may be linked to long-term enrichment of B on a local scale, and cannot be resolved unambiguously with the limited data presently available.

The New Zealand lavas also present a complex enigma in that they have low δ^{11}B and relatively low B/Nb. Their radiogenic isotopes appear to require enhanced inputs of a crustal nature, and this may also account for their low δ^{11}B values. A quandary pertains to whether this can be attributed to greater subduction input of terrigenous sediment to mantle domains in southern reaches of the arc system versus inheritance (or contamination) from the underlying mantle or basement [cf. *Rooney and Deering*, 2014]. With regard to B systematics, in some diagrams, sediment compositions lie far afield from the lavas and we do not see a compelling control of magma compositions by the analyzed sediments. Because the terrigenous sediments shed off New Zealand likely are similar to basement rocks [Torlesse and similar metasediments; *Price et al*., 2015] they are hard to distinguish chemically. In any case, there is ample evidence that modern magmas of the Taupo Volcanic Zone have interacted with such basement rocks [e.g., *Gamble et al*., 1993a; *Price et al*., 2007, 2012]. Although we have no direct data on the local basement, comparison with high-grade metamorphic rocks from other regions suggest that they may have low B/Nb and δ^{11}B [cf. *Leeman et al*., 1992; *Palmer and Swihart*, 1996]. Also, low B/Nb and δ^{11}B may simply reflect ambient mantle composition as such characteristics are also observed in back-arc regions in many arcs, and in the northern Tonga region (this study), and may be typical of much of the Earth's mantle where it has not been impacted by subduction processes (such as has been proposed for the Cascades arc; *Leeman et al*. [2004]).

How boron is transported to domains within the mantle wedge, where arc magmas are produced, has been a long-standing question. The fact that the TKNZ arc system is one of the coolest subduction zones worldwide raises the possibility that slab temperatures beneath the arc front are below the solidus of most components in the slab. Predicted sub-arc slab surface temperatures range from ca. 800° beneath New Zealand to ca. 700°C beneath Tonga [*Syracuse et al*., 2010]. The latter is below estimates of the wet-solidi for pelitic sediments [*Johnson and Plank*, 1999; *Hermann and Spandler*, 2008, Figure 2], and both are well below the dry solidi at those depths. Moreover, the thermal models suggest the existence of a large temperature

gradient (>400°C) within the upper 10 km of the slab. Under such conditions fluids could be gradually released throughout hydrated portions of the slab. Such fluids would act as suitable transport media for fluid-mobile elements like B, and could trigger melting in overlying mantle wedge domains where temperatures exceed the wet solidus [*Spandler and Pirard*, 2013]. The extent to which other elements besides B are mobilized in such fluids and/or melts is not entirely clear owing to uncertainties in existing experimental constraints on element partitioning [*Johnson and Plank*, 1999, *Spandler et al*., 2007, 2014]. However, experimental studies indicate that at sufficiently high T-P conditions to form melts and/or supercritical fluids, it becomes increasingly difficult to selectively fractionate B from other incompatible elements as the "carrying capacities" of these media increase and virtually all elements become mobile to a significant extent [*Kessel et al*., 2005; *Dvir et al*., 2011; *Spandler et al*., 2014]. Our observations for the unusually cool TKNZ subduction system suggest that such conditions are not generally attained because B is selectively enriched in the arc magmas. As noted earlier, the propensity for B to be mobilized from progressively dehydrated and metamorphosed marine sediments and oceanic crustal rocks distinguishes it from refractory fluid-immobile elements (e.g., Zr, Hf, Nb, Ta, all of which have low fluid solubility and may be retained in accessory minerals). Conversely, because of its mobility, the B inventory in subducting oceanic crustal rocks and sediments is likely to be strongly attenuated long before the solidus is reached. Many aspects of TKNZ arc geochemistry are consistent with a dominantly fluid-based transport mechanism, with little compelling need to invoke melting of slab components except possibly in the vicinity of New Zealand. The common perception that a melt or supercritical fluid phase is required to explain element transport from subducting slabs to arc magma sources hinges to some extent on whether or not aqueous fluids are up to the task. The apparent correlations between B-enrichment, U-series isotopes and, tentatively, ^{10}Be provide support that this is the case, particularly for the Tonga-Kermadec sectors of the arc.

Finally, estimates of source compositions for a range of trace elements demonstrate systematic along-strike variations in melt-depletion for the TKNZ mantle, being most severe for southern Tonga. This is reflected in the chemistry of the arc lavas in that region (e.g., TiO_2 contents and Nb/Zr ratios well below values for average NMORB). Sources of these lavas must have had depleted incompatible element inventories that were easily leveraged by inputs from the subducting slab. For example, calculated sources for the modern arc lavas are systematically enriched in B, Ba, Th, U, LREE, and Be, with strongest enrichments corresponding to the most (previously) melt-depleted localities. Source abundances for more refractory (i.e., less fluid-mobile) elements Hf, Nb, and Zr are similarly depleted relative to MORB source mantle, and source Yb is relatively consistent along most of the arc, with notable compositional gradients at its the northern and southern ends. Calculated melt proportions needed to produce the arc lavas from these sources range from <10 to more than 30%, and show systematic gradients along the arc with maxima at Tonga, where sources are otherwise refractory. This implies that melt production is generally proportional to the magnitude of fluid flux beneath the arc, as represented by proxy ratios such as B/Nb, U/Nb, and Be/Nb. Boron isotopic compositions are loosely correlated with these latter parameters, but observed along-strike variations indicate a gradient in the nature of the subduction component, with δ^{11}B decreasing from Tonga to New Zealand, that could reflect warmer subduction zone conditions and stronger isotopic fractionation (i.e., ^{11}B losses) to the south.

These observations and inferences raise interesting questions regarding how arc magma sources are established in detail, and what actually causes melt generation. Correlated behavior of B and perhaps Be systematics with U-series systematics implies that transfer of these and other fluid-mobile elements by infiltration of slab-derived fluids must occur on time scales as short as millennia. However, details of the B systematics imply that the overall process could be cumulative and protracted over much longer time scales. A further implication is that regions of potential arc magma genesis could develop over broad temporal and spatial scales, say in relatively static domains within the lithospheric portion of the mantle wedge as well as in asthenospheric portions that may be convecting. It remains to be determined, then, what actually triggers melt production. It is tempting to conclude from the apparent correlation between melting degree and magnitude of B-enrichment in the TKNZ arc, that both are proportional to the amount of water added to the source (i.e., flux melting dominates). And, on the basis of our current understanding of short-lived isotopes, we infer that at least one pulse of fluid addition must be essentially synchronous with melt generation. However, evidence that B-enrichment is incremental and cumulative would imply that the full amount of aqueous fluid required to attain a given level of enrichment need not be present at the time of melt

production. Of course, the short-lived radioisotopes will not retain a complete record of this—leading to underestimates of magnitude of slab inputs. In which case, what was the physical effect of earlier fluid additions and where did they go? Moreover, the relatively high liquidus temperatures estimated for most TKNZ mafic magmas (cf. Table S1; *Cooper et al*. [2010]) seem inconsistent with melting simply due to fluid-induced solidus reduction. Certainly melting could be triggered by other means, some time following fluid additions—possibly due to decompression in ascending mantle flow. It remains to be evaluated whether this or other melting scenarios can be reconciled with the available temporal constraints.

6. Conclusions

New B concentration and isotope data from the Tonga-Kermadec-New Zealand arc show that many of the arc lavas extend to higher B/Nb and δ^{11}B than the subducting sediments. This observation implies that source B-enrichments are likely to derive from addition of aqueous fluids from the subducting altered oceanic crust or, more likely, underlying ultramafic rocks under relatively cool (i.e., subsolidus) conditions; contributions from sedimentary components are considered to be of second order to negligible importance except possibly in the southern reaches of the arc. Comparisons of B systematics with U-series isotopes and ^{10}Be systematics collectively support the concept that all are strongly influenced by fluid transport from a subducted slab. Such a model represents a significant departure from previous studies of this arc that stress the importance of element transport via sediment melts [e.g., *Turner et al*., 1997, 2012; *Ewart et al*., 1998; *George et al*., 2005; *Caulfield et al*., 2012a]. For example, elements such as Be and Th, that have been considered difficult to mobilize in aqueous fluids, display spatial variations in source enrichments (i.e., relative to Nb) similar to those of B, U (Figures 6 and 7), and Ba, suggesting that all are to some extent fluid-mobile. Thus, it appears possible to scavenge components such as ^{10}Be or Nd from subducted sediments (where they are concentrated) into ascending fluids, as has also been suggested previously for Hf [*Woodhead et al*., 2001] and for Th [*Hergt and Woodhead*, 2007]. This notion should be appraised by further studies of fluid partitioning under P-T conditions appropriate to this arc since the data presently available are to some extent contradictory [e.g., *Johnson and Plank*, 1999 or *Brenan et al*., 1995, 1998a, 1998b versus *Spandler et al*., 2007].

We also discern an inverse relation between source depletion and extent of B-enrichment. In detail, gradients in lava (and source) B/Nb ratios along the arc suggest that slab influence (e.g., fluid input, melting degree) peaks near southern Tonga (ca. 21°S) and systematically diminishes to the north and south. This pattern is consistent with overprinting of fluid additions on previously melt-depleted mantle, whereby the fluid has greatest leverage on the more depleted mantle domains [cf. *Gamble et al*., 1993; *Woodhead et al*., 1993; *Ewart et al*., 1998]. However, because degree of source depletion appears to be fairly uniform along much of the Tonga-Kermadec arc, the observed systematic spatial variations in lava compositions are likely dominated by the magnitude of overall subduction flux, which increases progressively with subduction rate northward from New Zealand. Second-order variations in lava chemistry (e.g., δ^{11}B, Th/Nb, La/Nb, Be/Nb) can be attributed to along-strike differences in the compositions and/or proportions of subducted materials.

Acknowledgments

We are especially grateful to Tony Ewart, John Gamble, Bill Hackett, Julian Pearce, Terry Plank, Tony Reay, Ian Smith, and Tracy Vallier for generously providing samples and information. We thank Peter Clift, Richard Price, Jeff Ryan, and Tim Worthington for discussions and Tim Elliott for encouragement. Richard Price kindly provided unpublished data for New Zealand samples. Finally, we thank Peter van Keken for sharing details of thermal models for the TKNZ arc, and Christoph Beier for drafting Figure 1 using GMT software. This work was partly supported by National Science Foundation grants EAR00-03612 and EAR04-09423 to WPL. Analytical work at Pisa was facilitated by support from Gruppo Nazionale de Volcanologia. SPT acknowledges support by a Royal Society University Research Fellowship and an Australian Federation Fellowship. Comments by three anonymous reviewers and editorial advice from Janne Blickert-Toft were helpful in improving this paper. Supporting data and citations of all original data sources are included in the supporting information (Table S1); any additional data information may be obtained from WPL (email: leeman@rice.edu).

References

Bali, E., A. Audétat, and H. Keppler (2011), The mobility of U and Th in subduction zone fluids: An indicator of oxygen fugacity and fluid salinity, *Contrib. Mineral. Petrol.*, *161*, 597–613, doi:10.1007/s00410-010-0552-9.

Barker, S. J., C. J. N. Wilson, J. A. Baker, M.-A. Millet, M. D. Rotella, I. C. Wright, and R. J. Wysoczanski (2013), Geochemistry and petrogenesis of silicic magmas in the intra-oceanic Kermadec arc, *J. Petrol.*, *54*, 351–391, doi:10.1093/petrology/egs071.

Bebout, G. E., J. G. Ryan, W. P. Leeman, and A. E. Bebout (1999), Fractionation of trace elements by subduction-zone metamorphism—Effect of convergent margin thermal evolution, *Earth Planet. Sci. Lett.*, *171*, 63–81, doi:10.1016/S0012-821X(99)00135-1.

Benton, L. D., J. G. Ryan, and F. Tera (2001), Boron isotope systematics of slab fluids as inferred from a serpentine seamount, Mariana forearc, *Earth Planet. Sci. Lett.*, *187*, 273–282, doi:10.1016/S0012-821X(01)00286-2.

Bevis, M., et al. (1995), Geodetic observations of very rapid convergence and back-arc extenstion at the Tonga arc, *Nature*, *374*, 249–251, doi:10.1038/374249a0.

Bonatti, E., J. R. Lawrence, and N. Morundi (1984), Serpentinization of oceanic peridotite: Temperature dependence of mineralogy and boron content, *Earth Planet. Sci. Lett.*, *70*, 88–94, doi:10.1016/0012-821X(84)90211-5.

Bourdon, B., S. Turner, and C. Allègre (1999), Melting dynamics beneath the Tonga-Kermadec island arc inferred from ^{231}Pa-^{235}U systematics, *Science*, *286*, 2491–2493, doi:10.1126/science.286.5449.2491.

Brenan, J. M., H. F. Shaw, F. J. Ryerson, and D. L. Phinney (1995), Mineral-aqueous fluid partitioning of trace elements at 900°C and 2.0 GPa: Constraints on the trace element chemistry of mantle and deep crustal fluids, *Geochim. Cosmochim. Acta*, *59*, 3331–3350, doi:10.1016/0016-7037(95)00215-L.

Brenan, J. M., E. Neroda, C. C. Lundstrom, H. F. Shaw, F. J. Ryerson, and D. L. Phinney (1998a), Behaviour of boron, beryllium, and lithium during melting and crystallization: Constraints from mineral-melt partitioning experiments, *Geochim. Cosmochim. Acta*, *62*, 2120–2141, doi:10.1016/S0016-7037(98)00131-8.

Brenan, J. M., F. J. Ryerson, and H. G. Shaw (1998b), The role of aqueous fluids in the slab-to-mantle transfer of boron, beryllium, and lithium during subduction, Experiments and models, *Geochim. Cosmochim. Acta*, *62*, 3337–3347, doi:10.1016/S0016-7037(98)00224-5.

Brounce, M., M. Feineman, P. LaFemina, and A. Gurenko (2012), Insights into crustal assimilation by Icelandic basalts from boron isotopes in melt inclusions from the 1783–1784 Lakagígar eruption, *Geochim. Cosmochim. Acta*, *94*, 164–180, doi:10.1016/j.gca.2012.07.002.

Burns, R. E., et al. (1973), Initial report for Site 203, *Initial Reports of the Deep-Sea Drilling Project*, vol. 21, pp. 33–56, Gov. Print. Off., Washington, D. C., doi:10.2973/dsdp.proc.21.103.1973.

Castillo, P. R., P. F. Lonsdale, C. L. Moran, and J. W. Hawkins (2009), Geochemistry of mid-Cretaceous Pacific crust being subducted along the Tonga-Kermadec Trench: Implications for the generation of arc lavas, *Lithos*, *112*, 87–102, doi:10.1016/j.lithos.2009.03.041.

Catanzaro, E. J., C. E. Champion, E. L. Garner, G. Malinenko, K. M. Sappenfield, and W. R. Shields (1970), Boric acid: Isotopic, and assay standard reference materials, *U.S. Nat. Bur. Stand. Spec. Publ. 260-17*, pp. 17–70, U.S. Gov. Print. Off., Washington, D. C.

Caulfield, J. T., S. P. Turner, A. Dosseto, N. J. Pearson, and C. Beier (2008), Source depletion and extent of melting in the Tongan sub-arc mantle, *Earth Planet. Sci. Lett.*, *273*, 279–288, doi:10.1016/j.epsl.2008.06.040.

Caulfield, J., S. Turner, R. J. Arculus, C. Dale, F. Jenner, J. Pearce, J., C. Macpherson, and H. Handley (2012a), Mantle flow, volatiles, slab-surface temperatures and melting dynamics in the north Tonga arc-Lau back-arc basin, *J. Geophys. Res.*, *117*, B11209, doi:10.1029/2012JB009526.

Caulfield, J. T., S. P. Turner, I. E. M. Smith, L. B. Cooper, and G. A. Jenner (2012b), Magma evolution in a primitive, intra-oceanic arc setting: Petrogenesis of basaltic-andesites at Tofua volcano, Tonga, *J. Petrol.*, *53*, 1197–1230, doi:10.1093/petrology/egs013.

Chan, L. H., W. P. Leeman, and C.-F. You (1999), Lithium isotopic composition of Central American Volcanic Arc lavas: Implications for modification of subarc mantle by slab-derived fluids, *Chem. Geol.*, *160*, 255–280, doi:10.1016/S0009-2541(99)00101-1.

Chan L. H., W. P. Leeman, and C.-F. You (2002), Lithium isotopic composition of Central American volcanic arc lavas: Implications for modification of subarc mantle by slab-derived fluids: A correction, *Chem. Geol.*, *182*, 293–300, doi:10.1016/S0009-2541(01)00298-4.

Chaussidon, M., and G. Libouret (1993), Boron partitioning in the upper mantle: An experimental and ion probe study, *Geochim. Cosmochim. Acta*, *57*, 5053–5062, doi:10.1016/0016-7037(93)90607-X.

Class, C., D. M. Miller, S. L. Goldstein, and C. H. Langmuir (2000), Distinguishing melt and fluid subduction components in Umnak volcanics. Aleutian arc, *Geochem. Geophys. Geosyst.*, *1*(6), 1004, doi:10.1029/1999GC000010.

Clift, P. D., E. Rose, N. Shimizu, G. Layne, A. E. Draut, and M. Regelous (2001), Tracing the evolving flux from the subducting plate in the Tonga-Kermadec arc system using boron in volcanic glass, *Geochim. Cosmochim. Acta*, *65*, 3347–3364, doi:10.1016/S0016-7037(01)00670-6.

Conder, J. A., and D. A. Wiens (2007), Rapid mantle flow beneath the Tonga volcanic arc, *Earth Planet. Sci. Lett.*, *264*, 299–307, doi:10.1016/j.epsl.2007.10.014.

Contreras-Reyes, E., I. Grevemeyer, A. B. Watts, E. R. Fluch, C. Peirce, S. Moeller, and C. Papenburg (2011), Deep seismic structure of the Tonga subduction zone: Implications for mantle hydration, tectonic erosion, and arc magmatism, *J. Geophys. Res.*, *116*, B10103, doi:10.1029/2011JB008434.

Cooper, L. B., T. Plank, R. J. Arculus, E. H. Hauri, P. S. Hall, and S. W. Parman (2010), High-Ca boninites from the active Tonga Arc, *J. Geophys. Res.*, *115*, B10206, doi:10.1029/2009JB006367.

Cooper, L. B., D. M. Ruscitto, T. Plank, P. J. Wallace, E. M. Syracuse, and C. E. Manning (2012), Global variations in H_2O/Ce, 1: Slab surface temperatures beneath volcanic arcs, *Geochem. Geophys. Geosyst.*, *13*, Q03024, doi:10.1029/2011GC003902.

Davidson, J., S. Turner, and T. Plank (2013), Dy/Dy*: Variations arising from mantle sources and petrogenetic processes, *J. Petrol.*, *54*, 525–538, doi:10.1093/petrology/egs076.

Deering, C. D., O. Bachmann, J. Dufek, and D. M. Gravley (2011), Rift-related transition from andesite to rhyolitic volcanism in the Taupo Volcanic Zone (New Zealand) controlled by crystal-melt dynamics in mush zones with variable mineral assemblages, *J. Petrol.*, *52*, 2243–2263, doi:10.1093/petrology/egr046.

Deschamps, F., M. Godard, S. Guillot, and K. Hattori (2013), Geochemistry of subduction zone serpentinites: A review, *Lithos*, *178*, 96–127, doi:10.1016/j.lithos.2013.05.019.

Dunn, R. A., and F. Martinez (2011), Contrasting crustal production and rapid mantle transitions beneath back-arc ridges, *Nature*, *469*, 198–202, doi:10.1038/nature09690.

Dvir, O., T. Pettke, P. Fumagali, and R. Kessel (2011), Fluids in the peridotite-water system up to 6 GPa and 800°C: New experimental constraints on dehydration reactions, *Contrib. Mineral. Petrol.*, *161*, 829–844, doi:10.1007/s00410-010-0567-2.

Elliott, T., T. Plank, A. Zindler, W. M. White, and B. Bourdon (1997), Element transport from subducted slab to juvenile crust at the Mariana Arc, *J. Geophys. Res.*, *102*, 14,991–15,019.

Ellis, A. J., and J. R. Sewell (1963), Boron in waters and rocks of New Zealand hydrothermal areas, *N.Z. J. Sci.*, *6*, 589–606.

England, P. C., and C. Wilkins (2004), A simple analytical approximation to the temperature structure in subduction zones, *Geophys. J. Int.*, *159*, 1138–1154, doi:10.1111/j.1365-246X.2004.02419.x.

England, P. C., and R. F. Katz (2010), Melting above the anhydrous solidus controls the location of volcanic arcs, *Nature*, *467*, 700–704, doi:10.1038/nature09417.

Escrig, S., A. Bézos, S. L. Goldstein, C. H. Langmuir, and P. J. Michael (2009), Mantle source variations beneath the Eastern Lau Spreading Center and the nature of subduction components in the Lau basin-Tonga arc system, *Geochem. Geophys. Geosyst.*, *10*, Q04014, doi:10.1029/2008GC002281.

Escrig, S., A. Bézos, C. H. Langmuir, P. J. Michael, and R. Arculus (2012), Characterizing the effect of mantle source, subduction input and melting in the Fonualei Spreading Center, Lau Basin: Constraints on the origin of the boninitic signature of the back-arc lavas, *Geochem. Geophys. Geosyst.*, *13*, Q10008, doi:10.1029/2012GC004130.

Ewart, A., and C. J. Hawkesworth (1987), The Pleistocene-Recent Tonga-Kermadec arc lavas: Interpretation of new isotopic and rare earth data in terms of a depleted mantle source model, *J. Petrol.*, *28*, 495–530, doi:10.1093/petrology/28.3.495.

Ewart, A., W. B. Bryan, and J. Gill (1973), Mineralogy and geochemistry of the younger volcanic islands of Tonga, southwest Pacific, *J. Petrol.*, *14*, 429–465, doi:10.1093/petrology/14.3.429.

Ewart, A., K. D. Collerson, M. Regelous, J. I. Wendt, and Y. Niu (1998), Geochemical evolution within the Tonga-Kernadec-Lau arc-back-arc systems: The role of varying mantle wedge composition in space and time, *J. Petrol.*, *39*, 331–368, doi:10.1093/petroj/39.3.331.

Falloon, T. J., L. V. Danyushevsky, T. J. Crawford, R. Maas, J. D. Woodhead, S. M. Eggins, S. H. Bloomer, D. J. Wright, S. K. Zlobin, and A. R. Stacey (2007), Multiple mantle plume components involved in the petrogenesis of subduction-related lavas from the northern termination of the Tonga Arc and northern Lau Basin: Evidence from the geochemistry of arc and back-arc submarine volcanics, *Geochem. Geophys. Geosyst.*, *8*, Q09003, doi:10.1029/2007GC001619.

Gale A., C. A. Dalton, C. H. Langmuir, Y. Su, and J.-G. Schilling (2013), The mean composition of ocean ridge basalts, *Geochem. Geophys. Geosyst.*, *14*, 489–518, doi:10.1029/2012GC004334.

Gamble, J. A., I. E. M., Smith, I. J. Graham, B. P. Kokelaar, J. W. Cole, B. F. Houghton, and C. J. N. Wilson (1990), The petrology, phase relations and tectonic setting of basalts from the Taupo Volcanic Zone, New Zealand and the Kermadec Island Arc-Havre Trough, S.W. Pacific, *J. Volcanol. Geotherm. Res.*, *43*, 253–270, doi:10.1016/0377-0273(90)90055-K.

Gamble, J. A., I. E. M. Smith, M. T. McCulloch, I. J. Graham, and P. Kokelaar (1993a), The geochemistry and petrogenesis of basalts from the Taupo Volcanic Zone and Kermadec Arc, S.W. Pacific, *J. Volcanol. Geotherm. Res.*, *54*, 265–290, doi:10.1016/0377-0273(93)90067-2.

Gamble, J. A., I. C. Wright, and J. A. Baker (1993b), Seafloor geology and petrology in the oceanic to continental transition zone of the Kermadec-Harve-Taupo Volcanic arc system, New Zealand, *N.Z. J. Geol. Geophys.*, *36*, 417–435, doi:10.1080/00288306.1993.9514588.

Gamble, J. A., J. D. Woodhead, I. C. Wright, and I. E. M. Smith (1996), Basalt and sediment geochemistry and magma petrogenesis in a transect from oceanic island arc to rifted continental margin arc: The Kermadec-Hikurangi margin, SW Pacific, *J. Petrol.*, *37*, 1523–1546, doi:10.1093/petrology/37.6.1523.

Gamble, J. A., R. H. K. Christie, I. C. Wright, and R. J. Wysoczanski (1997), Primitive K-rich magmas from Clark volcano, southern Kermadec Arc: A paradox in the K-depth relationship, *Can. Min.*, *35*, 275−290.

Gamble, J. A., C. P. Wood, R. C. Price, I. E. M. Smith, R. B. Stewart, and T. Waight (1999), A fifty year perspective of magmatic evolution on Ruapehu Volcano, New Zealand: Verification of open system behaviour in an arc volcano, *Earth Planet. Sci. Lett.*, *170*, 301–314, doi:10.1016/S0012-821X(99)00106-5.

Genske, F. S., S. P. Turner, C. Beier, M.-F. Chu, S. Tonarini, N. J. Pearson, and K. M. Haase (2014), Lithium and boron isotope systematics in lavas from the Azores islands reveal crustal assimilation, *Chem. Geol.*, *373*, 27–36, doi:10.1016/j.chemgeo.2014.02.024.

George, R., S. Turner, J. Morris, T. Plank, C. Hawkesworth, and J. Ryan (2005), Pressure-temperature-time paths of sediment recycling beneath the Tonga-Kermadec arc, *Earth Planet. Sci. Lett.*, *233*, 195–211, doi:10.1016/j.epsl.2005.01.020.

Gonfiantini, R., et al. (2003), Intercomparison of boron isotope and concentration measurements. Part II: Evaluation of results, *Geostand. Newslett.*, *27*, 41–57, doi:10.1111/j.1751-908X.2003.tb00711.x.

Govindaraju, K. (1994), 1994 compilation of working values and sample description for 383 geostandards, *Geostand. Newslett.*, *18*(S1), 158 pp., doi:10.1046/j.1365-2494.1998.53202081.x-i1.

Graham, I. J., and W. R. Hackett (1987), Petrology of calc-alkaline lavas from Ruapehu volcano and related vents, Taupo Volcanic Zone, New Zealand, *J. Petrol.*, *28*, 531–567, doi:10.1093/petrology/28.3.531.

Gribble, R. F., R. J. Stern, S. Newman, S. H. Bloomer, and T. O'Hearn (1998), Chemical and isotopic composition of lavas from the Northern Mariana Trough: Implications for magma genesis in back-arc basins, *J. Petrol.*, *39*, 125–154, doi:10.1093/petroj/39.1.125.

Haase, K. M., T. J. Worthington, P. Stoffers, D. Garbe-Schönberg, and I. Wright (2002), Mantle dynamics, element recycling, and magma genesis beneath the Kermadec Arc-Havre Trough, *Geochem. Geophys. Geosyst.*, *3*(11), 1071, doi:10.1029/2002GC000335.

Harmon, N., and D. K. Blackman (2010), Effects of plate boundary geometry and kinematics on mantle melting beneath the back-arc spreading centers along the Lau Basin, *Earth Planet. Sci. Lett.*, *298*, 334–346, doi:10.1016/j.epsL2010.08.004.

Harvey, J., C. J. Garrido, I. Savov, S. Agostini, J. A. Padrón, C. Marchesi, V. L. Sánchez-Vizcaíno, and M. T. Gómez-Pugnaire (2014), ^{11}B-rich fluids in subduction zones: The role of antigorite dehydration in subducting slabs and boron isotope heterogeneity in the mantle, *Chem. Geol.*, *376*, 20–30, doi:10.1016/j.chemgeo.2014.03.015.

Hattori, K. H., and S. Guillot (2003), Volcanic fronts form as a consequence of serpentinite dehydration in the forearc mantle wedge, *Geology*, *31*, 525–528, doi:10.1130/0091-7613(2003)031 < 052.

Hayes, G. P., D. J. Wald, and R. L. Johnson (2014), Slab 1.0: A three-dimensional model of global subduction zone geometries, *J. Geophys. Res.*, *117*, B01302, doi:10.1029/2011JB008524.

Hergt, J. M., and J. D. Woodhead (2007), A critical evaluation of recent models for Lau—Tonga arc—Back-arc basin magmatic evolution, *Chem. Geol.*, *245*, 9–44, doi:10.1016/j.chemgeo.2007.07.022.

Hermann, J., and C. Spandler (2008), Sediment melts at sub-arc depths: An experimental study, *J. Petrol.*, *49*, 717–740, doi:10.1093/petrology/egm073.

Heyworth, Z., S. Turner, B. Schaefer, B. Wood, R. George, K. Berlo, H. Cunningham, R. Price, C. Cook, and J. Gamble (2007), ^{238}U-^{230}Th-^{226}Ra-^{210}Pb constraints on the genesis of high-Mg andesites at White Island, New Zealand, *Chem. Geol.*, *243*, 105–121, doi:10.1016/j.chemgeo.2007.05.012.

Ishikawa, T., and E. Nakamura (1992), Boron isotope geochemistry of the oceanic crust from DSDP/ODP Hole 504B, *Geochim. Cosmochim. Acta*, *56*, 1633–1639, doi:10.1016/0016-7037(92)90230-G.

Ishikawa, T., and E. Nakamura (1993), Boron isotope systematics of marine sediments, *Earth Planet. Sci. Lett.*, *117*, 567–580, doi:10.1016/0012-821X(93)90103-G.

Ishikawa, T., and E. Nakamura (1994), Origin of the slab component in arc lavas from across-arc variation of B and Pb isotopes, *Nature*, *370*, 205–208, doi:10.1038/370205a0.

Ishikawa, T., and F. Tera (1997), Source, composition and distribution of the fluid in the Kurile mantle wedge: Constraints from across-arc variations of B/Nb and B isotopes, *Earth Planet. Sci. Lett.*, *152*, 123–138, doi:10.1016/S0012-821X(97)00144-1.

Ishikawa, T., and F. Tera (1999), Two isotopically distinct fluid components involved in the Mariana arc: Evidence from Nb/B and B, Sr, Nd, and Pb isotope systematics, *Geology*, *27*, 83–86, doi:10.1130/0091-7613(1999)027 < 008.

Ishikawa, T., F. Tera, and T. Nakazawa (2001), Boron isotope and trace element systematics of the three volcanic zones in the Kamchatka arc, *Geochim. Cosmochim. Acta*, *65*, 4523–4537, doi:10.1016/S0016-7037(01)00765-7.

Jochum, K. P., U. Nohl, K. Herwig, E. Lammel, B. Stoll, and A. W. Hofmann (2005), GeoReM: A new geochemical database for reference materials and isotopic standards, *Geostand. Geoanal. Res.*, *29*, 333–338, doi:10.1111/j.1751-908X.2005.tb00904.x.

Johnson, M. C., and T. Plank (1999), Dehydration and melting experiment constrain the fate of subducted sediments, *Geochem. Geophys. Geosyst.*, *1*(12), 1007, doi:10.1029/1999GC000014.

Kamenetsky, V. S., A. J. Crawford, S Eggins, and R. Mibe (1997), Phenocryst and melt inclusion chemistry of near-axis seamounts, Valu Fa Ridge, Lau Basin: Insight into mantle wedge melting and the addition of subduction components, *Earth Planet. Sci. Lett.*, *151*, 205–223, doi:10.1016/S0012-821X(97)81849-3.

Keller, N. S., R. J. Arculus, J. Hermann, and S. Richards (2008), Submarine back-arc lava with arc signature: Fonualei Spreading Center, northeast Lau Basin, Tonga, *J. Geophys. Res.*, *113*, B08S07, doi:10.1029/2007JB005451.

Kelley, K. A., T. Plank, J. Ludden, and H. Staudigel (2003), Composition of altered oceanic crust at ODP sites 801 and 1149, *Geochem. Geophys. Geosyst.*, *4*, doi:10.1029/2002GC000435.

Kelley, K. A., T. Plank, T. L. Grove, E. M. Stolper, S. Newman, and E. Hauri (2006), Mantle melting as a function of water content beneath back-arc basins, *J. Geophys. Res.*, *111*, B09208, doi:10.1029/2005JB003732.

Kessel, R., M. W. Schmidt., P. Ulmer, and T. Pettke (2005), Trace element signature of subduction-zone fluids, melts and supercritical liquids at 120–180 km depth, *Nature*, *437*, 724–727, doi:10.1038/nature03971.

Klimm, K., J. D. Blundy, and T. H. Green (2008), Element partitioning and accessory phase saturation during H_2O-saturated melting of basalt with implications for subduction zone chemical fluxes, *J. Petrol.*, *49*, 523–553, doi:10.1093/petrology/egn001.

Kodolányi, J., T. Pettke, C. Spandler, B. S. Kamber, and K. Gméling (2012), Geochemistry of ocean floor and fore-arc serpentinites: Constraints on the ultramafic input to subduction zones, *J. Petrol. 53*, 235–270, doi:10.1093/petrology/egr058.

Konrad-Schmolke, M., and R. Halama (2014), Combined thermodynamic-geochemical modeling in metamorphic geology: Boron as tracer of fluid-rock interaction, *Lithos*, *208*, 393–414, doi.org/10.1016/j.lithos.2014.09.021.

Korschinek, G., et al. (2010), A new value for the half-life of ^{10}Be by heavy-ion elastic recoil detection, *Nucl. Instr. Meathods Phys. Res. B*, *268*, 187–191, doi:10.1016/j.nimb.2009.09.020.

Lee, C.-T. A., P. Luffi, T. Plank, H. Dalton, and W. P. Leeman (2009), Constraints on the depths and temperatures of basaltic magma generation on Earth and other terrestrial planets using new thermobarometers for mafic magmas, *Earth Planet. Sci. Lett.*, *279*, 20–33, doi:10.1016/j.epsl.2008.12.020.

Leeman, W. P. (1988), Boron contents in selected international geochemical reference samples, *Geostand. Newslett.*, *12*, 61–62, doi:10.1111/j.1751-908X.1988.tb00043.x.

Leeman, W. P. (1996), Boron and other fluid-mobile elements in volcanic arc lavas: Implications for subduction processes, in *Subduction Top to Bottom, Geophys Monogr. Ser.*, vol. 96, edited by G. E. Bebout et al., pp. 269–276, AGU, Washington, D. C., doi:10.1029/GM096p0269.

Leeman, W. P., and V. B. Sisson (1996), Geochemistry of boron and its implications for mantle and crustal processes, in *Boron: Mmineralogy, Ppetrology and Geochemistry. Reviews in Mineralogy*, vol. 33, edited by E. S. Grew and L. M. Anovitz, pp. 645–707, Min. Soc. Am., Washington, D. C.

Leeman, W. P., V. B. Sisson, and M. R. Reid (1992), Boron geochemistry of the lower crust: Evidence from granulite terranes and deep crustal xenoliths, *Geochim. Cosmochim. Acta*, *56*, 775–788, doi:10.1016/0016-7037(92)90097-3.

Leeman, W. P., M. J. Carr, and J. D. Morris (1994), Boron geochemistry of the Central American volcanic arc: Constraints on the genesis of subduction-related magmas, *Geochim. Cosmochim. Acta*, *58*, 149–168, doi:10.1016/0016-7037(94)90453-7.

Leeman, W. P., S. Tonarini, L. H. Chan, and L. M. Borg (2004), Boron and lithium isotopic variations in a hot subduction zone—The southern Washington Cascades, *Chem. Geol.*, *212*, 101–124, doi:10.1016/j.chemgeo.2004.08.010.

Leeman, W. P., J. F. Lewis, R. C. Evarts, R. M. Conney, and M. J. Streck (2005a), Petrologic constraints on the thermal structure of the Cascades arc, *J. Volcanol. Geotherm. Res.*, *140*, 67–105, doi:10.1016/j.jvolgeores.2004.07.016.

Leeman, W. P., S. Tonarini, M. Pennisi, and G. Ferrara (2005b), Boron isotopic variation in fumarolic condensates and thermal waters from Vulcano Island, Italy: Implications for evolution of volcanic fluids, *Geochim. Cosmochim. Acta*, *69*, 143–163, doi:10.1016/j.gca.2004.04.004.

LeRoux, P. J., S. B. Shirey, L. Benton, E. H. Hauri, and T. D. Mock (2004), In situ, multiple multiplier, laser ablation ICP-MS measurement of boron isotopic composition (δ^{11}B) at the nanogram level, *Chem. Geol.*, *203*, 123–138, doi:10.1016/j.chemgeo.2003.09.006.

Lytle, M. L., K. A. Kelley, E. H. Hauri, J. B. Gill, D. Papia, and R. J. Arculus (2012), Tracing mantle sources and Samoan influence in the northwestern Lau back-arc basin, *Geochem. Geophys. Geosyst.*, *13*, Q10019, doi:10.1029/2012GC004233.

Macpherson, C. G., J. A. Gamble, and D. P. Mattey (1998), Oxygen isotope geochemistry of lavas from an oceanic to continental arc transition, Kermadec-Hikurangi margin, SW Pacific, *Earth Planet. Sci. Lett.*, *160*, 609–621, doi:10.1016/S0012-821X(98)00115-0.

Manea, V. C., W. P. Leeman, T. Gerya, M. Manea, and G. Zhu (2014), Subduction of fracture zones controls mantle melting and geochemical signature above slabs, *Nat. Comm.*, *5*, 5095, doi:10.1038/ncomms6095.

Marschall, H. R., T. Ludwig, R. Altherr, A. Kalt, A., and S. Tonarini (2006), Syros metasomatic tourmaline: Evidence for very high-δ^{11}B fluids in subduction zones, *J. Petrol.*, *47*, 1915–1942, doi:10.1093/petrology/egl031.

Marschall, H. R., R. Altherr, and L. Rüpke, (2007), Squeezing out the slab—Modeling the release of Li, Be and B during progressive high-pressure metamorphism, *Chem. Geol.*, *239*, 323–335, doi:10.1016/j.chemgeo.2006.08.008.

Marschall, H. R., R. Altherr, K. Gmelling, and Z. Kasztovsky (2009), Lithium, boron and chlorine as tracers for metasomatism in high-pressure metamorphic rocks: A case study from Syros (Greece), *Mineral. Petrol.*, *95*, 291–302, doi10.1007/s00710-008-0032-3.

Martin, C., K. E. Flores, and G. E. Harlow (2016) Boron isotopic discrimination for subduction-related serpentinites, *Geology*, *44*, 899–902, doi:10.1130/G38102.1.

McCulloch, M. T., and J. A. Gamble (1991), Geochemical and geodynamical constraints on subduction zone magmatism, *Earth Planet. Sci. Lett.*, *102*, 358–374, doi:10.1016/0012-821X(91)90029-H.

McDonough, W. F., and S.-S. Sun (1995), The composition of the Earth, *Chem. Geol.*, *120*, 223–253, doi:10.1016/0009-2541(94)00140-4.

Menke, W., Y. Zha, S. C. Webb, and D. K. Blackman (2015), Seismic anisotropy indicates ridge-parallel asthenospheric flow beneath the Eastern Lau Spreading Center, *J. Geophys. Res. Solid Earth*, *120*, 976–992, doi:10.1002/2014JB011154.

Millot, R., A. Hegan, and P. Négrel (2012), Geothermal waters from the Taupo Volcanic Zone, New Zealand: Li, B and Sr isotopes characterization, *Appl. Geochem.*, *27*, 677–688, doi:10.1016/j.apgeochem.2011.12.015.

Moran, A. E., V. B. Sisson, and W. P. Leeman (1992) Boron depletion during progressive metamorphism: Implications for subduction processes, *Earth Planet. Sci. Lett.*, *111*, 331–349, doi:10.1016/0012-821X(92)90188-2.

Morris, J. D., W. P. Leeman, and F. Tera (1990), The subducted component in island arc lavas: Constraints from Be isotopes and B-Be systematics, *Nature*, *344*, 31–36, doi:10.1038/344031a0.

Nagaishi, K., and T. Ishikawa (2009), A simple method for the precise determination of boron, zirconium, niobium, hafnium and tantalum using ICP-MS and new results for rock reference samples, *Geochem. J.*, *43*, 133–141.

Noll, P. D., H. Newsom, H., W. P. Leeman, and J. G. Ryan (1996), The role of hydrothermal fluids in the production of subduction zone magmas: Evidence from siderophile and chalcophile trace elements and boron, *Geochim. Cosmochim. Acta*, *60*, 587–611, doi:10.1016/0016-7037(95)00405-X.

Ottolini, L., B. Le Fevre, and R. Vannucci (2004), Direct assessment of mantle boron and lithium contents and distribution by SIMS analyses of peridotite minerals, *Earth Planet. Sci. Lett.*, *228*, 19–36, doi:10.1016/j.epsl.2004.09.027.

Pabst, S., T. Zack, I. P. Savov, T. Ludwig, D. Rost, S. Tonarini, and E. Vicenzi (2012), The fate of subducted oceanic slabs in the shallow mantle: Insights from boron isotopes and light element composition of metasomatized blueschists from the Mariana forearc, *Lithos*, *132–133*, 162–179, doi:10.1016/j.lithos.2011.11.010.

Padrón-Navarta, J. A., V. López Sánchez-Vizcaino, J. Hermann, J. A. D. Connolly, C. J. Garrido, M. T. Gómez-Pugnaire, and C. Marchesi (2013), Tschermak's substitution in antigorite and consequences for phase relations and water liberation in high-grade serpentinites, *Lithos*, *15*, 186–196, doi:10.1016/j.lithos.2013.02.001.

Palmer, M. R., and G. H. Swihart (1996), Boron isotope geochemistry: An overview, in *Boron: Mineralogy, Petrology and Geochemistry, Reviews in Mineralogy*, vol. 33, edited by E. S. Grew and L. M. Anovitz, pp. 709–744, Min. Soc. Am., Washington, D. C.

Peacock, S. M., and R. L. Hervig (1999), Boron isotopic composition of subduction-zone metamorphic rocks, *Chem. Geol.*, *160*, 281–290, doi: 10.1016/S0009-2541(99)00103-5.

Pearce, J. A., and D. W. Peate (1995), Tectonic implications of the composition of volcanic arc magmas, *Annu. Rev. Earth Planet. Sci. Lett.*, *23*, 251–285, doi:10.1146/annurev.ea.23.050195.001343.

Pearce, J. A., R. J. Stern, S. H. Bloomer, and P. Fryer (2005), Geochemical mapping of the Mariana arc-basin system: Implications for the nature and distribution of subduction components, *Geochem. Geophys. Geosyst.*, *6*, Q07006, doi:10.1029/2004GC000895.

Pennisi, M., W. P. Leeman, S. Tonarini A. Pennisi, and P. Nabelek (2000), Boron, Sr, O, and H isotope geochemistry of groundwaters from Mt. Etna (Sicily)—Hydrologic implications, *Geochim. Cosmochim. Acta*, *64*, 961–974, doi:10.1016/S0016-7037(99)00382-8.

Pfänder, J. A., C. Munker, A. Stracke, and K. Mezger (2007), Nb/Ta and Zr/Hf in ocean island basalts—Implications for crust-mantle differentiation and the fate of niobium, *Earth Planet. Sci. Lett.*, *254*, 158–172, doi:10.1016/j.epsl.2006.11.027.

Plank, T. (2005), Constraints from Thorium/Lanthanum on sediment recycling at subduction zones and the evolution of the continents, *J. Petrol.*, *46*, 921–944, doi:10.1093/petrology/egi005.

Plank, T. (2014), The chemical composition of subducting sediments, in *Treatise on Geochemistry*, 2nd ed., vol. 4, edited by H. D. Holland and K. K. Turekian, pp. 607–629, Elsevier, Amsterdam, doi:10.1016/B978-0-08-095975-7.00319-3.

Plank, T., and C. H. Langmuir (1998), The chemical composition of subducted sediment and its consequences for the crust and mantle, *Chem. Geol.*, *145*, 325–394, doi:10.1016/S0009-2541(97)00150-2.

Price, R. C., J. A. Gamble, I. E. M. Smith, R. B. Stewart, S. Eggins, and I. C. Wright (2005), An integrated model for the temporal evolution of andesites and rhyolites and crustal development in New Zealand's North Island, *J. Volcanol. Geotherm. Res.*, *140*, 1–24, doi:10.1016/j.jvolgeores.2004.07.013.

Price, R. C., R. George, J. A. Gamble, S. Turner, I. E. M. Smith, C. Cook, B Hobden, and A. Dosseto (2007), U-Th-Ra fractionation during crustal-level andesite formation at Ruapehu volcano, New Zealand, *Chem. Geol.*, *244*, 437–451, doi:10.1016/j.chemgeo.2007.07.001.

Price, R. C., S. Turner, C. Cook, B. Hobden, I. E. M. Smith, J. A. Gamble, H. Handley, R. Maas, and A. Möbis (2010), Crustal and mantle influences and U-Th-Ra disequilibrium in andesitic lavas of Ngauruhoe volcano, New Zealand, *Chem. Geol.*, *277*, 355–373, doi:10.1016/j.chemgeo.2010.08.021.

Price, R. C., J. A. Gamble, I. E. M. Smith, R. Maas, T. Waight, R. B. Stewart, and J. Woodhead (2012), The anatomy of an andesite volcano: A time-stratigraphic study of andesite petrogenesis and crustal evolution at Ruapehu Volcano, New Zealand, *J. Petrol.*, *53*, 2139–2189, doi: 10.1093/petrology/egs050.

Price, R. C., N. Mortimer, I. E. M. Smith, and R. Maas (2015), Whole-rock geochemical reference data for Torlesse and Waipapa terranes, North Island, New Zealand, *N.Z. J. Geol. Geophys.*, *58*, 213–228, doi:10.1080/00288306.2015.1026832.

Regelous, M., K. D. Collerson, A. Ewart, and J. I. Wendt (1997), Trace element transport rates in subduction zones: Evidence from Th, Sr and Pb isotope data for Tonga-Kermadec arc lavas, *Earth Planet. Sci. Lett.*, *150*, 291–302, doi:10.1016/S0012-821X(97)00107-6.

Regelous, M., S. Turner, T. J. Falloon, P. Taylor, J. Gamble, and T. Green (2008), Mantle dynamics and mantle melting beneath Niuafo'ou Island and the northern Lau back-arc basin, *Contrib. Mineral. Petrol.*, *156*, 103–118, doi:10.1007/s00410-007-0276-7.

Regelous, M., J. A. Gamble, and S. P. Turner (2010), Mechanism and timing of Pb transport from subducted oceanic crust and sediment to the mantle source of arc lavas, *Chem. Geol.*, *273*, 46–54, doi:10.1016/j.chemgeo.2010.02.011.

Rooney, T. O., and C. D. Deering (2014), Conditions of melt generation beneath the Taupo Volcanic Zone: The influence of heterogeneous mantle inputs on large-volume silicic systems, *Geology*, *42*, 3–6, doi:10.1130/G34868.1.

Romer, R. L., A. Meixner, and K. Hahne (2014), Lithium and boron isotopic composition of sedimentary rocks—The role of source history and depositional environment: A 250 Ma record from the Cadomian orogeny to the Variscan orogeny, *Gond. Res.*, *26*, 1093–1110, doi: 10.1016/j.gr.2013.08.015.

Rosner, M., J. Erzinger, G. Franz, and R. B. Trumbull (2003), Slab-dervied boron isotope signatures in arc volcanic rocks from the Central Andes and evidence for boron isotope fractionation during progressive slab dehydration, *Geochem. Geophys. Geosyst.*, *4*(8), 9005, doi: 10.1029/2002GC000438.

Ryan, J. G., and C. H. Langmuir (1993), The systematics of boron abundances in young volcanic rocks, *Geochim. Cosmochim. Acta*, *57*, 1489–1498, doi:10.1016/0016-7037(93)90008-K.

Ryan, J. G., and C. Chauvel (2014), The subduction-zone filter and the impact of recycled materials on the evolution of the mantle, in *Treatise on Geochemistry*, 2nd ed., vol. 3.13, edited by H. D. Holland and K. K. Turekian, pp. 479–508, Elsevier, Amsterdam, doi:10.1016/B978-0-08-095975-7.00211-4.

Ryan, J. G., J. Morris, F. Tera, W. P. Leeman, and A. Tsvetkof (1995), Cross-arc grochemical variations in the Kurile arc as a function of slab depth, *Science*, *270*, 625–628, doi:10.1126/science.270.5236.625.

Ryan, J. G., W. P. Leeman, J. D. Morris, and C. H. Langmuir (1996), The boron systematics of intraplate lavas: Implications for crust and mantle evolution, *Geochim. Cosmochim. Acta*, *60*, 415–422, doi:10.1016/0016-7037(95)00402-5.

Ryan, W. B. F., et al. (2009), Global multi-resolution topography synthesis, *Geochem. Geophys. Geosyst.*, *10*, Q03014, doi:10.1029/2008GC002332.

Salters, V. J. M., and A. Stracke (2004), Composition of the depleted mantle, *Geochem. Geophys. Geosyst.*, *5*, Q05004, doi:10.1029/2003GC000597.

Savov, I. P., J. G. Ryan, M. D'Antonio, K. Kelley, and P. Mattie (2005), Geochemistry of serpentinized peridotites from the Mariana forearc Conical Seamount, ODP Leg 125: Implications for the elemental recycling at subduction zones, *Geochem. Geophys. Geosyst.*, *6*, Q04J15, doi:10.1029/2004GC000777.

Scambelluri, M., and S. Tonarini (2012), Boron isotope evidence for shallow fluid transfer across subduction zones by serpentinized mantle, *Geology*, *40*, 907–910, doi:0.1130/G33233.1

Scambelluri, M., O. Muntener, L. Ottolini, T. T. Pettke, and R. Vannucci (2004), The fate of B, Cl, and Li in the subducted oceanic mantle and in the antigorite breakdown fluids, *Earth Planet. Sci. Lett.*, *222*, 217–234, doi:10.1016/j.epsl.2004.02.012.

Seyfried, W. E., D. R. Janecky, and M. J. Mottl (1983), Alteration of the oceanic crust: Implications for geochemical cycles of lithium and boron, *Geochim. Cosmochim. Acta*, *48*, 557–569, doi:10.1016/0016-7037(84)90284-9.

Singer, B. S., B. R. Jicha, W. P. Leeman, N. W. Rogers, M. F. Thirlwall, and J. Ryan (2007), Along strike trace element and isotopic variation in Central Aleutian Island arc basalt: Subduction melts sediments and dehydrates serpentine, *J. Geophys. Res.*, *112*, B06206, doi:10.1029/2006JB004897.

Smith, G. P., D. A. Wiens, K. M. Fischer, L. M. Dorman, S. C. Webb, and J. A. Hildebrand (2001), A complex pattern of mantle flow in the Lau back-arc, *Science*, *292*, 713–716, doi:10.1126/science.1058763.

Smith, H. J., A. J. Spivack, H. Staudigel, and S. R. Hart (1995), The boron isotopic composition of altered oceanic crust, *Chem. Geol.*, *126*, 119–135, doi:10.1016/0009-2541(95)00113-6.

Smith, I. E. M., and R. C. Price (2006), The Tonga-Kermadec arc and Havre-Lau back-arc system: Their role in the development of tectonic and magmatic models for the western Pacific, *J. Volcanol. Geotherm. Res.*, *156*, 315–331, doi:10.1016/j.jvolgeores.2006.03.006.

Smith, I. E. M., R. B. Stewart, R. C. Price, and T. J. Worthington (2010), Are arc-type rocks the products of magma crystallization? Observations from a simple oceanic arc volcano: Raoul Island, Kermadec Arc, SW Pacific, *J. Volcanol. Geotherm. Res.*, *190*, 219–234, doi:10.1016/j.jvolgeores.2009.05.006.

Spandler, C., and C. Pirard (2013), Element recycling from subducting slabs to crust: A review, *Lithos*, *170–171*, 208–223, doi:10.1016/j.lithos.2013.02.016.

Spandler, C., J. Mavrogenes, and J. Hermann (2007), Experimental constraints on element mobility from subducted sediments using high-P synthetic fluid/melt inclusions, *Chem. Geol.*, *239*, 228–249, doi:10.1016/j.chemgeo.2006.10.005.

Spandler, C., T. Pettke, and J. Hermann (2014), Experimental study of trace element release during ultrahigh-pressure serpentinite dehydration, *Earth Planet. Sci. Lett.*, *391*, 296–306, doi:10.1016/j.epsl.2014.02.010.

Spivack, A. J., and J. M. Edmond (1987), Boron isotope exchange between seawater and oceanic crust, *Geochim. Cosmochim. Acta*, *51*, 1033–1043, doi:10.1016/0016-7037(87)90198-0.

Stolper, E., and S. Newman (1994), The role of water in the petrogenesis of Mariana trough magmas, *Earth Planet. Sci. Lett.*, *121*, 293–325, doi:10.1016/0012-821X(94)90074-4.

Staudigel, H., T. Plank, B. White, and H.-U. Schminke (1996), Geochemical fluxes during seafloor alteration of the basaltic upper oceanic crust, DSDP Sites 417 and 418, in *Subduction Top to Bottom, Geophys Monogr. Ser.*, vol. 96, edited by G. E. Bebout et al., pp. 19–38, AGU, Washington, D. C., doi:10.1029/GM096p0019

Straub, S. M., and G. D. Layne (2002), The systematics of boron isotopes in Izu arc front volcanic rocks, *Earth Planet. Sci. Lett.*, *198*, 25–39, doi:10.1016/S0012-821X(02)00517-4.

Straub, S. M., and G. D. Layne (2003), Decoupling of fluids and fluid-mobile elements during shallow subduction: Evidence from halogen-rich andesite melt inclusions from the Izu zrc volcanic front, *Geochem. Geophys. Geosys.*, *4*(7), 9003, doi:10.1029/2002GC000349.

Straub, S. M., G. D. Layne, A. Schmidt, and C. H. Langmuir (2004), Volcanic glasses at the Izu arc volcanic front: New perspectives on fluid and sediment melt recycling in subduction zones, *Geochem. Geophys. Geosys.*, *5*, Q01007, doi:10.1029/2002GC000408.

Syracuse, E. M., P. E. van Keken, and G. A. Abers (2010), The global range of subduction zone thermal models, *Phys. Earth Planet. Inter.*, *183*, 73–90, doi:10.1016/j.pepi.2010.02.004.

Tanaka, R., and E. Nakamura (2005), Boron isotopic constraints on the source of Hawaiian shield lavas, *Geochim. Cosmochim. Acta*, *69*, 3385–3399, doi:10.1016/j.gca.2005.03.009.

Taylor, B., and F. Martinez (2003), Back-arc basin basalt systematics. *Earth Planet. Sci. Lett.*, *210*, 481–497, doi.org/10.1016/S0012-821X(03)00167-5.

Tenthorey, E., and J. Hermann (2004), Composition of fluids during serpentinite breakdown in subduction zones: Evidence for limited boron mobility, *Geology*, *32*, 865–868, doi:10.1130/G20610.1.

Thompson, G., and W. G. Melson (1970), Boron contents of serpentinites and metabasalts in the oceanic crust: Implications for the boron cycle in the oceans, *Earth Planet. Sci. Lett.*, *8*, 61–65, doi:10.1016/0012-821X(70)90100-7.

Tian, L., P. R. Castillo, D. R. Hilton, J. W. Hawkins, B. B. Hanan, and A. J. Pietruszka (2011), Major and trace element and Sr-Nd isotope signatures of the northern Lau Basin lavas: Implications for the composition and dynamics of the back-arc basin mantle, *J. Geophys. Res.*, *116*, B11201, doi:10.1029/2011JB008791.

Till, C. B., T. L. Grove, and A. C. Withers (2012), The beginnings of hydrous mantle wedge melting, *Contrib. Mineral. Petrol.*, *163*, 669–688, doi:10.1007/s00410-011-0692-6.

Timm, C., I. J. Graham, C. E. J. de Ronde, M. I. Leybourne, and J. Woodhead (2011), Geochemical evolution of Monowai volcanic center: New insights into the northern Kermadec arc subduction system, SW Pacific, *Geochem. Geophys. Geosyst.*, *12*, Q0AF01, doi:10.1029/2011GC003654.

Timm, C., D. Bassett, I. J. Graham, M. I. Leybourne, C. J. E. De Ronde, J. Woodhead, D. Layton-Matthews, and A. B. Watts (2013), Louisville seamount subduction and its implication on mantle flow beneath the central Tonga-Kermadec arc, *Nat. Commun.*, *4*, 1720, doi:10.1038/ncomms2702.

Timm, C., et al. (2014), Subduction of the oceanic Hikurangi Plateau and its impact on the Kermadec arc, *Nat. Commun.*, *5*, 4923, doi:10.1038/ncomms5923.

Todd, E., J. B. Gill, R. J. Wysoczanski, M. R. Handler, I. C. Wright, and J. A. Gamble (2010), Sources of constructional cross-chain volcanism in the southern Havre Trough: New insights from HFSE and REE concentration and isotope systematics, *Geochem. Geophys. Geosyst.*, *11*, Q04009, doi:10.1029/2009GC002888.

Todd, E., J. B. Gill, R. J. Wysoczanski, J. Hergt, I. C. Wright, M. I. Leybourne, and N. Mortimer (2011), Hf isotopic evidence for small-scale heterogeneity in the mode of mantle wedge enrichment: Southern Havre Trough and South Fiji Basin back-arcs, *Geochem. Geophys. Geosyst.*, *12*, Q09011, doi:10.1029/2011GC003683.

Tonarini, S., M. Pennisi, and W. P. Leeman (1997), Precise boron isotopic analysis of complex silicate (rock) samples using alkali carbonate fusion and ion exchange separation, *Chem. Geol.*, *142*, 129–137, doi:10.1016/S0009-2541(97)00087-9.

Tonarini, S., W. P. Leeman, and G. Ferrara (2001), Boron isotopic variations in lavas of the Aeolian volcanic arc, South Italy, *J. Volcanol. Geotherm. Res.*, *110*, 155–170, doi:10.1016/S0377-0273(01)00203-7.

Tonarini, S., M. Pennisi, A. Adorni-Braccesi, A., Dini, G. Ferrara, R. Gonfiantini, M. Wiedenbeck, and M. Groning (2003), Intercomparison of boron isotope and concentration measurements. Part 1: Selection, preparation and homogeneity tests of the intercomparison materials, *Geostand. Newslett.*, *27*, 21–39, doi:10.1111/j.1751-908X.2003.tb00710.x.

Tonarini, S., S. Agostini, C. Doglioni, F. Innocenti, and P. Manetti (2007), Evidence for serpentinite fluid in convergent margin systems: The example of El Salvador (Central America) arc lavas, *Geochem. Geophys. Geosyst.*, *8*, Q09014, doi:10.1029/2006GC001508.

Tonarini, S., W. P. Leeman, and P. T. Leat (2011), Subduction erosion of forearc mantle wedge implicated in the genesis of the South Sandwich Island (SSI) arc: Evidence from boron isotope systematics, *Earth Planet. Sci. Lett.*, *301*, 275–284, doi:10.1016/j.epsl.2010.11.008.

Turner, S., and C. Hawkesworth (1997), Constraints on flux rates and mantle dynamics beneath island arcs from Tonga-Kermadec lava geochemistry, *Nature*, *389*, 568–573, doi:10.1038/39257.

Turner, S., and C. Hawkesworth (1998), Using geochemistry to map mantle flow beneath the Lau Basin, *Geology*, *26*, 1019–1022, doi:10.1130/0091-7613(1998)026 < 1019:UGTMMF > 2.3.CO;2.

Turner, S., C. Hawkesworth, N. Rogers, J. Bartlett, T. Worthington, J. Hergt, J. Pearce, and I. Smith (1997), ^{238}U-^{230}Th disequilibria, magma petrogenesis and flux rates beneath the depleted Tonga-Kermadec island arc, *Geochim. Cosmochim. Acta*, *61*, 4855–4884, doi:10.1016/S0016-7037(97)00281-0.

Turner, S., B. Bourdon, C. Hawkesworth, and P. Evans (2000), ^{226}Ra-^{230}Th evidence for multiple dehydration events, rapid melt ascent and the time scales of differentiation beneath the Tonga-Kermadec island arc, *Earth Planet. Sci. Lett.*, *179*, 581–593, doi:10.1016/S0012-821X(00)00141-2.

Turner, S., M. Handler, I. Bindeman, and K. Suzuki (2009), New insights into O-Hf-Os isotope signatures in arc lavas from Tonga-Kermadec, *Chem. Geol.*, *266*, 196–202, doi:10.1016/j.chemgeo.2009.05.027.

Turner, S., J. Caulfield, T. Rushmer, M. Turner, S. Cronin, I. Smith, and H. Handley (2012), Magma evolution in a primitive, intra-oceanic arc setting: Rapid petrogenesis of dacites at Fonualei volcano, Tonga, *J. Petrol.*, *53*, 1231–1253, doi:10.1093/petrology/egs005.

Ulmer, P. (2001), Partial melting in the mantle wedge—The role of H_2O in the genesis of mantle-derived 'arc-related' magmas, *Phys. Earth Planet. Inter.*, *127*, 215–232, doi:10.1016/S0031-9201(01)00229-1.

Van Keken, P. E. (2003), The structure and dynamics of the mantle wedge, *Earth Planet. Sci. Lett.*, *215*, 323–338, doi:10.1016/S0012-821X(03)00460-6.

Vils, F., L. Pelletier, A. Kalt, O. Müntener, and T. Ludwig (2008), The lithium, boron and beryllium content of serpentinized peridotites from ODP Leg 209 (Sites 1272A and 1274A): Implications for lithium and boron budgets of oceanic lithosphere, *Geochim. Cosmochim. Acta*, *72*, 5475–5504, doi:10.1016/j.gca.2008.08.005.

Vils, F., S. Tonarini, A. Kalt, and H.-M. Seitz (2009), Boron, lithium and strontium isotopes as tracers of seawater-serpentinite interaction at Mid-Atlantic ridge, ODP Leg 209, *Earth Planet. Sci. Lett.*, *286*, 414–425, doi:10.1016/j.epsl.2009.07.005.

Walowski, K. L., P. J. Wallace, E. H. Hauri, I. Wada, and M. A. Clynne (2015), Slab melting beneath the Cascade arc driven by dehydration of altered oceanic peridotite, *Nat. Geosci.*, *8*, 404–408, doi:10.1038/ngeo2417.

Wei, S. S., D. A. Wiens, Y. Zha, T. Plank, S. C. Webb, D. K. Blackman, R. A. Dunn, and J. S. Conder (2015), Seismic evidence of effects of water on melt transport in the Lau back-arc mantle, *Nature*, *518*, 395–398, doi:10.1038/nature14113.

Wendt, J. I., M. Regelous, K. D. Collerson, and A. Ewart (1997), Evidence for a contribution from two mantle plumes to island arc lavas from northern Tonga, *Geology*, *25*, 611–614, doi:10.1130/0091-7613(1997)025 < 0611:EFACFT>2.3.CO;2.

Wiens, D. A. (2001), Seismological constraints on the mechanism of deep earthquakes: Temperature dependence of deep earthquake source properties, *Phys. Earth Planet. Inter.*, *127*, 145–163, doi:10.1016/S0031-9201(01)00225-4.

Wiens, D. A., and H. J. Gilbert (1996), Effect of slab temperature on deep earthquake aftershock productivity and magnitude-frequency relations, *Nature*, *384*, 153–156, doi:10.1038/384153a0.

Wood, B., and S. Turner (2009), Origin of primitive high-Mg andesite: Constraints from natural examples and experiments, *Earth Planet. Sci. Lett.*, *283*, 59–66, doi:10.1016/j.epsl.2009.03.032.

Woodhead, J., S. Eggins, and J. Gamble, (1993), High field strength and transition element systematics in island arc and back-arc basin basalts: Evidence for multi-phase melt extraction and a depleted mantle wedge, *Earth Planet. Sci. Lett.*, *114*, 491–504, doi:10.1016/0012-821X(93)90078-N.

Woodhead, J. D., J. M. Hergt, J. P. Davidson, and S. M. Eggins (2001), Hafnium isotope evidence for 'conservative' element mobility during subduction zone processes, *Earth Planet. Sci. Lett.*, *192*, 331–346, doi:10.1016/S0012-821X(01)00453-8.

Workman, R. K., E. Hauri, S. R. Hart, J. Wang, and J. Blusztajn (2006), Volatile and trace elements in basaltic glasses from Samoa: Implications for water distribution in the mantle, *Earth Planet. Sci. Lett.*, *241*, 932–951, doi:10.1016/j.epsl.2005.10.028.

Wysoczanski, R. J., I. C. Wright, J. A. Gamble, E. H. Hauri, J. F. Luhr, S. M. Eggins, and M. R. Handler (2006), Volatile contents of Kermadec Arc—Havre Trough pillow glasses: Fingerprinting slab-derived aqueous fluids in the mantle sources of arc and back-arc lavas, *J. Volcanol. Geotherm. Res.*, *152*, 51–73, doi:10.1016/j.jvolgeores.2005.04.021.

Yamaoka, K., T. Ishikawa, O. Matsubaya, D. Ishiyama, K. Nagaishi, Y. Hiroyasu, H. Chiba, and H. Kawahata (2012), Boron and oxygen isotope systematics for a complete section of oceanic crustal rocks in the Oman ophiolite, *Geochim. Cosmochim. Acta*, *84*, 543–559, doi:10.1016/j.gca.2012.01.043.

You, C.-F., A. J. Spivack, J. H. Smith, and J. M. Gieskes (1993), Mobilization of boron in convergent margins: Implications for the boron geochemical cycle, *Geology*, *21*, 207–210, doi:10.1130/0091-7613(1993)021 < 0207:MOBICM>.

You, C. F., J. D. Morris, J. M. Gieskes, R. Rosenbauer, S. H. Zheng, X. Xu, T. L. Ku, and J. L. Bischoff (1994), Mobilization of Be in the sedimentary column at convergent margins, *Geochim. Cosmochim. Acta*, *58*, 4887–4898, doi:10.1016/0016-7037(94)90219-4.

You, C.-F., L. H. Chan, A. J. Spivack, and J. M. Gieskes (1995), Lithium, boron, and their isotopes in sediments and pore waters of Ocean Drilling Program Site 808, Nankai Trough: Implications for fluid expulsion in accretionary prisms, *Geology*, *23*, 37–40, doi:10.1130/0091-7613(1995)023 < 0037:LBATII>2.3.CO;2.

Zellmer, K. E., and B. Taylor (2001), A three-plate kinematic model for Lau Basin opening, *Geochem. Geophys. Geosyst.*, *2*(5), 1020, doi:10.1029/2000GC000106.

Geophysics, Geochemistry, and Geosystems

Supporting Information for

Boron isotope variations in Tonga-Kermadec-New Zealand arc lavas: Implications for the origin of subduction components and mantle influences

William Leeman[1, 4], Sonia Tonarini[2] and Simon Turner[3]

[1] Department of Earth Science, Rice University, U.S.A.

[2] Instituto di Geoscienze e Georisorse, Via Moruzzi 1, 56127 Pisa, Italy

[3] Department of Earth and Planetary Sciences, Macquarie University, Sydney NSW 2109, Australia

[4] Current address: 642 Cumbre Vista, Santa Fe, NM 87501

Contents of this file

Additional Supporting Information (Files uploaded separately)

Table S1. Supplemental information including: I. Mantle source models calculated from compositions of primitive magmas; II, Average primitive melt compositions considered; and III. Reference compositions used in figures and text

Introduction

• This document provides supplemental information used in the main text and figures. Table S1 comprises three sections: I. Mantle source models calculated from compositions of primitive magmas; II. Average primitive melt compositions considered; and III.

Reference compositions used in figures and text. Reference citations are provided for the sources of this information where appropriate. Also, a description is provided for the methods used to compute level of source depletion, degree of melting to produce the arc lavas, and the compositions of their respective sources. This is followed by a brief assessment of the results, including estimated temperatures of melt segregation from the mantle. Selected figures are also included. Figure S1 shows systematic variations for TiO_2, Yb, and Y concentrations in TKNZ lavas, Figure S2 presents latitudinal variation in source composition for selected elements, and Figure S3 shows variation of B and $\delta^{11}B$ vs. Sr and Nd isotopic compositions for individual samples analyzed in this study.

Text S1.

Description of Table S1 - Supplemental Information

Source compositions reported in Part I were calculated using model parameters provided there, following the procedure described below. In this section are provided source elemental concentrations (in ppm unless otherwise noted), and melt fractions (F) used to calculate source composition from the average analyses in Part II. Also reported are temperature, pressure, and equivalent 'segregation' depth at which the primitive magmas could have equilibrated with a source with Mg# = 90. These values are averages from calculations on individual samples using the method of *Lee et al.* [2009] (see details below; also *Leeman et al*., 2005a). Note that the tabulated source concentrations are not corrected for fractional crystallization. However, based on the *Lee et al.* [2009] computations, a value for [Mf/Mo] is provided for each locality average that represents the final mass of primitive magma after olivine addition to achieve equilibrium with Mg#90 mantle divided by the initial mass of uncorrected magma. Division of the reported concentrations by this number gives the 'FC'-corrected source compositions; these corrections range from 0 (New Zealand) to 37% (L'Esperance), and typically are between 10-20% (average = 15%). Finally, we tabulate depth to slab for each locality [a] as determined from the SLIP 1.0 model of *Hayes et al.* [2014], or [b] from the compilation of *Syracuse et al.* [2006].

Primitive melt compositions tabulated in Part II are calculated using analyses of selected samples from each locality, restricted to less than 55% SiO_2, and at least 5% MgO where possible. No samples from Hunga Ha'apai and L'Esperance in our database

met the second criterion, so the most primitive samples were used. Also, because no samples from Niuatoputapu, Fonualei, Metis Shoal or Curtis met either criterion, these localities are not represented here. Prior to averaging, all major element analyses were normalized to total 100% on an anhydrous basis with all iron calculated as FeO. Averages, standard deviation, and number of samples included are provided for each element. In some cases, for B and a few other elements, there was only a single analysis available. For New Zealand, the TVZ average is based on two of the most primitive basalts from the Ruapehu area; because the Kakuki lava is distinctly more primitive it was treated separately. References for the analyses used are provided in Part I).

Our extrapolation to mantle conditions necessarily implies that the analyzed magmas are primitive and only moderately removed from compositions of mantle partial melts. This is difficult to prove, but we note that virtually all basalts from the Kermadec – TVZ sectors are multiply saturated with plagioclase, olivine, ± clinopyroxene (± orthopyroxene in some basaltic andesites), and in the highest-MgO samples the olivines are magnesian (up to Fo_{89}) which supports their primitive nature [*Gamble et al.*, 1990, 1993, 1997]. Mafic lavas from the Tonga sector (esp. Late and Hunga Ha'apai) are dominantly saturated with plagioclase and pyroxene, and olivine is rare [*Ewart et al*., 1973]; accordingly, extrapolations to mantle conditions are less certain for these lavas.

End member compositions in Part III are taken from the cited references, with B data from this study included where noted; in some cases B content was estimated. The sediment average for DSDP 596 was calculated using only the samples analyzed in this study, using our B data, with data for other elements and lithological weightings from *Plank and Langmuir* [1998]. It should be noted that B contents in other sediment averages from *Plank* [2014] are estimates, and not based on direct analyses.

Calculations of source depletion, degree of melting, and source compositions

The level of prior melt depletion in the source for each locality was estimated based on contents of TiO_2, Y, and Yb in primitive samples, and assuming that source concentrations for these components were not enhanced in any way by subduction contributions [cf. *McCulloch and Gamble*, 1991; *Pearce and Peate*, 1995; *Ewart et al*, 1998; *Gribble et al.*, 1998; *Kelley et al*., 2006]. The latter authors use TiO_2/Y ratios in a

given sample, the same ratio in MORB, and estimated TiO_2 content (0.133%) for DMM [*Salters and Stracke*, 2004] to calculate TiO_2 content in the source for the sample. The formulation used is as follows: $C_o\text{-Ti} = [(TiO_2/Y)_{sa}/(TiO_2/Y)_{NMORB}] \bullet C_{DMM}\text{-Ti}$.

We follow this approach but use both TiO_2/Y and TiO_2/Yb sample ratios with average NMORB values (0.0461 and 0.4665, respectively; *Gale et al*. [2013]) to obtain two independent solutions for source TiO_2 content. The resulting values provide parallel estimates of the source TiO_2 content for a given sample normalized to the value in an average NMORB source. We find that, for the samples considered in our study (and using high precision trace element data; cf. *Davidson et al*., [2013]), the different estimates based on ratios with Y or Yb typically agree within 10% or better. The source TiO_2 values reported (Table S1, Part I and also Part II) represent averages of multiple samples from each locality, and in most cases standard deviations indicate that agreement among samples is better than 10%. An advantage of this approach is that lava compositions do not require correction for fractional crystallization because solid/melt distribution coefficients for all three elements are sufficiently similar that the element ratios are not significantly modified during differentiation of basaltic magmas. This is supported by Figure S1, in which it is shown that Ti-Yb and Ti-Y concentrations are highly correlated in TKNZ lavas with < 56% SiO_2. Specifically in magmas with > 5-6% MgO, titanomagnetite fractionation is expected to be negligible [cf. *Taylor and Martinez*, 2003]. Estimated source TiO_2 values can be used with magmatic TiO_2 contents and a batch melting model to calculate the extent of melting (or melt fraction, F) required to produce said magma (cf. *Kelley et al.,* 2006). Their formulation is as follows: $F = [(C_o/C_{liq}) - D]/(1 - D)$, where C_o and C_{liq} are concentrations of TiO_2 in the source and the magma (adjusted to Mg# = 90). D is the bulk solid/melt partition coefficient during source melting, and for the spinel lherzolite model assumed, a value of 0.04 is used; although this parameter will decrease with degree of melting (as clinopyroxene is consumed), this effect is of secondary importance because the absolute value is so low. C_{liq} values (Ti_{90}) were determined from individual lava compositions, extrapolated back to the equivalent melt composition in equilibrium with a source having Mg# = 90. This source composition is used in the references cited above and allows comparison with results of those studies. However, actual source Mg# could differ. For example, *Cooper*

et al. [2010] provide evidence for Mg# as high as 92 for some TKNZ boninites at submarine Volcano A). Calculations are presented in Table S1 for Volcano A; although the estimated source compositions are very similar to those for nearby Hunga Ha'apai, they are not included in our figures because of the uncertainty in source Mg#. Assumption of Mg# > 90 will lower the absolute source concentrations reported here (and vice versa), but relative abundances and element ratios for incompatible elements will not be significantly affected.

The FRACTIONATE3 worksheet of *Lee et al*. [2009] was used for this extrapolation; it incrementally adds equilibrium olivine to the original lava composition until the target source Mg# is attained. This approach does not strictly replicate liquid lines of descent for magmas that are multiply saturated with phases other than olivine (e.g., plagioclase and/or clinopyroxene) but, because TiO_2 is negligible in the major liquidus phases, simple olivine addition reasonably approximates the incompatible element concentrations in a primitive melt (i.e., TiO_2 content is essentially diluted by the mass of solid material added to achieve the primitive composition). This approach effectively incorporates a comprehensive adjustment for crystal fractionation effects back to equilibrium with the assumed source. Implicit corrections for cotectic plagioclase or clinopyroxene have only small effect on the final liquid composition for the incompatible elements and for Ti as long as these mineral modes are small. Additionally, these calculations can be sensitive to redox conditions, and for our purposes we assumed a ferric iron fraction appropriate for calcalkaline magmas ($X_{Fe3} = 0.18$, on molar basis; cf. *Leeman et al*., [2005a]). F values were calculated for individual samples, using the corrected Ti_{90} values and estimated source TiO_2 contents for each; most of the values reported in Table S1, Part II represent averages of multiple samples from each locality (in some cases only one sample was used). Coefficients of variation (CV = % SD) are typically better than 15% but range up to 26% for New Zealand.

Taking the average F value for each locality from above, and using a batch melting model with the primitive melt compositions in Table S1, Part II and distribution coefficients in Table S1, Part I, source compositions were calculated for selected incompatible elements. These are presented in Table S1, Part I for TKNZ localities, along with estimates for the backarc FSC calculated using data of *Keller et al*. [2008];

using data of *Escrig et al*. [2012] we obtain essentially the same estimates (not shown) despite the fact that they made initial adjustments for fractional crystallization and we did not. The uncertainties in F values (melt fraction) propagate directly to these calculations. Coupled with uncertainties in the primitive melt averages (in each case using average CV for all tabulated elements), the pooled uncertainties on source compositions are between 8-31% (a measure of precision only). The greatest uncertainties are for New Zealand (TVZ), Kao, Raoul, and Mangatolo Triple Junction (MTJ), and these reflect heterogeneity in the populations of primitive basaltic magmas from these localities. We also note that use of lower TiO_2/Y and TiO_2/Yb ratios (e.g., those of DMM instead of NMORB) in the above process results in systematically higher estimates for source TiO_2, F, and other element concentrations in the arc lava sources. However, relative differences in source element concentrations are not affected and element ratios are robust. The latter are used in the main text figures and discussion.

Brief summary of source compositions

Estimated source compositions ('FC'-corrected as explained above; plotted vs. latitude in Figure S2) reveal important spatial variations along the arc. These are discussed briefly with reference to nominal compositions of primitive ('PM'; OIB-source), depleted ('DMM'; MORB-source), and ultra-depleted ('DMM-1'; MORB-source minus 1% melt) mantle compositions (cf. Table S1, Part III). Estimates for FSC lavas conform closely to patterns defined by the TKNZ lavas (cf. Fig. S2), and are not discussed separately. Yb concentrations are relatively consistent along the arc, decreasing slightly at the south end, but near estimates for PM, DMM, and DMM-1 (all close to 0.4 ppm). Zr is also fairly consistent along most of the arc, near DMM-1, hence more depleted than MORB-source mantle; values above PM occur at Clark and TVZ. Nb is conspicuously depleted (at or below DMM-1) for most of the Tonga-Kermadec locations, but rises to DMM levels in the north and slightly higher levels in the south (but still well below PM values). These elements corroborate the overall depleted nature of the main arc, and indicate that the level of depletion is relatively consistent except at the extreme ends where compositions approach (or exceed, at New Zealand) estimated MORB source values.

Th and, to lesser extent, La and Be source abundances display southward-increasing gradients ranging from near DMM in the north to values approaching PM from Kermadec to New Zealand; these elements have similar concentrations in the FSC and backarc region in general. U and Ba source abundances are more uniformly enriched along the arc, near or above PM values for U and well above PM for Ba. Assuming that these elements must have been extremely depleted by processes (melt extraction) that produced the Nb and Zr patterns, it is evident that Th, La, Be, and especially Ba and U have been enhanced by subduction contributions. B displays the most dramatic gradient in which source abundances increase strongly to the north from New Zealand, and are everywhere well above PM estimates. The trend for B extends to the northern island of Tafahi, whereas Ba in that region drops slightly in source enrichment. Both B and Ba source abundances decrease sharply in the backarc in a coherent fashion that is well defined by the FSC lavas and ends with MTJ and Niuafo'ou still above estimated DMM composition. For the arc sources, it is clear that essentially all of the B and Ba enrichment must be of slab derivation. The spatial variations are discussed further in the main text in terms of element ratios and their relation to isotopic compositions.

The main observations drawn from Figure S2 are that: [1] prior source depletion was relatively consistent beneath the entire arc, with exception of the extreme ends; [2] northward enrichment of the most fluid-mobile element (B) is consistent with northward increasing inputs of slab-derived fluids, and this appears to extend more or less steadily as far as Tafahi; [3] by the same measures, fluid inputs (B, Ba) diminish sharply in the northern backarc region; [4] U and Ba enrichments are relatively consistent along the arc and U diminishes only slightly in the backarc region; and [5] Th, Be, and La enrichments are significant but generally increase to the south; the anticorrelation with B is particularly significant. This latter point strongly suggests that Th, La, and perhaps Be are decoupled from B and Ba, but the reason is not entirely clear. One possibility is that Th, La, and Be are less soluble in aqueous fluid than B or Ba, and this may imply an alternate mode of transport for them – for example in silicate melts (as has commonly been proposed). Supporting this viewpoint are models of subduction zone thermal structures that suggest greater likelihood of melting of the uppermost slab approaching New Zealand. Another possibility is that, proceeding from north to south, sources for Th

and La (i.e. sedimentary components) make up systematically greater proportions of the material being subducted; this is in accord with geological observations. The anticorrelation noted above might suggest that two transfer processes have operated (i.e., fluid vs. melt), and that their relative efficacy changes along-strike. This would presumably be related to changing conditions in the subducting slab since the mantle wedge appears to be more or less uniformly depleted by earlier processes.

Another important facet concerns melting processes along the arc. If the level of source refractoriness is near constant (point [1] above), then increasing flux of slab-derived fluids to the north (e.g., in proportion to convergence rate along the arc) can explain the parallel increase in degree of melting inferred to produce the main arc magmas. This might imply that melting is catalyzed in proportion to the amount of available aqueous fluid (but see below).

Implications of P-T constraints

One other outcome of modeling primitive melt compositions with FRACTIONATE 3, is that temperature and pressure are estimated for equilibrium of the calculated melts with the assumed source. While the absolute T-P values are certainly dependent on assumptions regarding redox conditions and of specific source composition (e.g., Mg#), the relative values are more robust. These are shown in Table S1, Part I. Estimated temperatures range between 1250-1440 °C, and pressures between 0.64-1.53 GPa (depths of 20-50 km) for the TKNZ locations (overlapping estimates by *Cooper et al.* [2010]), and 1286-1323°C, 0.40-0.92 GPa (depths of 15-30 km) for FSC, and imply extremely warm conditions at relatively shallow depths (essentially just below the base of the arc crust), presumably in a zone of magma accumulation. The predicted temperatures are well above experimentally determined water-saturated solidi for mantle lithologies [cf. *Ulmer*, 2001; *Till et al*., 2012], and inconsistent with melting in response to solidus reduction by addition of fluids. However, the amount of fluid required to produce estimated enrichments of B in the magma sources may be small (possibly <<1%), depending on the assumed fluid composition and on the process of enrichment. In the main text, we discuss evidence that source enrichments are incremental and occur over protracted duration; only a portion of the enrichment is ‘real time’ or recent, as reflected

in the presence of short-lived radioisotopes. Thus, 'fluid transport' need not imply that the full amount of fluid required to account for a given enrichment level be present at one moment. We envision that concentrations of fluid-mobile elements accumulate over time due to interactions between transient fluids and the host rock, and this domain of modified mantle can later produce partial melts when P-T conditions are appropriate. This could occur in different ways, including: [1] when a domain of modified mantle is convected into warmer regions of the mantle wedge, [2] some external heat source (e.g., magma infiltration) is applied, or [3] a new pulse of fluid lowers the ambient solidus. We do not attempt to resolve these issues here, but the temperature constraints outlined above are more consistent with scenarios that involve melting at conditions not far removed from the anhydrous mantle solidus. The relatively high melt proportions (up to >30%) estimated here would be favored by high temperatures.

B systematics vs. Sr-Nd isotopic compositions

Figure S3 shows details of relations between B systematics (as B/Zr ratios and $\delta^{11}B$) vs. Sr and Nd compositions for all individual lavas investigated in this study. This figure complements text Fig. 8, that shows averages of Sr-Nd-Pb compositions as a function of Zr/Nb ratios (proportional to source depletion) estimated for the respective source compositions. Note that the average NMORB $^{87}Sr/^{86}Sr$ ratio (0.70281) plots just off scale in panels B and D. Symbols are same as in text Figure 3.

Key observations include the following. As B/Zr ratios increase (i.e., greater slab fluid input to magma sources) $^{87}Sr/^{86}Sr$ ratios decrease systematically (ca. 0.7045 for New Zealand to < 0.7035 for Tonga) whereas $^{143}Nd/^{144}Nd$ ratios remain fairly consistent, near MORB values (0.5130-0.5131). Lavas from New Zealand and the backarc are exceptional in that their $^{143}Nd/^{144}Nd$ ratios are shifted lower, and their $^{87}Sr/^{86}Sr$ ratios are the highest observed. Both features could be attributed to involvement of sedimentary material but, in general, sediment fields are displaced far from and at high angles to the lava trends. If the lava trends reflect the addition of subduction components to the mantle wedge, it appears that the B-rich additive must have Sr and Nd compositions similar to MORB or possibly altered oceanic crust. B isotopic compositions are more clustered, and do not define strong trends. $\delta^{11}B$ values are elevated compared to sedimentary

components and require additions of heavy boron from other sources - most likely serpentinized ultramafic rocks or possibly altered oceanic crust within the subducting slab (cf. analyses of these types of materials in Table S1, Part III). Of all the arc lavas, the anomalous Ata samples have Sr-Nd compositions most similar to average NMORB [*Gale et al*., 2013].

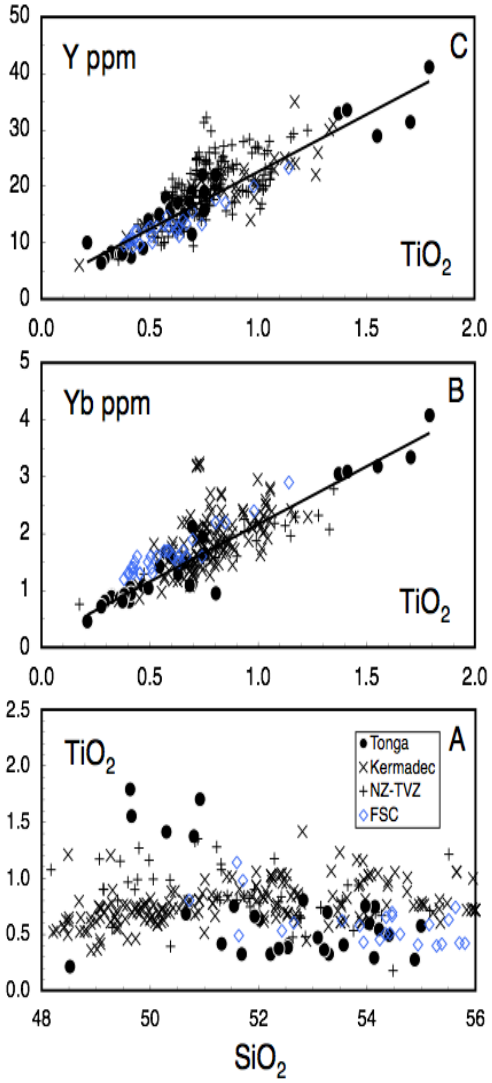

Figure S1. TiO_2-Yb-Y systematics: (a) TiO_2 vs. SiO_2 in lavas from Tonga, Kermadec, New Zealand (TVZ), and the backarc Fonualei Spreading Center (FSC). Tonga group samples with > 1.3 % TiO_2 are from backarc Niuafo'ou. Data are from the GEOROC data base for samples having < 56% SiO_2. (b) TiO_2 vs. Yb and (c) TiO_2 vs. Y are highly correlated, consistent with their similar incompatibility during melting and subsequent

fractional crystallization for magmas in this compositional range. Trend lines in (b) and (c) for the Tonga data show correlations as follows: for Yb, $y = 2.023x + 0.1405$ ($R^2 = 0.92$); for Y, $y = 20.281 + 2.26$ ($R^2 = 0.91$). Despite that the GEOROC data are compiled from various sources with data of varying quality, overall the correlations are remarkably good and the data internally consistent.

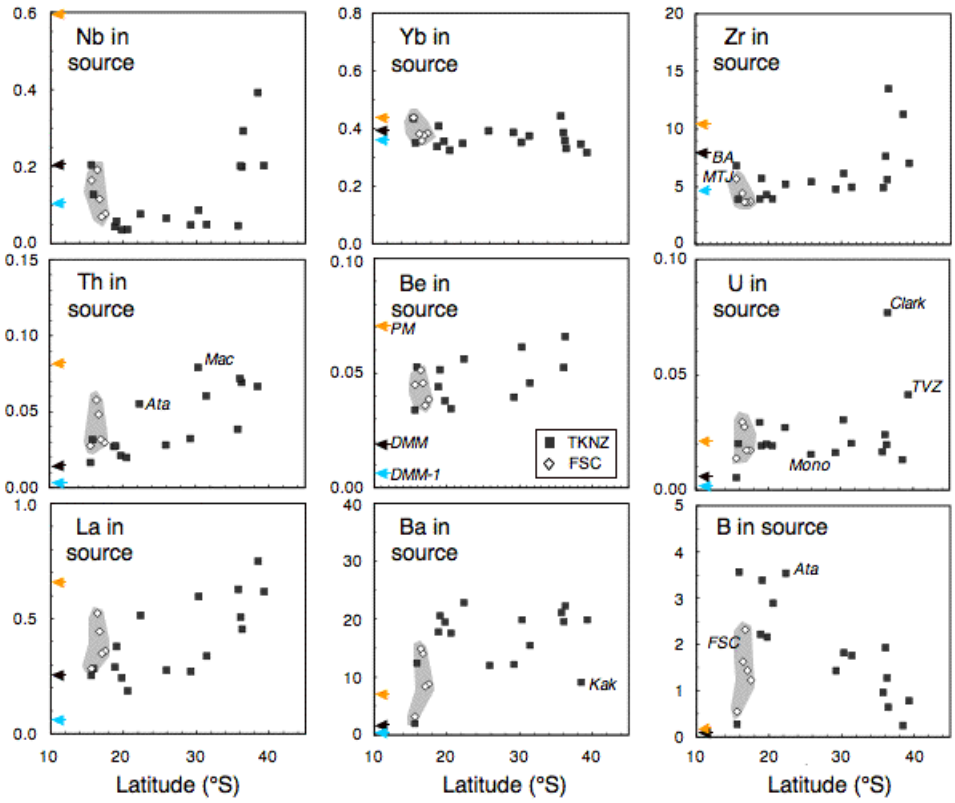

Figure S2. Latitudinal variation in estimated source compositions for selected elements in TKNZ and Fonualei Spreading Center (FSC) localities. Corrections for FC have been applied to data tabulated in Table S1 (see text). Estimated mantle compositions are indicated by triangles (on left hand side) for PM (orange), DMM (black), and DMM-1 (blue).

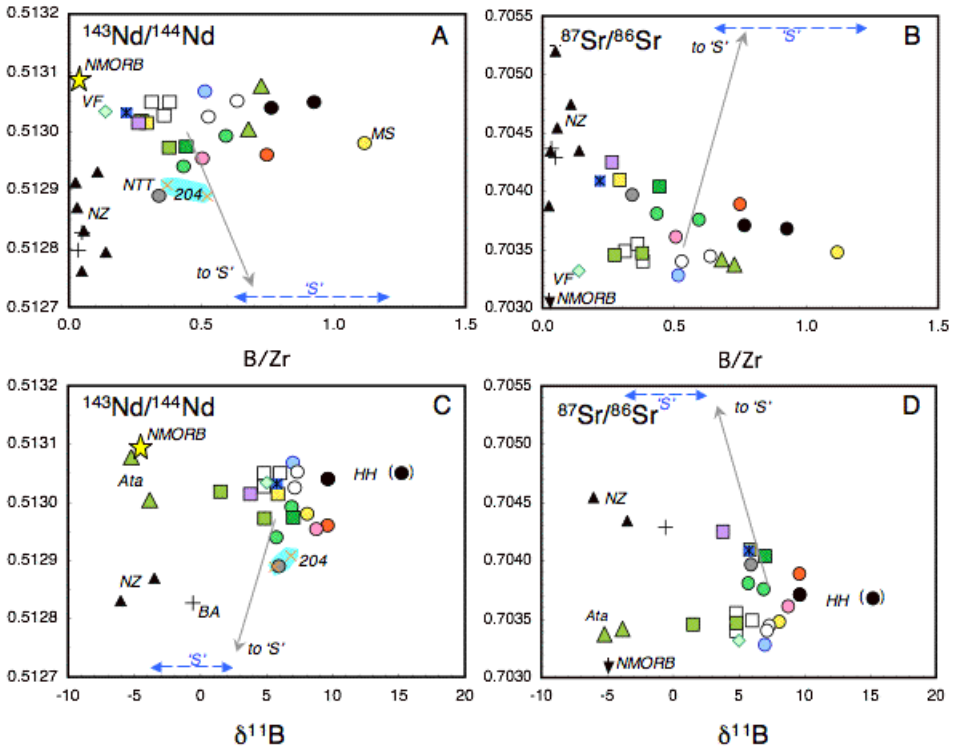

Figure S3. Variation of B and $\delta^{11}B$ vs. Sr and Nd isotopic compositions for individual samples analyzed in this study. Symbols as in text Fig. 3. Gray arrows point to fields for locally subducting sediments ('S') that plot off-scale; blue horizontal arrows delimit their ranges in B/Zr and $\delta^{11}B$. Average NMORB $^{87}Sr/^{86}Sr$ (0.70281; *Gale et al*. [2013]) plots slightly off-scale.

Table S1. Supplemental information including: I. Mantle source models calculated from compositions of primitive magmas; II, Average primitive melt compositions considered; and III. Reference compositions used in figures and text.